

DISSERTATION / DOCTORAL THESIS

Titel der Dissertation /Title of the Doctoral Thesis

„Unravelling rescue mechanisms of stalled proteasome complexes“

verfasst von / submitted by

mag. biol. mol. Katarina Belačić

angestrebter akademischer Grad / in partial fulfilment of the requirements for the degree of

Doctor of Philosophy (PhD)

Wien, 2022 / Vienna 2022

Studienkennzahl lt. Studienblatt /
degree programme code as it appears on the student
record sheet:

UA 794 685 490

Dissertationsgebiet lt. Studienblatt /
field of study as it appears on the student record sheet:

Molekulare Biologie

Betreut von / Supervisor:

Jun. Prof. Dr. David Haselbach

Table of Contents

Acknowledgements	1
Abstract	2
Zusammenfassung	3
1. Introduction	4
1.1. Ubiquitin-proteasome system	4
1.2. Proteasome complex	6
1.2.1. Diversity of proteasome complexes	6
1.2.2. Structure of the 26S proteasome	8
1.2.2.1. Structure of the 20S core particle	8
1.2.2.2. Structure of the 19S regulatory particle	10
1.2.3. Function of the 26S proteasome	13
1.2.3.1. Substrate binding and engagement with the 26S proteasome	15
1.2.3.2. Substrate unfolding, translocation and deubiquitination	18
1.2.3.3. Substrate proteolysis	21
1.3. Regulation of the 26S proteasome	22
1.4. UPS impairment	24
1.4.1. Malfunction of the 26S proteasome	25
1.4.2. Polyglutamine disorders – the case of Huntington’s disease	26
1.4.3. 26S proteasome malfunction in Huntington’s disease	29
1.4.4. 26S proteasome as a therapeutic target	32
1.5. Regulation of 26S proteasome under malfunctioning conditions	34
1.5.1. Potential rescue mechanisms of malfunctioning 26S proteasomes	34
1.5.2. 26S proteasome regulation by ZFAND protein family	36
2. Aims of the study	43
3. Materials and Methods	44
3.1. Materials	44
3.1.1. Standard chemicals	44
3.1.2. Stains and reagents	44
3.1.3. Standards, commercial kits, and enzymes	44
3.1.4. <i>Escherichia coli</i> strains, mammalian cell lines and expression plasmids	44
3.1.5. Bacterial and cell culture media	45
3.2. Methods	45
3.2.1. Molecular cloning	45

3.2.1.1. Polymerase chain reaction (PCR)	45
3.2.1.2. Agarose gel electrophoresis.....	46
3.2.1.3. PCR product purification	46
3.2.1.4. Gibson assembly	47
3.2.1.5. Transformation of chemically competent DH5a <i>E. coli</i> cells	47
3.2.1.6. Miniprep and sequencing.....	48
3.2.2. Biochemical methods.....	48
3.2.2.1. Sodium dodecyl sulfate polyacrylamide gel electrophoresis (SDS-PAGE)	48
3.2.2.2. Western blot	49
3.2.2.3. Analytical size exclusion chromatography	50
3.2.2.4. Determination of protein concentration	50
3.2.2.5. Sucrose density gradient ultracentrifugation.....	51
3.2.3. Recombinant protein expression and purification	52
3.2.3.1. Transformation of chemically competent <i>E. coli</i> cells.....	52
3.2.3.2. Protein expression in autoinduction media	52
3.2.3.3. Cell lysis	52
3.2.3.4. MBPTrap affinity chromatography.....	53
3.2.3.5. MagneGST Glutathione Particles affinity purification	53
3.2.3.6. Ion-exchange chromatography.....	54
3.2.3.7. Size-exclusion chromatography.....	55
3.2.4. Purification of human 26S proteasomes	55
3.2.4.1. Purification from HeLa cytoplasmic extracts using GST-UBL method	55
3.2.4.2. Purification from HEK293GP cells using Streptavidin affinity chromatography	56
3.2.5. <i>In vitro</i> assays	58
3.2.5.1. Ubiquitination assay	58
3.2.5.2. Degradation assay.....	59
3.2.5.3. Reconstitution assay	60
3.2.6. Cryo-electron microscopy	60
3.2.6.1. Sample preparation	60
3.2.6.2. Grid screening and data collection.....	61
3.2.6.3. Movie preprocessing and 2D image processing	62
3.2.6.4. 3D processing	63
4. Results & Discussion	64
4.1. <i>In vitro</i> approach for investigation of ZFAND2a-bound 26S proteasome complex .	64

4.1.1. Affinity purification of human 26S proteasome complexes.....	64
4.1.2. Purification of recombinant ZFAND2a-MBP-6xHis protein	68
4.1.3. Generation of proteasomal substrates	70
4.1.3.1. Strategy in substrate protein design	71
4.1.3.2. Purification of designed substrate proteins.....	73
4.1.3.3. Ubiquitination of substrate proteins	76
4.1.3.4. Initial degradation screen with K48-polyubiquitinated substrates	80
4.1.3.5. Separation of polyubiquitinated from non-ubiquitinated substrate species	83
4.3. Functional analysis of ZFAND2a-bound 26S proteasome complex.....	85
4.3.1. SDS-PAGE analysis of degradation assay	86
4.4. Structural analysis of ZFAND2a-bound 26S proteasome complex	90
4.4.1. Reconstitution of ZFAND2a-bound 26S proteasome complex.....	91
4.4.2. Cryo-EM analysis of ZFAND2a-bound 26S proteasome complex.....	95
4.4.3. Comparison of ZFAND2a-bound and ZFAND2a-free 26S proteasome complexes	102
4.4.4. Rigid body fitting of ZFAND2a predicted structure into ZFAND2a density	105
5. Summary and Conclusions	107
5.1. <i>In vitro</i> system preparation for investigation of ZFAND2a potential role in rescuing stalled 26S proteasome complex.....	108
5.2. 26S proteasome degradation of model substrates in the presence or absence of ZFAND2a	109
5.3. Structural characteristics of ZFAND2a-bound 26S proteasome complex	111
6. Appendix.....	114
7. References.....	121

Acknowledgements

First and foremost, I would like to express my gratitude to my Ph.D. supervisor David Haselbach for entrusting me to independently drive this project. David's passion about science and curious mindset have inspired me to push further and have had tremendous impact on my scientific as well as personal growth.

I am grateful for the opportunity to work with all previous and present members of the Haselbach lab, whose admirable scientific knowledge and expertise as well as friendly and supportive spirit have made this experience so much richer and unforgettable.

This work would have never reached its goals if it had not been for many amazing people and their contributions. Especially I would like to emphasize and express my thankfulness to all the members of the VBCF EM Facility and IST EM Facility, Clausen and Plaschka group and to our collaborators Nick G. Brown, Philipp Kukura and Ariel Stanhill.

My deepest gratitude to Bojan Žagrović, Daniel Wolfram Gerlich and Florian Schur for their involvement in this project as members of my Thesis Advisory Committee. Their professional advice, feedback, guidelines, and support greatly shaped and steered this project to its completion.

I also thank Sebastian Falk, Georg Winter and Yasin Dagdas for their willingness to be the reviewers and/or examiners of my work.

I am deeply thankful for the unconditional support and love that I have received from my parents – Ksenka and Djuro and siblings – Kristina and Djuro, that gave me strength to fiercely pursue my professional and personal ambitions; moreover, to overcome many hurdles on the way.

Furthermore, I also want to thank my dearest friends Sofija, Susanne, Ana, Sofia, Hanna, Zuzana, and Kimi for their unique and unlimited support.

The person I will be thankful forever and ever is my boyfriend Stjepan. Because of him I could do more even when I thought I couldn't. I turned my failures into lessons and my weaknesses into strengths. Without him, it would have not been possible.

Lastly, I want to thank my Mino Lino for every cuddle after work that took away the stress, for every walk during which I got a clear mind and for teaching me to have patience and a mindset that makes what seems impossible possible by effort and perseverance.

Abstract

Efficient removal of proteins whose presence in cells is not required or have toxic properties is crucial for maintaining cellular homeostasis. The 26S proteasome complex represents a final destination of proteins targeted for degradation via the ubiquitin-proteasome system. Malfunction of the 26S proteasome has been implicated in several human pathologies, including neurodegenerative disorders, where mutant proteins accumulate due to their resistance towards proteasomal degradation. Although general regulation of the 26S proteasome has been widely investigated, the potential rescue mechanisms of malfunctioning 26S proteasomes are fairly unknown.

The ZFAND protein family in humans has been implicated in the regulation of the 26S proteasome under conditions that require increased proteasomal activity such as muscle atrophy and proteotoxic conditions. Particularly, ZFAND2a is induced upon heat stress, arsenite intoxication, and proteasome inhibition; after which, it directly binds the 26S proteasome. This points towards ZFAND2a's potential role as a rescue factor for malfunctioning 26S proteasomes. Moreover, the *C.elegans* homolog of ZFAND2a increases proteasomal degradation of A β peptide and polyglutamine protein present in Alzheimer's and Huntington's disease, respectively.

Here, I investigated the functional characteristics of the 26S proteasome complexed with ZFAND2a and a control substrate or a toxic substrate containing a polyglutamine repeat. I showed under *in vitro* conditions that ZFAND2a binding to the 26S proteasome does not enhance overall protein degradation and does not allow efficient degradation of proteins with polyglutamine repeats. Structural analysis of ZFAND2a-bound 26S proteasome complex revealed that ZFAND2a has an elongated shape bound to the proteasomal subunits Rpn1 and Rpn7. The observation that ZFAND2a-bound 26S proteasome complex is in substrate accepting state suggests that ZFAND2a binding performs a regulatory role that is prior to substrate engagement. Thus, the ZFAND2a role might have more of a structural rather than functional purpose, such as inferring more stability or recruiting additional factors required for the rescue to occur.

Zusammenfassung

Die effiziente Beseitigung von Proteinen, deren Anwesenheit in Zellen nicht mehr erforderlich ist oder die toxischen Eigenschaften haben, ist für die Aufrechterhaltung der zellulären Homöostase von entscheidender Bedeutung. Der 26S-Proteasom-Komplex ist das endgültige Ziel von Proteinen, die über das Ubiquitin-Proteasom-System abgebaut werden sollen. Eine Fehlfunktion des 26S-Proteasoms wurde bei mehreren menschlichen Erkrankungen festgestellt, darunter auch bei einer Reihe von neurodegenerativen Erkrankungen, bei denen sich mutierte Proteine aufgrund ihrer Resistenz gegenüber dem proteasomalen Abbau ansammeln. Obwohl die allgemeine Regulierung des 26S-Proteasoms weitgehend erforscht ist, sind die potenziellen Mechanismen zur Rettung von schlecht funktionierenden 26S-Proteasomen noch weitgehend unbekannt.

Die ZFAND-Proteinfamilie wurde beim Menschen in die Regulierung des 26S-Proteasoms unter Bedingungen einbezogen, die eine erhöhte proteasomale Aktivität erfordern, wie Muskelschwund und proteotoxische Bedingungen. Insbesondere ZFAND2a wird unter Bedingungen wie Hitzestress, Arsenitvergiftung und Proteasominhibition induziert und bindet dann direkt an das 26S-Proteasom, was auf eine mögliche Rolle von ZFAND2a als Rettungsfaktor für schlecht funktionierende 26S-Proteasome hinweist. Darüber hinaus erhöht das *C.elegans*-Homolog von ZFAND2a den proteasomalen Abbau von A β -Peptid und Polyglutamin-Protein, die bei der Alzheimer- bzw. Huntington-Krankheit vorkommen.

Hier untersuchten wir die funktionellen Eigenschaften des 26S-Proteasom-Komplexes in Anwesenheit von ZFAND2a unter Verwendung eines Modell-Kontrollsubstrats und eines toxischen Substrats mit Polyglutamin-Wiederholung. Ich konnte zeigen, dass die Bindung von ZFAND2a an das 26S-Proteasom unter *in vitro* Bedingungen weder den allgemeinen Proteinabbau verstärkt noch einen effizienten Abbau von Proteinen mit Polyglutamin-Wiederholungen ermöglicht. Die Strukturanalyse des an den 26S-Proteasom-Komplexe gebundenen ZFAND2a ergab, dass ZFAND2a an die 26S Untereinheiten Rpn1 und Rpn7 bindet und eine längliche Form aufweist. Die Beobachtung, dass sich der an ZFAND2a gebundene 26S-Proteasom-Komplex in einem Substrat-akzeptierenden Zustand befindet, lässt vermuten, dass die Bindung von ZFAND2a eine regulatorische Rolle spielt, die vor der Substratbindung liegt. Somit könnte die Rolle von ZFAND2a eher einen strukturellen als einen funktionellen Zweck haben, wie z. B. die Erhöhung der Stabilität oder die Rekrutierung zusätzlicher Faktoren, die für die Rettung erforderlich sind, um zu erfolgen.

1. Introduction

1.1. Ubiquitin-proteasome system

Inside all cells a myriad of proteins that perform biological functions need to be synthesized or removed from the cellular interior in a spatially and temporally controlled fashion. To ensure targeted protein degradation, the cells employ a very complex network of enzymes that work together comprising the ubiquitin-proteasome system (UPS) (Ciechanover and Brundin, 2003). UPS plays a role in the turnover of more than 80% of all the cellular proteins (Tanaka, 2009). Thus, this pathway is one of the key regulators of merely all cellular processes including transcription, cell division, DNA repair, antigen processing, signaling, metabolism, development, and cell death (Tanaka, 2009).

Targeted protein degradation by the UPS can be divided in two major events. The first event involves the attachment of the targeting signal onto a protein destined to be degraded. The second event is the delivery of the protein to the degradation machinery and its subsequent degradation. Hence, the enzymatic machinery of the UPS system includes the enzymes which catalyze the addition of the targeting signal followed by the action of the enzyme that proteolyzes the targeted proteins (Nandi et al., 2006).

For a targeting purpose, the highly conserved, 76-amino acid protein ubiquitin is conjugated via the formation of an isopeptide bond between the ubiquitin's carboxy-terminal glycine to the ϵ -amino group of a lysine residue in the target protein sequence (**Figure 1.1 A**) (Hershko and Ciechanover, 1998). However, the addition of a single ubiquitin moiety (termed monoubiquitination) is in most cases not sufficient for targeting the protein to the degradation machinery. Therefore, additional ubiquitin moieties are added to the already substrate-attached ubiquitin (termed polyubiquitination) using one of the seven internal lysine residues inside ubiquitin's sequence (Shabek et al., 2012). Polyubiquitination can result in either linear or branched polyubiquitin chains on a substrate protein (**Figure 1.1 B**). Consequently, polyubiquitin chains can be either homotypic where only one internal lysine residue is used to build the chain or they can be heterotypic where different internal lysine residues are used (Akutsu et al., 2016). Apart from its role in targeting proteins for degradation, ubiquitin modifications have also been implicated in many other regulatory processes such as signaling, modulation of localization, activities, and interactions (Husnjak and Dikic, 2012).

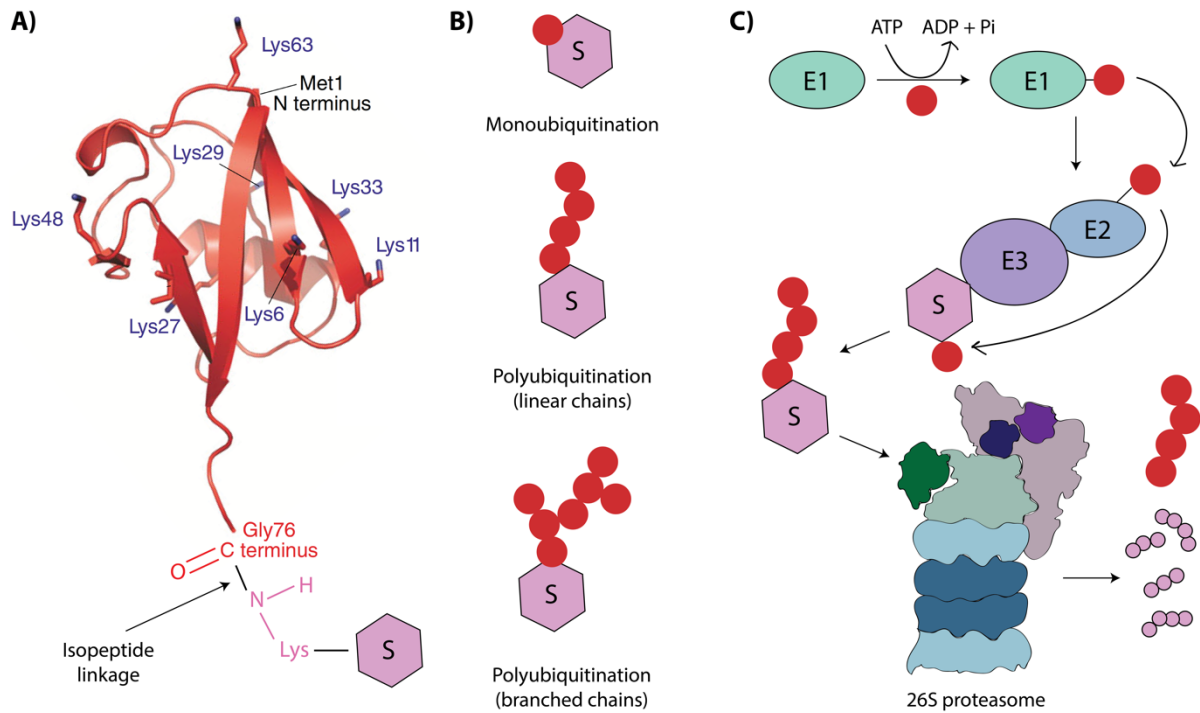


Figure 1.1. Components of the ubiquitin-proteasome system (UPS).

A) Ribbon diagram representation of ubiquitin molecule (PDB ID: 1UBQ). The N-terminal, C-terminal, internal lysine residues, and the isopeptide bond with a substrate's lysine residue are indicated. Taken and adapted from (Traub and Lukacs, 2007).

B) Schematic representation of monoubiquitinated (top) and polyubiquitinated substrate with either linear (middle) or branched (bottom) chain configuration. The ubiquitin moiety is represented with a red circle.

C) Schematic representation of ubiquitination machinery and substrate shuttling for degradation by the 26S proteasome. The depicted components of the UPS are ubiquitin-activating enzyme (E1), ubiquitin-conjugating enzyme (E2), ubiquitin ligase (E3), ubiquitin (red circle) and polyubiquitinated substrate (S). During ubiquitination reaction, adenosine triphosphate (ATP) is hydrolyzed, and adenosine diphosphate (ADP) and inorganic phosphate (Pi) are released.

The attachment of the first ubiquitin to the target protein and subsequent ubiquitin chain elongation is catalyzed by the ubiquitination cascade consisting of three different enzymes (**Figure 1.1 C**). The first enzyme, the ubiquitin-activating enzyme E1, activates ubiquitin in an ATP-dependent manner and attaches it covalently to its active site cysteine residue (Haas et al., 1982). The second enzyme, the ubiquitin-conjugating enzyme E2, binds the E1 and ubiquitin is being transferred onto an E2's active site cysteine residue. Then, E2 binds the third enzyme in the cascade, ubiquitin ligase E3, which in turn simultaneously binds the substrate

protein. E3 subsequently catalyzes the final transfer of ubiquitin from E2's active site onto a lysine residue in the target substrate protein (Hershko et al., 1983). The substrate specificity in UPS degradation is inferred through substrate identification and binding by E3 ubiquitin ligase (David et al., 2011). The substrate recognition by E3 ligases is often based on the presence of specific sequences. For example, destruction box motif in cyclin proteins; or large basic or hydrophobic amino-terminal residues in the substrate that confers higher instability (the so-called N-end rule pathway). Alternatively, misfolded proteins are recognized through exposed hydrophobic patches and interactions with chaperones. Posttranslational modifications such as oxidation or phosphorylation are also found to play a role in substrate targeting (Ravid and Hochstrasser, 2008).

In the cells, the proteins with attached polyubiquitin chains are directed for destruction via the ATP-dependent proteolytic machine called the 26S or 30S proteasome (Hershko et al., 1984). The proteasome degrades the substrate proteins to small polypeptides that are 3-22 amino acids long (**Figure 1.1 C**) (Kisselev et al., 1999). These oligopeptides are being released into the surrounding medium and further proteolyzed to individual amino acids by other cytosolic aminopeptidases and endopeptidases (Saric et al., 2004).

The indispensable role of the UPS in the regulation of cellular proteostasis places a heavy burden on the impeccable functioning of its components. Consequently, any perturbations in this system result in severe disturbances that can manifest from the cellular to the organismal level. The perturbations can originate from mutations of UPS's components or of substrate proteins; also, due to cellular conditions that prevent its normal function or overwhelm the capacity (Bedford et al., 2008). Indeed, malfunctioning UPS is brought forward as a major contributor to various human conditions and diseases including neurodegeneration, cancer, autoimmunity, and cardiomyopathies as discussed in the Section 1.4 (Lecker et al., 2006).

1.2. Proteasome complex

1.2.1. Diversity of proteasome complexes

The “proteasome” is a collective term that refers to a group of complexes whose main component is the 20S core particle (20S CP). The 20S CP can exist as an isolated entity in the cells acting as a standalone proteolytic machine or it can be found complexed with its regulatory particle or activators. A single 20S CP complex contains two activator binding sites,

and these sites seem to be independent of one another (Baumeister et al., 1998). Based on the type of 20S CP - mediated degradation when associated with different activators, two separate groups of activators have been defined as ubiquitin- and ATP-independent activators and ubiquitin- and ATP-dependent activators of the 20S CP (**Figure 1.2**) (Rechsteiner and Hill, 2005).

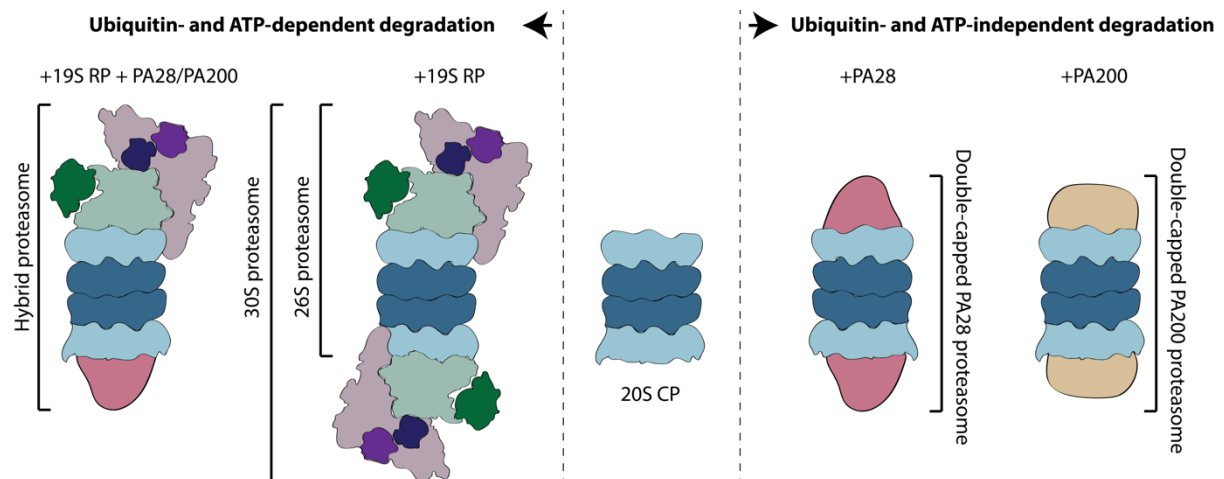


Figure 1.2. Diversity of proteasome complexes.

Single 20S CP can associate with one or two activator complexes of the same type (19S RP or PA28/PA200 complex) thus forming single-capped or double-capped complexes or it can bind two distinct activator complexes (19S RP and PA28 or PA200) thus forming the hybrid proteasome complex.

The proteasome activator family PA28 (also known as REG or 11S) and PA200 (Blm10 in yeast) belong to the ubiquitin- and ATP-independent activators of the 20S CP. In higher eukaryotes three different isoforms of PA28 regulators are expressed: PA28 α and PA28 β that form heteroheptameric PA28 $\alpha\beta$ complex and PA28 γ that forms homoheptameric complex (Stadtmueller and Hill, 2011). When bound to 20S CP, these activators do not mediate the degradation of standard polyubiquitinated UPS substrate proteins. However, their binding leads to an increase of peptidase activity of the 20S CP as measured by accelerated degradation of fluorogenic peptides *in vitro* (Rechsteiner and Hill, 2005). The 20S CP-PA28 and the 20S CP-PA200 complexes have been implicated in the degradation of oxidized and misfolded proteins and naturally unfolded intracellular proteins in an ubiquitin-independent manner (Mao et al., 2008; Pickering and Davies, 2012).

The 19S regulatory particle (19S RP) is the only known proteasome activator complex that belongs to the class of 20S CP activators that mediate ubiquitin- and ATP-dependent degradation of polyubiquitinated substrate proteins. The 20S CP capped by one 19S RP is termed the 26S proteasome complex, whereas the 30S proteasome complex consists of the 20S CP capped by two 19S RPs (Schmidt and Finley, 2014). So far, experimental results have not indicated any functional differences nor distinct roles between single-capped or double-capped 20S CP complexes (Sahu and Glickman, 2021a).

Almost all of the above-described types of active proteasome complexes can be found in the nucleus and in the cytoplasm. In addition, it was observed that one portion of the proteasomes displays association with plasma and ER membrane and with the elements of the cytoskeleton (Coux et al., 1996).

1.2.2. Structure of the 26S proteasome

The 26S proteasome architecture represents an intricate composition of 46 constitutive protein subunits of which 28 are found as part of the 20S CP and the remaining 18 subunits belong to the 19S RP. The structure of the 20S CP alone from several different organisms was extensively studied by X-ray crystallography (Groll et al., 1997; Löwe et al., 1995; Unno et al., 2002) long before the first complete 26S proteasome structure from yeast and humans were determined (Förster et al., 2013; Schweitzer et al., 2016). This delay in overall 26S proteasome structure determination was due to the inability to crystalize such a large and inherently flexible complex. Hence, another approach, named as single-particle cryo-electron microscopy (single-particle cryo-EM), was developed to allow the visualization and structure determination of bigger and more flexible entities (Bai et al., 2015).

1.2.2.1. Structure of the 20S core particle

Crystallographic, and later also cryo-EM studies showed that the subunits of the mammalian 20S CP complex arrange in a barrel-like structure consisting of four stacked heteroheptameric rings (**Figure 1.3 A**). The 20S CP subunits are termed to be either of the α -type (α_1 - α_7) or the β -type (β_1 - β_7), with the major structural difference between these subunits being the absence of the N-terminal H0-helix in the β -type subunits (Löwe et al., 1995). The outer two rings are composed of seven different α -type subunits and the inner two rings are

composed of seven different β -type subunits (Dahlmann, 2016). The molecular mass of individual 20S CP subunits ranges from 22 to 30 kDa and each subunit occupies a specific position inside its respective ring. Hence, the two outer α -rings and the two inner β -rings are identical in composition, thus the complex possesses C2 symmetry.

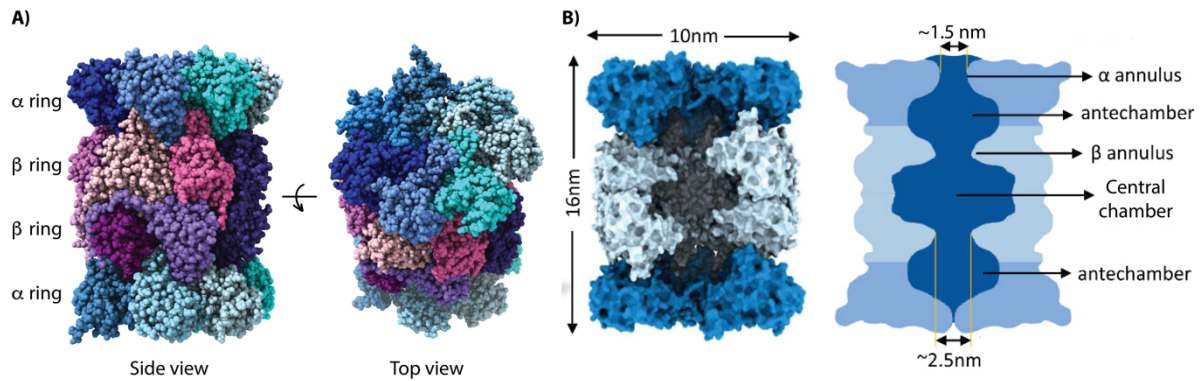


Figure 1.3. Structure and interior organization of the mammalian 20S core particle.

A) Side and top view of the 20S CP model in surface representation. Individual α and β subunits are shown in different shades of blue and purple colors, respectively (PDB ID: 7PG9).

B) Slice through the 20S CP interior organization. On the surface representation of sliced 20S CP, the length, and the diameter of the 20S CP complex are indicated. On the schematic illustration, individual compartments, and constrictions with their corresponding diameters are highlighted. Taken and adapted from (Sahu and Glickman, 2021b).

The approximate length of the 20S CP is 16 nm and the diameter is around 10 nm (**Figure 1.3 B**) (Unno et al., 2002). The inner cavity of the 20S CP is compartmentalized into three sub-cavities, two antechambers and one central chamber, separated by four narrow constrictions (**Figure 1.3 B**). The outer constrictions called α -annulus are positioned at either side of the 20S CP complex, slightly below the surface of outer α -rings, and are formed by loops in the α -subunits. The antechambers are defined by α -annulus and inner constriction formed at the α/β ring interface termed β -annulus. The central chamber is restricted from both sides by β -annulus and harbors the proteasome's proteolytic active sites (Stadtmueller and Hill, 2011).

1.2.2.2. Structure of the 19S regulatory particle

The 19S RP is organized in a rather complex shape and is biochemically divided into two independently assembling subcomplexes termed the “lid” and the “base” (Glickman et al., 1998). Single-particle cryo-EM studies of either isolated 19S RP lid or fully assembled 19S RP in the context of the 26S proteasome holocomplex have provided detailed structural insights into the structural arrangements among different subunits (**Figure 1.4**) (Förster et al., 2013; Schweitzer et al., 2016). In addition, X-ray crystallography analysis of individual subunits or particular subunit domains has allowed the building of a more detailed atomic model of the 20S CP-bound 19S RP (Förster et al., 2013).

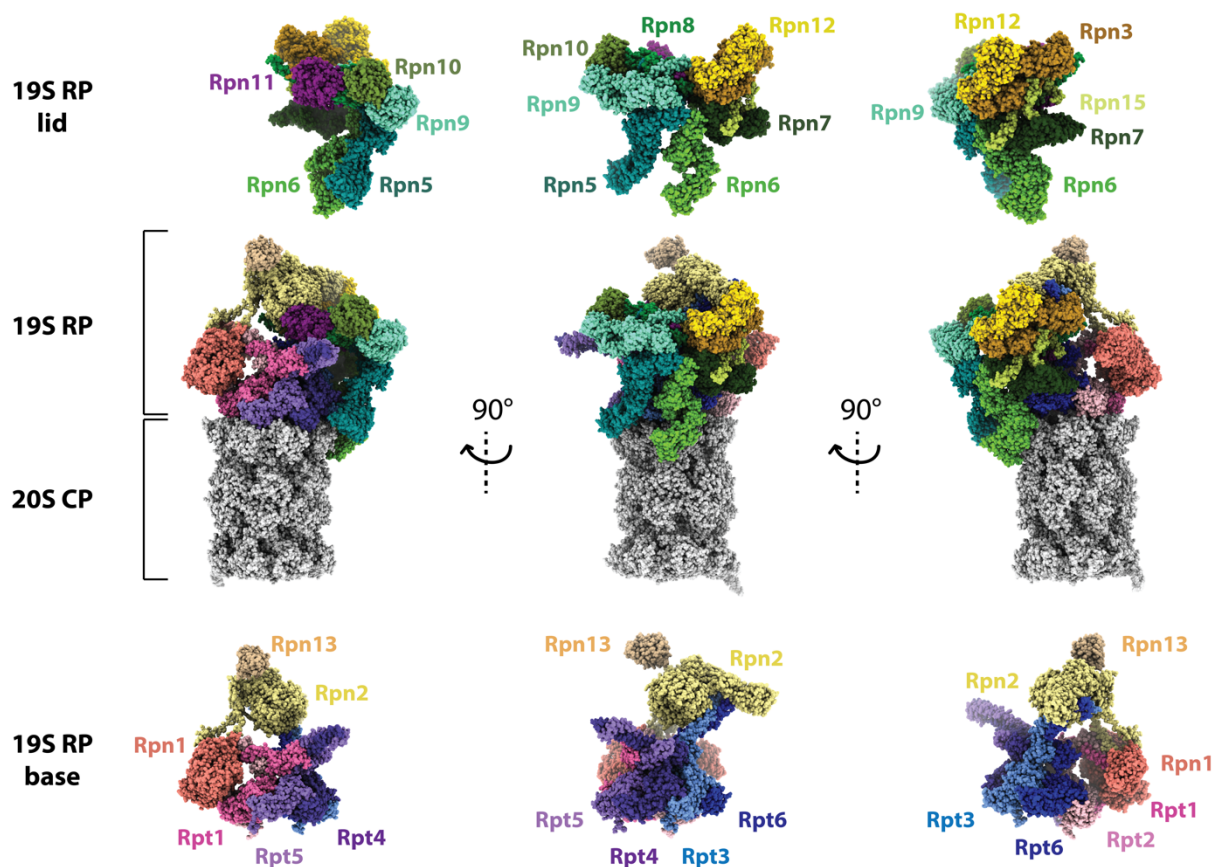


Figure 1.4. Structure and subunit composition of the 19S RP in the context of the 26S proteasome (PDB ID: 6FVT).

Surface representations of the 19S RP’s lid and base subcomplexes are shown as separated entities above and below the surface representation of the 19S RP bound to the 20S CP (colored in grey), respectively. Individual subunits of the 19S RP complex are colored differently and indicated with their corresponding color.

In the 20S CP-bound 19S RP, the base subcomplex establishes the majority of the contact surface between the two complexes by positioning its heterohexameric ring-like structure on top of the α -ring. The base ring is composed of six regulatory particle type AAA-protein (Rpt1 – Rpt6) subunits that are part of the family of ATPase-associated-with-different cellular activities (AAA+ ATPase family). All six Rpt subunits share the same domain composition (**Figure 1.5 A and B**). The N-terminus adopts a coiled-coil structure between pairs of neighboring Rpt subunits through which protein-protein interactions are established: Rpt1 binds to Rpt2, Rpt4 binds to Rpt5 and Rpt3 binds to Rpt6 (Ferrell et al., 2000). The N-terminal coiled-coil is followed by an oligonucleotide and oligosaccharide-binding domain (OB-fold) that forms an N-ring section. The N-ring section is considered to contribute to the structural stability of the Rpt ring. Below the N-ring, a section called AAA+ ring is formed by the stacking of a large and a small AAA+ subdomains of the neighboring Rpt subunits onto each other (Schweitzer et al., 2016).

In addition to the hexameric Rpt ring, the base subcomplex also includes three regulatory particle non-ATPase (Rpn) subunits, named Rpn1, Rpn2, and Rpn13. Rpn1 is positioned on the side of the Rpt ring in the region where Rpt1/2 dimer is located, whereas Rpn2 and Rpn13 are positioned in the apical region of the 19S RP (**Figure 1.4 and 1.5 C**). Rpn1 and Rpn2 share similar domain architecture consisting of an N-terminal rod-like domain, central domain built from 11 proteasome/cyclosome repeats, and C-terminal globular β -structure domain (**Figure 1.5 E**) (He et al., 2012). Rpn1 subunit serves as a ubiquitin receptor and a binding platform for proteasome interacting proteins (PIPs) for which two distinct binding sites in the Rpn1's C-terminal region have been identified. The polyubiquitinated substrates and ubiquitin-like - ubiquitin-associated (UBL-UBA) proteins bind the T1 site, whereas the UBL domain from Ubp6/USP14 proteasome associated deubiquitinating (DUB) enzyme binds the T2 site (**Figure 1.5 C**) (Boughton et al., 2021). Rpn1 subunit is one of the most flexibly connected subunits of the 19S RP complex; therefore, it is often resolved in a low-resolution cryo-EM reconstructions (Schweitzer et al., 2016). A high degree of Rpn1's positional flexibility is most likely required to accommodate and coordinate the binding of multiple associating factors and substrates. In addition, Rpn1 together with Rpn2 provides a functional connection between the Rpt ring and the lid subcomplex as a lid-binding scaffold (He et al., 2012). Finally, Rpn13 also serves as a ubiquitin receptor, and it binds polyubiquitinated substrates through its N-terminal pleckstrin-like receptor of ubiquitin (PRU) domain (**Figure 1.5 C and D**). The Rpn13's C-terminal region consists of a helical bundle that interacts with the DUB enzyme UCHL5/Uch37 (Jiang et al., 2018; Wang et al., 2017b). It is

important to note that in *Saccharomyces cerevisiae* Rpn13 is a constitutive 26S proteasome subunit, however, in mammalian cells it was found in sub-stoichiometric amounts (Schweitzer et al., 2016).

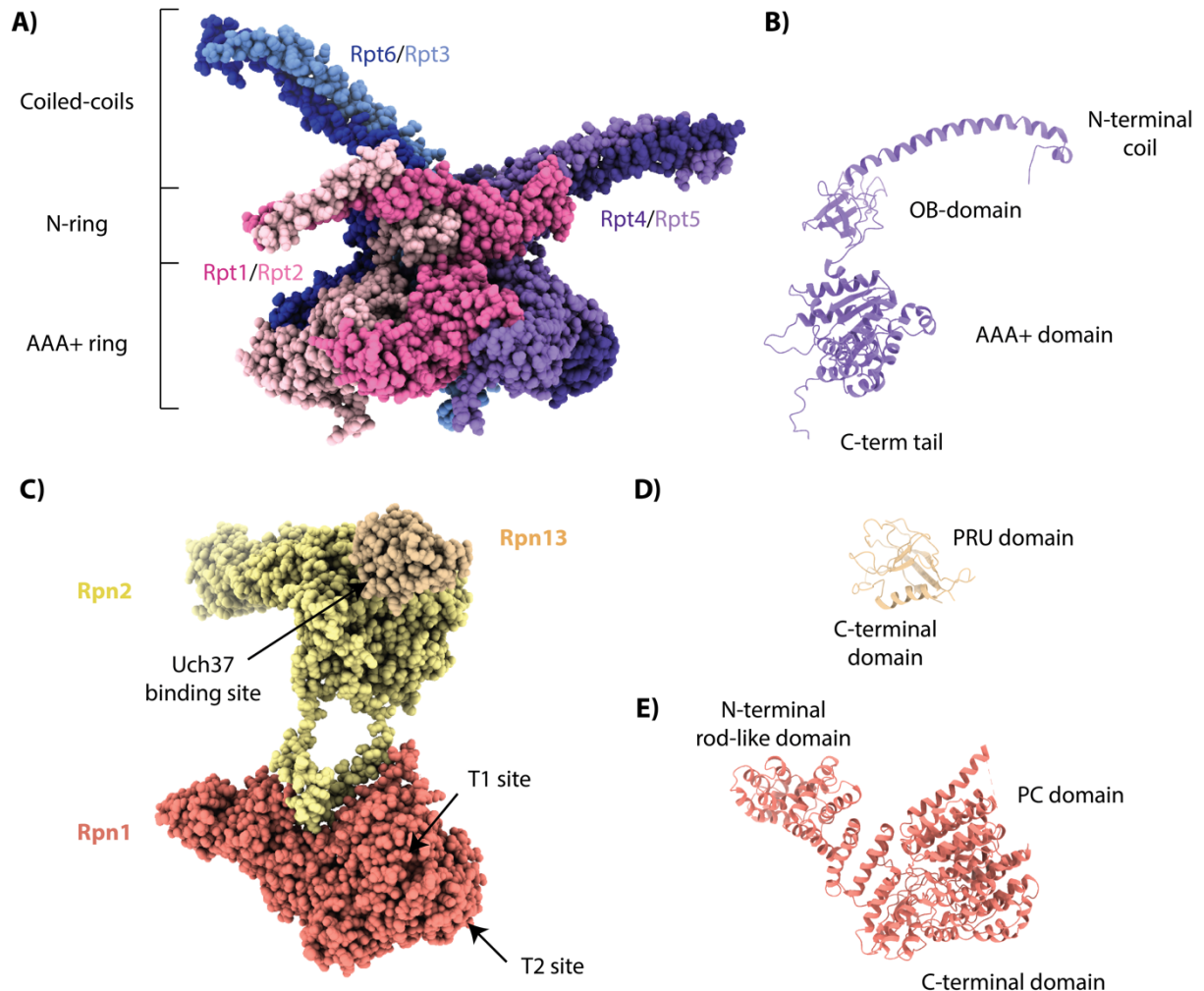


Figure 1.5. Close-up view of the 19S RP base subcomplex organization (PDB ID: 6FVT).

A) Architecture of the Rpt ring with indicated individual Rpt subunits and ring sections.

B) Ribbon diagram representation of a single Rpt subunit (Rpt5) with indicated domains.

C) Organization of the Rpn1, Rpn2 and Rpn13 19S RP base subunits. The T1 and T2 binding sites on the Rpn1 subunit and the Uch37 binding site on the Rpn13 subunit are indicated.

D) Ribbon diagram representation of Rpn13 subunit with indicated pleckstrin-like receptor of ubiquitin (PRU) and C-terminal domain.

E) Ribbon diagram representation of Rpn1 subunit with indicated N-terminal rod-like, proteasome/cyclosome (PC) and C-terminal domain.

The lid subcomplex of the 19S RP is described to have a horseshoe shape. It is composed of nine regulatory particle non-ATPase subunits (Rpn3, Rpn5-9, Rpn11, Rpn12, and Rpn15) (**Figure 1.4**). The Rpn subunits 3, 5, 6, 7, 9 and 12 share similar structural features consisting of a solenoid fold and a proteasome-CSN-eIF3 (PCI) domain which is considered to play a role in lid-scaffolding and inter-subunit contacts (Kish-Trier and Hill, 2013). Rpn11 and Rpn8 subunits contain an N-terminal Mpr-Pad1 (MPN) domain but only Rpn11 possesses enzymatic activity for substrate deubiquitination. Rpn15 subunit is a small acidic protein that, similarly to Rpn13, is found in sub-stoichiometric amounts in mammalian 26S proteasome samples. Rpn15 is assumed to function as a molecular glue between Rpn3 and Rpn7 subunits (Tomko and Hochstrasser, 2013).

One subunit of the 19S RP, Rpn10, is neither considered to be part of the base nor the lid. Rpn10 is the bridge between the lid and the base in a fully assembled 19S RP complex. At its C-terminus, Rpn10 contains ubiquitin-interacting motifs (UIMs) that serve as a primary binding site for polyubiquitin chains and for UBL domains present in the proteasomal substrates. On its N-terminus, Rpn10 contains a von Willebrand factor type A (VWA) domain responsible for the 19S RP stability maintenance (Bard et al., 2018; Wang et al., 2017b). Together with Rpn1 ubiquitin receptor, Rpn10 shows a high degree of conformational flexibility (Bard et al., 2018).

1.2.3. Function of the 26S proteasome

Numerous genetic, biochemical, and structural studies have focused on the 26S proteasome function (reviewed in Bard et al., 2018). The merge of all the discoveries led to today's current understanding of how the 26S proteasome carries out protein degradation of numerous regulatory and damaged or misfolded proteins. The structural features of both complexes, the 20S CP and the 19S RP, ensure that the protein degradation is tightly selective in order to perform timely and spatially accurate shaping of eukaryote proteome (Wolf and Hilt, 2004). The stages of the degradation cycle required for efficient destruction of proteins include recognition and binding of protein substrates marked by polyubiquitin chain on the 19S RP, substrate re-orientation and accommodation to enable engagement of substrate's initiation region, substrate unfolding and initial translocation through the central channel of the 19S RP, translocation-coupled deubiquitination and opening of the 20S CP gate, threading of unfolded

polypeptide inside the central chamber of 20S CP for degradation and finally releasing of generated peptides (**Figure 1.6**) (Coll-Martínez and Crosas, 2019).

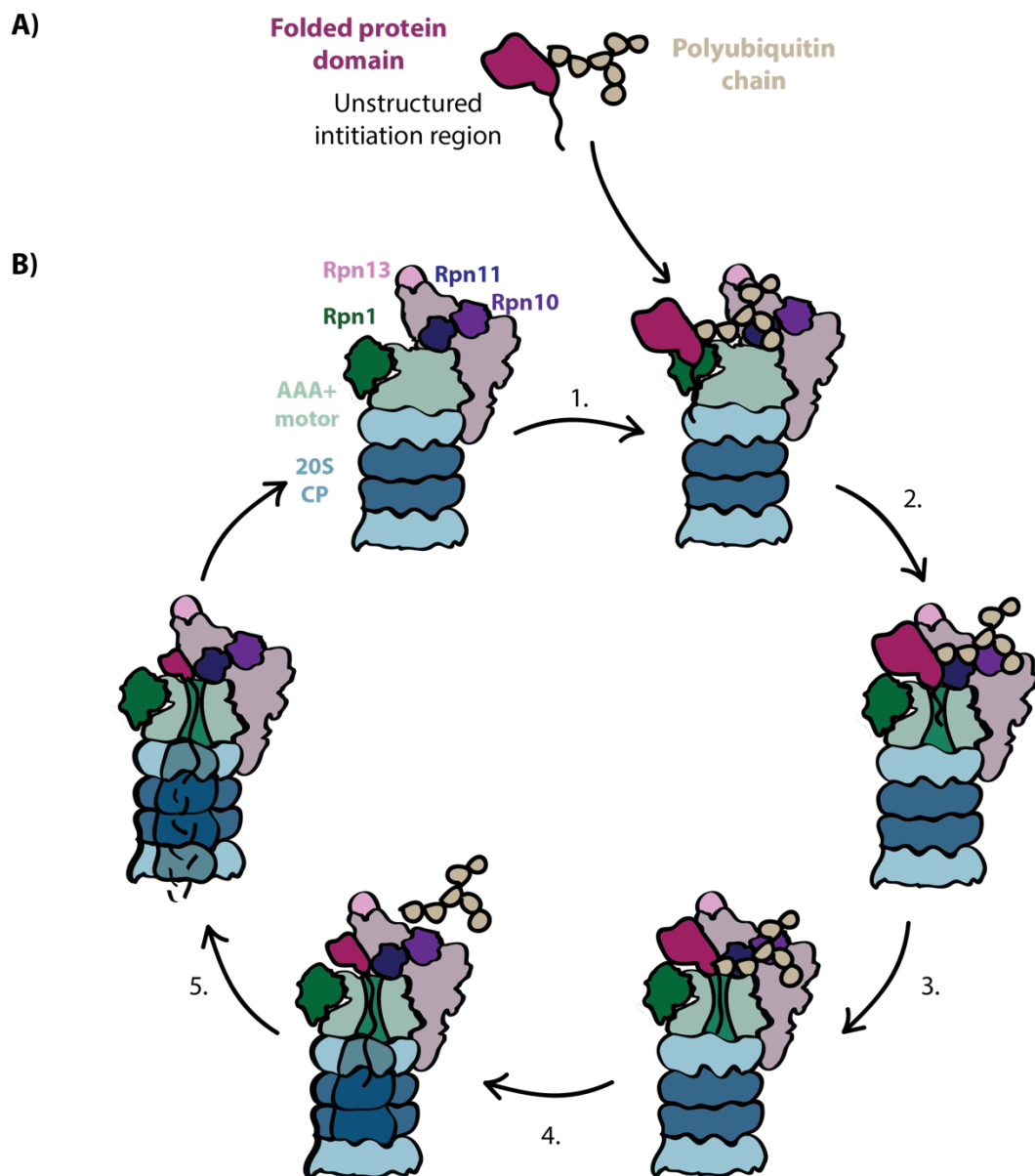


Figure 1.6. Degradation cycle of the 26S proteasome.

A) Schematic illustration of individual proteasome substrate elements required for efficient binding and engagement with the 26S proteasome.

B) Polyubiquitinated substrate with unstructured initiation region binds the 26S proteasome (1) through ubiquitin receptors Rpn1, Rpn10, and/or Rpn13. Substrate tail insertion into the ATPase motor and engagement (2) initiates substrate's translocation (3) inside the proteolytic chamber of the 20S CP. Gates of the 20S CP open (4) to allow substrate entrance and degradation (5). During translocation, the polyubiquitin chain is cleaved by DUB enzyme Rpn11 (4).

Cryo-EM studies of the 26S proteasome allowed concomitant analysis of complex dynamics alongside structural features, resulting in the classification of different proteasome conformational states. The observed states were brought to a most feasible sequence that would provide mechanistical description of the 26S proteasome degradation cycle. The current nomenclature assigns state's s1, s2, s3, and s4 or S_A, S_B, S_C, S_{D1-3} to yeast and human 26S proteasome, respectively (Chen et al., 2016; Ding et al., 2017). The different conformational states of the 26S proteasome have also been observed in cells using *in situ* cryo-EM approach (Guo et al., 2018). The most striking structural rearrangements throughout transition between all states are taking place in the 19S RP where the lid and the base change relative orientations to each other, while the 20S CP structure remains firmly static in most of its regions. The only observed rearrangement observed for the 20S CP is at the interface between the 19S RP and the 20S CP due to gate opening into the proteolytic chamber (Ding et al., 2017).

Kinetic analysis of individual steps during 26S proteasome degradation cycle revealed that the initial steps of substrate binding, tail insertion, and engagement of polypeptide chain happen very fast. In comparison, the subsequent steps of substrate's translocation-coupled deubiquitination, unfolding, and degradation are the most time consuming steps of the whole process (Bard et al., 2019). Consequently, the transition from S_A state which represents substrate accepting state to S_D state which represents substrate processing state through state's S_B and S_C is a rather rapid event when ideal model proteasome substrate is being processed.

1.2.3.1. Substrate binding and engagement with the 26S proteasome

The main targeting route to the 26S proteasome is via the polyubiquitin chain attached to the lysine residue of the substrate protein. The recognition of polyubiquitinated substrates is carried out directly at the 19S RP by the intrinsic ubiquitin receptor subunits. Alternatively, polyubiquitinated substrate recognition can occur through extrinsic shuttle ubiquitin receptors such as Rad23 or Dsk2 that subsequently deliver substrates to the 26S proteasome (Hartmann-Petersen et al., 2003). The intrinsic ubiquitin receptor sites are in the T1 site of Rpn1, UIM motifs of Rpn10, and in the PRU domain of Rpn13. The presence of several intrinsic ubiquitin receptors enables 19S RP to recognize and bind substrates marked with distinct ubiquitin chains assuming different configurations (Martinez-Fonts et al., 2020). Substrate recognition and binding through extrinsic ubiquitin receptors that only transiently bind the 19S RP provides

an additional layer of flexibility to select for and accommodate an even broader pool of substrates with varying geometries and ubiquitin chain configurations.

Though necessary, substrate binding is not sufficient to ensure efficient processing. In addition to the polyubiquitin chain targeting signal, tightly folded substrates require an unstructured initiation region necessary for substrate insertion and commitment to proteasomal processing (Prakash et al., 2004). The initiation region can either be in the form of a loose, 20-30 amino acid long unfolded terminus or in the form of an internal flexible loop. The relative positions of polyubiquitin chain and initiation region play an important role in the rate of proteasomal degradation (Inobe et al., 2011).

After the binding, the proper accommodation of a substrate results in the insertion of initiation region into the N-ring of the Rpt hexamer. The length of the initiation region plays a crucial role in bridging the gap between the constriction of the N-ring and the AAA+ ATPase region of the central channel. The polypeptide chain needs to reach the channel region formed by AAA+ domains, in order to get engaged with the proteasomal ATPases (Bard et al., 2018). The engagement is achieved through pore-1 and pore-2 loops that line the inner channel of the AAA+ ring (**Figure 1.7**). The direct contact for engagement is established through aromatic residues present in the characteristic aromatic-hydrophobic-glycine motif (Ar- Φ -G) of the pore-1 loops originating from the Rpt's large AAA+ subdomains (Schweitzer et al., 2016).

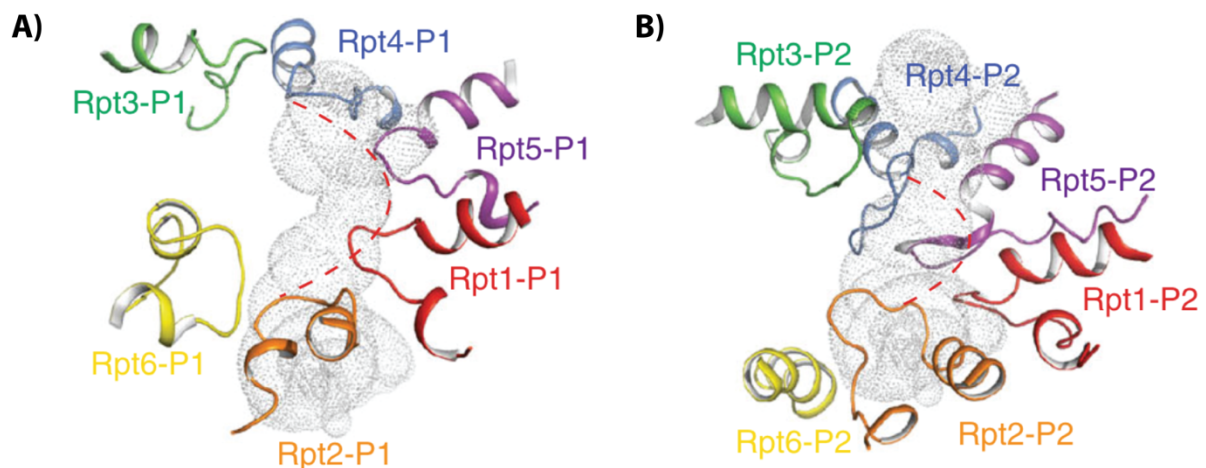


Figure 1.7. A) Pore-1 and B) pore-2 loop arrangement in substrate accepting state (S_A) of the 26S proteasome. The grey dots represent the solvent accessible surface of the AAA+ domain's inner channel. Taken and adapted from (Zhu et al., 2018).

Substrate recognition and binding followed by tail insertion and engagement are most likely taking place while the 26S proteasome is assuming the S_A state (**Figure 1.8**). This conclusion is based on the observation that in all other states except S_A , the Rpn11 subunit is positioned directly above the entrance into the Rpt ring channel which could interfere with and potentially restrict the insertion of the initiation region (Chen et al., 2016). Follow-up kinetic studies suggested that premature transition from S_A state to S_{B-D} states indeed prevented tail insertion and engagement to take place (Bard et al., 2019). Furthermore, cryo-EM analysis of 26S proteasomes with bound ATP purified without the addition of a substrate or additional factors resulted in cryo-EM reconstructions of the complex predominantly in S_A state. This observation further corroborated the notion that S_A represents the primary, substrate accepting as well as ground, resting conformation of the 26S proteasome (Unverdorben et al., 2014).

Upon substrate engagement, the 26S proteasome transitions between S_A to S_B state, where lid rotation of $\sim 30^\circ$ takes place (**Figure 1.8**) (Chen et al., 2016). This rotational movement results in a coaxially aligned position of Rpn11 with the central pore of the Rpt ring. The positioning of Rpn11 directly above the central channel sets the subunit arrangement necessary for the upcoming translocation coupled substrate deubiquitination (Worden et al., 2017). Concomitantly, Rpn10 is moved together with Rpn11 and establishes contact with the N-terminal coiled-coil region of Rpt4/5 dimer (Matyskiela et al., 2013). Upon transition from S_B to S_C state, the major conformational rearrangement is observed in Rpt subunits resulting in a wider and continuous central channel aligned with the pore of the 20S CP (**Figure 1.8**). Additionally, the interfaces between individual Rpt subunits become more uniform and a small AAA+ subdomain forms a rigid ATPase motor structure with a large AAA+ subdomain of a neighboring Rpt subunit (Wehmer et al., 2017). Upon continuous rounds of ATP binding and hydrolysis, the AAA+ domains change their relative arrangement. The movements of the ATPase motor structure are translated into substrate translocation movement through the pore loops contacting the polypeptide chain.

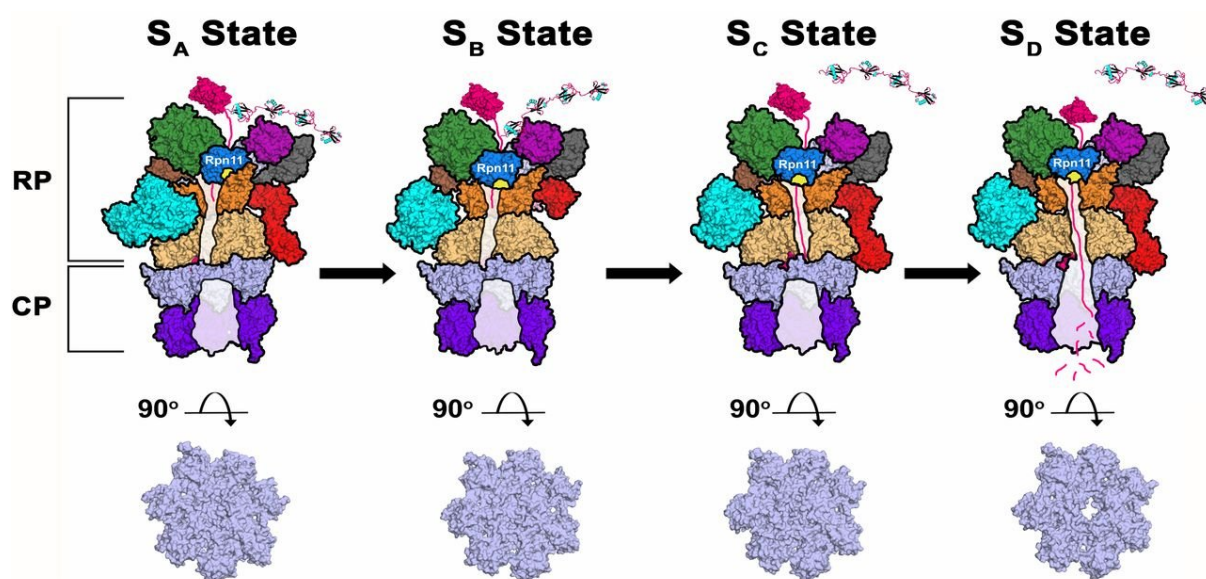


Figure 1.8. Conformational states of the 26S proteasome during substrate processing.

The conformational states of the 26S proteasome are termed S_A (ground or substrate-accepting state), S_B (substrate-binding state), S_C (substrate-engagement state) and S_D (substrate-processing state). At the bottom, the 20S CP gate in each conformational state is shown in surface representation. On the left side of the figure, the regulatory particle (RP) and the core particle (CP) are indicated. Taken from (Hochstrasser, 2016).

1.2.3.2. Substrate unfolding, translocation and deubiquitination

The translocation and unfolding of the polypeptide chain at certain point positions the isopeptide bond of the proximal ubiquitin in the active site of the intrinsic DUB enzyme Rpn11 (Figure 1.9 A and B) (Worden et al., 2017). In the absence of translocation mediated positioning of the substrate's ubiquitin, the Rpn11 active site is inhibited by the Insert-1 (Ins-1) loop that covers the groove into the catalytic center. This inhibition ensures that only committed substrates are getting deubiquitinated by Rpn11. The mechanical tension exerted on the substrate polypeptide chain through the interactions with the ATPase pore loops (Figure 1.9 C) and the interaction with proximal ubiquitin induces the conformational switch in Rpn11. This switch releases the Ins-1 loop inhibitory effect by forming an active β -hairpin structure and leads to hydrolysis of isopeptide bond and removal of polyubiquitin chain en bloc (Worden et al., 2017, 2014). It was observed that in the case of substrates with multiple polyubiquitin chains the overall degradation rate is unchanged in comparison to the same substrate with a single polyubiquitin chain (Bard et al., 2019). This suggests that Rpn11 activation by the first encountered polyubiquitin chain is maintained long enough until the second polyubiquitin

chain is positioned; thus, resulting in accelerated cleavage of all other subsequent polyubiquitin modifications on the substrate.

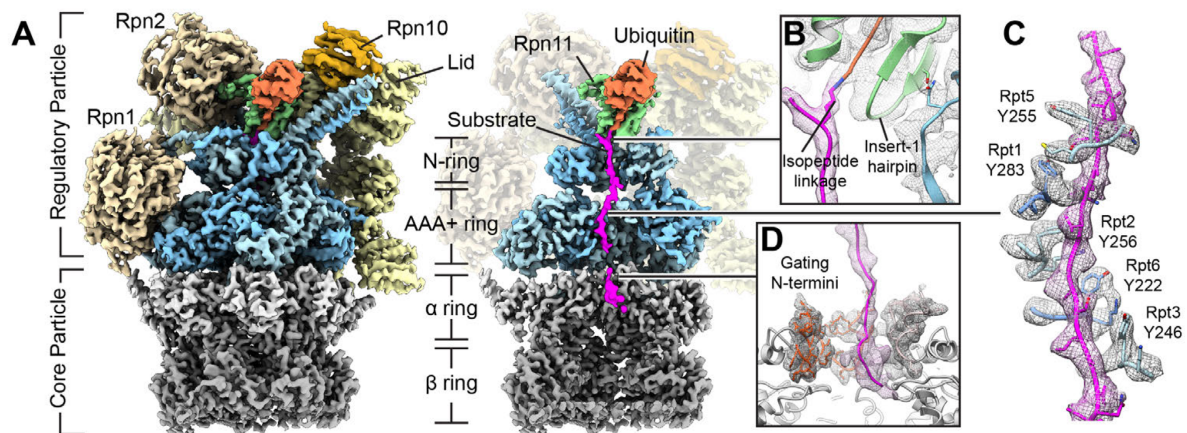


Figure 1.9. High-resolution cryo-EM structure of the 26S proteasome with engaged substrate stalled at the point of deubiquitination by Rpn11.

A) Complete (left) and cut-through (right) surface representation of substrate-engaged 26S proteasome. The substrate polypeptide chain (magenta) was stalled at the stage of Rpn11 (green) mediated deubiquitination (ubiquitin in orange) by the use of Rpn11 inhibitor capzimin. The substrate is visualized through the continuous channel formed by N-ring and ATPase motor (blue) and its entrance into the 20S CP (gray). **B)** Close-up view of the cryo-EM map and built-in atomic model of Rpn11's catalytic groove (green) with positioned isopeptide bond between the C-terminal glycine of ubiquitin and substrate's lysine (magenta). **C)** Resolved spiral staircase formed by pore-1 loops of the AAA+ domains that establish contacts with the substrate polypeptide chain. **D)** Close-up view of the cryo-EM map and built-in atomic model of the substrate polypeptide chain entering the 20S CP through the open gate. Taken from (Peña et al., 2018).

While the substrate is being unfolded through an axial channel of the 19S RP and translocated towards the central proteolytic chamber, the transition from S_C to S_D state results in an opening of the substrate entrance point into the 20S CP (Chen et al., 2016). The 20S CP without a bound activator, in addition to α -annulus constriction, contains one more seal on the entrance to the proteolytic chamber. This second restriction or the so-called 20S CP gate is formed by the N-termini of α -subunits which protrude in the direction of the ring's center (**Figure 1.10 A**) (Groll and Huber, 2003). The closed conformation of the 20S CP gate ensures on one hand that the access to proteolytic sites is tightly regulated to avoid undesired

degradation of cellular proteins and on the other hand to facilitate processive degradation of substrate proteins through restriction of the release of only partially digested peptides (Bajorek and Glickman, 2004). In the S_D state, the interactions of α -subunit's N-termini involved in closed gate conformation are destabilized and simultaneously new interactions are established that stabilize the 20S CP in open gate conformation to allow substrate translocation inside the proteolytic chamber (**Figure 1.9 D**) (Bajorek and Glickman, 2004).

The main trigger of the rearrangement of the N-termini is not only docking of the 19S RP onto the 20S CP, but rather a sequence of coordinated conformational changes initiated after substrate binding, engagement, and initial translocation are leading to the open gate conformation of the 20S CP. The open gate conformation is characterized by the insertion of the C terminal tails of Rpt1, Rpt2 and Rpt6 subunits into the $\alpha 4$ - $\alpha 5$, $\alpha 3$ - $\alpha 4$, and $\alpha 2$ - $\alpha 3$ pockets in addition to the previously inserted C terminal tails of Rpt3 and Rpt5 subunits into the $\alpha 1$ - $\alpha 2$ and $\alpha 5$ - $\alpha 6$ pockets, respectively (**Figure 1.10 B**) (Eisele et al., 2018). The C terminal tails of Rpt2, Rpt3, and Rpt5 subunits contain a hydrophobic-tyrosine-X (HbYX) motif, considered to be the critical element involved in gate opening. This was supported by the observation that the addition of peptides with HbYX motif alone induced 20S CP gate opening in solution (Rabl et al., 2008). In the S_D state, the 26S proteasome is actively translocating substrate from the N-ring and AAA+ domains all the way through the 20S CP gate into the proteolytic chamber for degradation. It is assumed that the coordination of substrate translocation between two physically separated regions, the initial binding site and the 20S CP gate, is carried out by Rpn1-Rpn2 asymmetrical solenoid structure (Rosenzweig and Glickman, 2008).

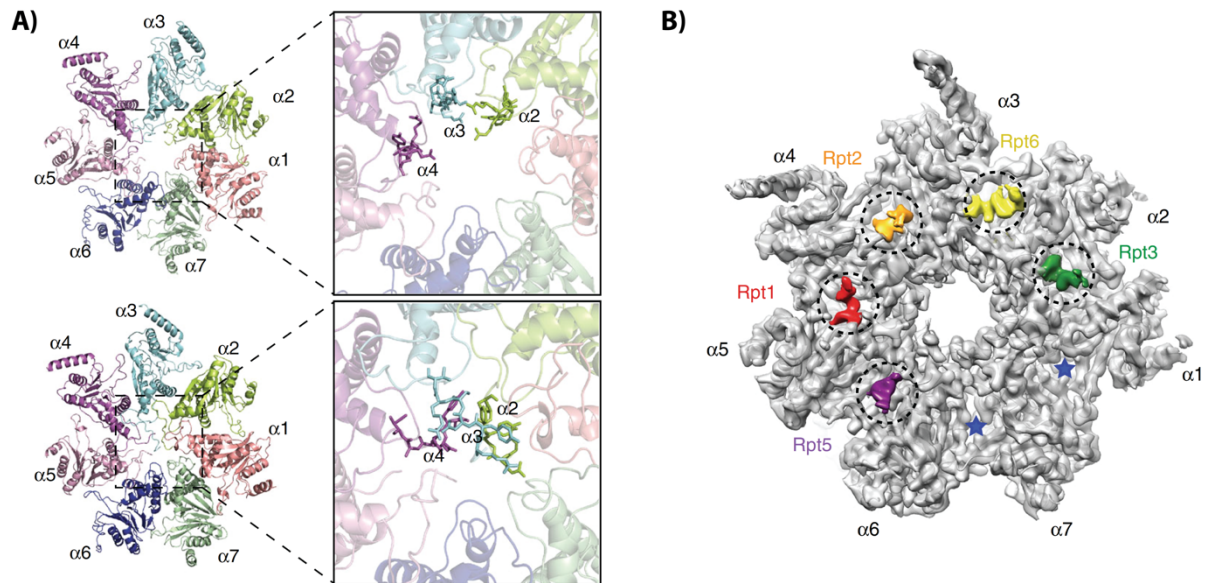


Figure 1.10. The 20S CP's gated channel towards the proteolytic chamber.

A) The atomic models of opened (upper panel) and closed (lower panel) 20S CP gates formed by N termini of α -subunits. The main closed-gate conformation forming subunits, $\alpha2$, $\alpha3$, and $\alpha4$, are indicated in close-up views in the right part of the figure. **B)** Cryo-EM map of α -ring in open-gate conformation with densities corresponding to inserted C-terminal tails of Rpt1, Rpt2, Rpt3, Rpt5, and Rpt6 subunits in their corresponding pockets in between α -subunits. Taken from (Zhu et al., 2018).

1.2.3.3. Substrate proteolysis

Once the substrate reaches the central chamber of the 20S CP where the proteolytic sites are, it is hydrolyzed to peptide fragments. The active sites in eukaryotic 20S CP reside in $\beta1$, $\beta2$, and $\beta5$ subunits of each of the β -rings, summing to a total of six proteolytic sites (Baumeister et al., 1998). The 20S CP catalytic β -subunits belong to the N-terminal nucleophile (Ntn) hydrolase family in which an N-terminal residue contains nucleophilic side chain. This side chain is exposed upon autocatalytic cleavage of an inactive β -subunit precursor during 20S CP assembly (Kunjappu and Hochstrasser, 2014). The active β -subunits contain N-terminal threonine (Thr1) whose side chain serves as an attacking nucleophile while the free N-terminal amine activates water molecule that is subsequently incorporated into the hydrolysis product (Stadtmueller and Hill, 2011). After each hydrolysis cycle, the Thr1 side chain is regenerated for another reaction, while the peptide fragment is released into the cytosol (Marques et al., 2009). The individual subunit cleavage specificities were determined in a

cleavage assay with fluorogenic substrates. β 1 subunit is associated with caspase-like/PGPH (peptidylglutamyl-peptide hydrolyzing) and the branched-chain amino acid-preferring (BrAAP) activity, hence it cleaves peptide bonds at the C-terminal side of acidic or branched-chain residues. β 2 subunit is associated with trypsin-like (TL) activity and cleaves peptide bonds at the C-terminal side of basic residues. Lastly, the β 5 subunit is mainly associated with chymotrypsin-like (ChTL) activity and cleaves peptide bonds at the C-terminal side of basic residues and it also contains BrAAP and small neutral amino acid-preferring (SNAAP) activity (Tanaka, 2009). Neighboring and catalytically inactive β -subunits make significant contributions in the selection of the cleavage sites.

In mammalian cells, active β -subunits can be encoded by three additional γ -interferon-inducible genes. These subunits termed β 1i/LMP2, β 2i/MECL-1, and β 5i/LMP7 can be incorporated into the 20S CP instead of constitutive active β subunits (β 1c, β 2c, and β 5c) and form a proteasome subtype termed immunoproteasome (Huber et al., 2012). The major functional difference between β c and β i containing 20S CP lies in their different cleavage specificities. The cleavage specificity of β i subunits favors the generation of peptides with desired sequence composition that can be used for antigen presentation (Cascio, 2014).

1.3. Regulation of the 26S proteasome

As the final executant of the UPS function, the 26S proteasome represents an entity at which the final decision about protein degradation is taking place. In accordance with the high significance of the 26S proteasome function, a sophisticated regulation network exists in each cell that ensures proper assembly, abundance, localization, and activity of the 26S proteasome in relation to cellular needs, development stage, and the existence of acute and chronic proteotoxic stress. The 26S proteasome regulation network includes various mechanisms acting on different levels such as transcriptional regulation, posttranslational modifications and binding of proteasome interacting proteins (PIPs) (reviewed in Marshall and Vierstra, 2019). PIPs bind the 26S proteasome in abundances that are lower than the canonical proteasomal subunits and play a direct regulatory role in decision making regarding which and at what rate are substrates being degraded. The most common PIPs co-purified with the 26S proteasome under normal conditions represent shuttle ubiquitin receptors, deubiquitination enzymes (DUBs), and E3 ubiquitin ligases.

Several shuttle ubiquitin receptors have been characterized in yeast (Rad23b, Dsk2, and Ddi1) and in humans (hHR23A, hHR23B, and ubiquilins). These proteins contain N-terminal Ubiquitin-Like (UBL) domain that mediates their association with the 26S proteasome mostly through Rpn1 subunit and C-terminal Ubiquitin-Associated (UBA) domain that interacts with polyubiquitin chains on substrate proteins (Livneh et al., 2016). The existence of additional ubiquitin receptors, apart from intrinsic ubiquitin receptors Rpn1, Rpn10, and Rpn13, could allow more tightly regulated substrate delivery, accommodation of a broader substrate repertoire, and more intricate substrate prioritization by the 26S proteasome as already briefly mentioned in Section 1.2.3.1. (Hartmann-Petersen et al., 2003).

In addition to the canonical DUB (metalloprotease Rpn11); two more DUBs bind the 19S RP, namely Ubiquitin-specific protease 14 (USP14, Ubp6 in yeast) and ubiquitin C-terminal hydrolase 37 (Uch37/UHL5, Uch2 in yeast) (Leggett et al., 2002). A smaller portion of 26S proteasomes can also be found in association with other DUBs (USP5, 7, 9x, 13, 15, 25, and 38), but the exact nature behind their contribution to substrate turnover is not yet known (Scanlon et al., 2009). While Rpn11 cleaves the ubiquitin chain at the base, thus performing *en bloc* substrate deubiquitination, USP14 and Uch37 preferentially remove ubiquitin moieties from the distal end of the ubiquitin chain. Uch37 releases monoubiquitin and USP14, in addition to monoubiquitin, releases di- and tri-ubiquitin (Livneh et al., 2016).

USP14 associates with the 26S proteasome by binding the T2 site of Rpn1 which in turn results in an increase of USP14 catalytic activity (Leggett et al., 2002). Deletion mutants of USP14 show several effects on protein and ubiquitin homeostasis such as enhancement of proteasome activity, sensitivity to stress, and ubiquitin depletion. These studies point towards USP14 role in ubiquitin recycling and regulation of substrate turnover by the 26S proteasome (Schmidt and Finley, 2014). USP14 primarily exerts its function on substrates that contain multiple polyubiquitin chains. Uch37 associates with the proteasome via Rpn13 subunit, and is positioned in close proximity to Rpn2 subunit of the 19S RP base (Hamazaki et al., 2006). Uch37 was primarily considered to release inadequately ubiquitinated proteins from the proteasome (Hamazaki et al., 2006). It was later also found that Uch37 has an ability to cleave K48-branched polyubiquitin chains and to enhance proteasomal degradation of substrates modified by branched chains (Deol et al., 2020). In addition, the role of Uch37 in the removal of regulatory ubiquitin modifications on the intrinsic 26S proteasome receptors has also been suggested (Bard et al., 2019). Ubiquitin chain cleavage by both, USP14 and Uch37 is assumed to take place prior to substrate commitment, contrary to Rpn11's deubiquitination, where it occurs after the substrate has been engaged. Thus, USP14 and Uch37 are considered to serve

as “timers” of substrate’s dwell time on the proteasome prior to engagement and are consequently thought to be the determinants for the likelihood of successful substrate degradation (Collins and Goldberg, 2017).

Deubiquitination activity of the 26S proteasome-associated DUBs is counteracted by the presence of E3 ubiquitin ligase enzymes that also bind the 19S RP. So far, several E3 enzymes have been identified as 26S interactors in mammalian cells – UBR4, Huwe1, UBE3A, UBE3C, and Rnfl81. The exact binding sites of the aforementioned E3 ligases are still not identified (Collins and Goldberg, 2017). 26S-bound E3 ligases are assumed to play a role in the remodeling of proteasome-bound ubiquitin chains. The remodeling is considered to either prolong substrate association with the 26S proteasome to ensure degradation (Xie and Varshavsky, 2002) and/or prevent the release of partially degraded substrates (Tai et al., 2010). Additionally, the 26S proteasome associated E3 ubiquitin ligases are also responsible for the addition of regulatory ubiquitin modifications on proteasomal subunits (Besche et al., 2014).

Apart from shuttle ubiquitin receptors, DUBs, and E3 ligases, the 26S proteasome can associate with many more regulators depending on the cell type, requirements, and conditions (Xie, 2010). The existence of multiple posttranslational modifications in addition to the transient binding of protein regulators reflects the complexity of the 26S proteasome function that is far beyond just simple protein degradation, but it clearly plays an important role in the final selectivity step of irreversible protein removal.

1.4. UPS impairment

The UPS consists of a large number of components that through their proper functioning maintain either directly or indirectly overall control of most cellular processes (Tanaka, 2009). Consequently, abrogation of proper function of any of the UPS aspects is almost instantly reflected as deterioration of cellular homeostasis. In a long run, UPS impairment can underlie the development of a wide range of human pathologies (Schwartz and Ciechanover, 1999). Many studies have been conducted and reviews compiled that give a broad insight into how dysregulation of UPS is involved in several cancers (Ding et al., 2014), genetic diseases (Paul, 2008), autoimmune and inflammatory disorders (Wang and Maldonado, 2006), muscular atrophy (Kitajima et al., 2020), cardiomyopathies (Powell et al., 2012) and neurodegenerative diseases (McKinnon and Tabrizi, 2014). The suggested mechanisms behind some of these diseases are based on faulty UPS substrates whose mutations or structural

characteristics lead to defects in recognition and/or processing by the components of the UPS. For others the cause may lie directly in the altered function of the UPS components or their regulation (Paul, 2008).

1.4.1. Malfunction of the 26S proteasome

A growing body of evidence points towards the fact that some of the mechanisms which underlie UPS-based pathologies are based on 26S proteasome malfunction. The 26S proteasome malfunction can occur upon the encounter with certain protein substrates or with some general protein features that the substrate contains. The encounters with such proteins do not only result in their own improper processing by the proteasome but can even cause general impairment of the 26S proteasome function by interfering with the degradation of other cellular proteins as well.

A general 26S impairment can be observed in the presence of persistent proteotoxic stress such as oxidative stress, heat shock, or arsenite intoxication (Grune et al., 2003; Reeg et al., 2020; Tillotson et al., 2017). These conditions lead to protein damage, by causing their misfolding. These damaged and misfolded proteins are subsequently polyubiquitinated and shuttled to the 26S proteasome for degradation (Brüning and Jückstock, 2015). It is not entirely clear whether the increase in misfolded protein species alone contributes to the observed decrease in the 26S proteasome function or perhaps also an inhibitory effect through interaction with misfolded proteins or a subset of them is directly causing 26S proteasome malfunction.

More specific events of 26S proteasome malfunction have been observed in the presence of specific viral proteins or native proteins that are mutated, contain aberrant posttranslational modifications, or have an altered oligomeric or conformational state. EBNA-1 and LANA-1 are viral proteins known to be able to avoid proteasomal degradation due to the existence of repetitive sequences, glycine-alanine repeats (GAR) and glutamine-glutamic acid-aspartic acid repeats (QEDr), respectively (Dantuma et al., 2000; Zaldumbide et al., 2007; Zhang and Coffino, 2004). These repeats are implicated in the interference with the normal translocation function of the 26S proteasome and thus with the disabling of processive unfolding and degradation (Hoyt et al., 2006; Levitskaya et al., 1997). Though the exact mechanism is not known, the resulting escape from proteasomal degradation renders these proteins invisible to the immune system since no antigenic peptides have been produced. As a

consequence, this allows prolonged viral infections that can lead to the development of malignant diseases (Ambagala et al., 2005).

The native proteins known to cause 26S proteasome malfunction are majorly connected to neurodegeneration phenotypes. These proteins are hallmarks of a large number of neurodegenerative disorders such as α -synuclein oligomers in Parkinson's disease, hyperphosphorylated tau and the A β peptide in Alzheimer's disease, the Sc conformational form of prion protein in prion disease, and huntingtin protein with expanded polyglutamine tract in Huntington's disease (Rao et al., 2015). Although the molecular mechanisms of the 26S proteasome functional impairment by these pathological proteins have been extensively investigated, they are not completely understood up today (reviewed in Deriziotis and Tabrizi, 2008; Lindersson et al., 2004; Oddo, 2008; Ortega and Lucas, 2014).

1.4.2. Polyglutamine disorders – the case of Huntington's disease

A group of neurodegenerative diseases collectively named polyglutamine (polyQ) repeat disorders are characterized by the presence of CAG trinucleotide expansion which encodes for the amino acid glutamine (Q) in disease-specific protein species (Michalik and Van Broeckhoven, 2004). There are in total nine polyQ disorders with the following proteins containing the polyQ expansion segments: huntingtin (HTT) in Huntington's disease (HD), androgen receptor (AR) in spinal and bulbar muscular atrophy (SBMA), atrophin-1 in dentatorubral and pallidoluysian atrophy (DRPLA) and ataxins-1,2,3,6 and 7 and TATA-binding proteins in several spinocerebellar ataxias (SCAs) (Michalik and Van Broeckhoven, 2004). PolyQ repeat of a certain length is a common appearance in some transcription factors and is assumed to mediate protein-protein interactions for the exertion of these protein's functions (Schipper-Krom et al., 2012). Likewise, proteins listed as causative factors of polyQ disorders themselves contain polyQ repeats. However, in healthy individuals this length never exceeds 35 glutamine residues, whereas individuals who develop polyglutamine-expansion pathologies contain a higher number (>35) of glutamine residues in these proteins (**Figure 1.11**). Moreover, a linear correlation was found between the number of CAG repeats and the degree of neurodegeneration in affected individuals (Penney Jr et al., 1997).

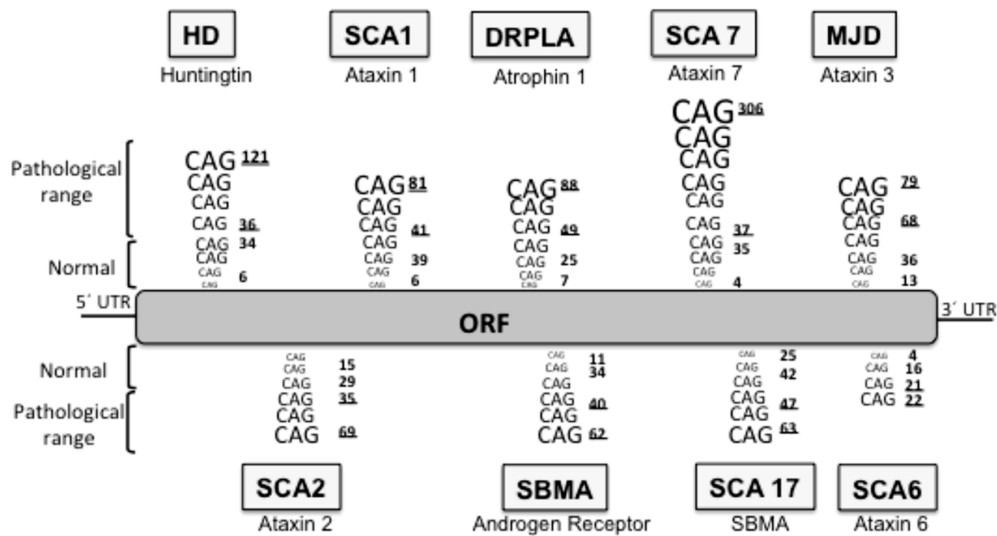


Figure 1.11. Overview of polyglutamine-expansion disorders with indicated pathological threshold length and position of a polyglutamine repeat in protein sequence for each of the individual causative protein species. HD – Huntington’s disease, SCA – spinocerebellar ataxia, DRPLA - dentatorubral and pallidolusian atrophy, MJD – Machado-Joseph disease, SBMA - spinal and bulbar muscular atrophy. Taken from (Ortega and Lucas, 2014).

One of the most extensively investigated polyglutamine-expansion disorder is Huntington’s disease (HD). Early symptoms of HD include mostly psychological perturbations such as concentration problems, memory lapses, depression, and mood swings with only minor motoric interferences like stumbling and clumsiness. In later stages, the motoric actions such as speaking, swallowing, breathing, and movement, in general, become increasingly jeopardized and accompanied by personality changes.

The polyQ expansion that causes HD is positioned within exon-1 of the Htt gene encoding protein huntingtin (HTT) (Gusella et al., 1993). Huntingtin, a ~350 kDa protein, is found ubiquitously expressed and it has been suggested to play a role in embryonal development, transcriptional regulation, axonal and vesicle transport, and as an antiapoptotic factor (Schipper-Krom et al., 2012). Once synthesized, full-length HTT was shown to get cleaved by caspases, calpains and endopeptidases resulting in an N-terminal fragment corresponding to a short sequence encoded by the exon-1 region of the gene. The N-terminal fragment is comprised of the N-terminal region of 17 residues (N17), followed by the polyQ tract and a 51 residue long proline-rich domain (PRD) (Harding and Tong, 2018). Wild-type huntingtin (HTT) as well as mutant huntingtin (mHTT) derived N-terminal fragments were

found to be targeted for degradation by the 26S proteasome through its ubiquitination by E2 enzyme UBE2W and a K48-specific E3 ligase UBE3A (Harding and Tong, 2018).

Despite being targeted for degradation by the proteasome, mHTT is in a time-dependent and polyQ length-dependent manner slowly accumulating in neuronal cells. Its accumulation results in the formation of intranuclear and cytoplasmic inclusion bodies (IB) through organized and hierarchical interactions among mHTT species (Ortega and Lucas, 2014). Monomers of mHTT N-terminal fragment associate into oligomers of globular structures that are 4-5 nm wide. Oligomeric species act as nucleation seeds that promote the formation of more complex structures through linear association thus giving rise to the formation of protofibrils with varying lengths. The individual protofibrils assemble into bigger structures called fibers through acquiring “polar zipper” conformations stabilized by cooperative hydrogen bonds between main-chain and side-chain amides. The preference for these interactions rises with the increasing length of the polyQ expansion (Li and Li, 1998). Ultimately, the fibrils assemble in unorganized assemblies called inclusion bodies (Arrasate and Finkbeiner, 2012).

The inefficient clearance of any of the above-mentioned species of mHTT N-terminal fragments pointed to the idea that the cell’s degradation pathways were faulty in dealing with the presence of such proteinaceous species becoming the main underlying cause of the pathology. Even though many studies aimed to investigate this connection, it is still undetermined whether the failure of the degradation pathway is a consequence of mHTT accumulation in cells or if the failure of degradation pathway is due to functional impairment leading to mHTT accumulation. Alternatively, the two scenarios might also be intertwined in a positive-feedback loop (Bence, 2001).

In addition to the UPS degradation pathway, whose main targets are short-lived proteins and damaged and misfolded monomeric proteins, the cells can employ another degradation pathway called autophagy. Through autophagy the cells get rid of long-lived proteins and larger structures such as damaged organelles and protein aggregates (Nedelsky et al., 2008). The involvement of both pathways has been implicated in HD pathology. The UPS is considered to be mainly responsible for removal of monomeric mHTT species both in cytoplasm and nucleus, and autophagy for removal of larger protein aggregates and IBs, but only in cytoplasmic area of the cell (Nedelsky et al., 2008).

1.4.3. 26S proteasome malfunction in Huntington's disease

The majority of conducted studies supports the view that mHTT accumulation is a consequence of direct UPS impairment and not the other way around. This hypothesis was tested by treating the 26S proteasome with proteasome inhibitor lactacystin, which led to a twofold increase of mHTT protein aggregates (Chai et al., 1999; Waelter et al., 2001). After this observation, most of the research focus has tried to untangle the question regarding which mHTT state: monomers, oligomers, or IBs, is the main culprit of 26S proteasome malfunction. However, the majority of this research is full of mutually contradictory findings, mainly attributed to the fact that they used different methods and different substrates to monitor the functionality of UPS in different systems or samples (Ortega and Lucas, 2014).

It was proposed that one of the obstacles in efficient mHTT, and in general removal of polyQ expansion containing proteins might arise from the inability of the 20S CP to cleave inside these long polyQ stretches. A study with *in vitro* purified 20S and 26S proteasomes postulated that the 20S CP catalytic sites are unable to bind polyQ expansions in their substrate recognition pockets and position them for hydrolysis (Venkatraman et al., 2004). Since these un-cleavable polyQ stretches would exceed the maximal length of proteasome peptide products, they were assumed to have difficulty exiting the 20S CP chamber. The inability to exit the chamber would lead to proteasome impairment by clogging the catalytic chamber. Alternatively, even if released, free un-cleaved polyQ peptides that are of disease-related length could still be toxic for the cell as they alone were shown to be able to promote aggregation and IB formation (Raspe et al., 2009). Furthermore, it was shown that allosteric alteration of 20S CP substrate binding pockets through association with PA28 γ activator, the eukaryotic 20S CP was able to cleave within shorter, 10 residues long, polyQ stretches (Pratt and Rechsteiner, 2008). Moreover, *in vitro* and *in vivo* assays with native polyubiquitinated N-terminal fragment of mHTT partially corroborated the hypothesis of 20S CP inability to digest polyQ repeats as only partially degraded fragments were detected as opposed to complete degradation (Holmberg et al., 2004).

In addition to impairment due to clogging, Holmberg et al. suggest that the impairment might originate from the need for polyQ expansion containing proteins to engage 26S proteasome longer in comparison to other substrates and thus indirectly compromise the overall substrate turnover by the 26S proteasome. Indeed, another study found that both HTT and mHTT were successfully degraded by the 26S proteasome, however, the rate of degradation was found to be inversely proportional to the polyQ extension length (Jana et al., 2001). A

similar observation was made for the degradation of SCA-1 causing polyQ expansion in ataxin-1 (Verhoef et al., 2002). Accordingly, when UPS function was measured through the production of the peptide products, a reduction in peptide levels was detected in cells expressing mHTT in comparison to cells that express HTT, pointing towards a decrease in the overall 26S proteasome degradation rate (Dasgupta et al., 2015).

In another study they did not observe drastic 26S proteasome impairment when using model proteasome substrate fused to pathological polyQ repeat (GFP-polyQ). However, they observed that the cell's ability to handle additional proteotoxic stress was significantly compromised (Ding et al., 2002). The discrepancy regarding 26S proteasome impairment seen with some, but not all polyQ containing substrates was later shown to also highly depend on the type and position of degradation signal used for protein targeting to the 26S proteasome (Juenemann et al., 2013; Michalik and Van Broeckhoven, 2004).

In conclusion, just the presence of polyQ expansion is not a key determinant of how efficiently a protein is degraded by the 26S proteasome and whether it leads to 26S proteasome malfunctioning. It is rather the totality of various aspects such as polyQ length and position inside the protein, targeting signal and overall cellular conditions that contribute to the extent of UPS impairment and 26S proteasome malfunction caused by monomeric species of polyQ expansion containing proteins. Moreover, UPS impairment by proteins containing polyQ expansions can vary depending on the protein's expression level, cellular localization, and cell-type (Bett et al., 2009). Nevertheless, more efficient handling of monomeric species through chaperone overexpression or removal through overexpression of E3 ligases that target them for degradation has already been shown to alleviate some of the hallmarks of HD (Cummings et al., 1998; Mishra et al., 2008; Nath and Lieberman, 2017; Rao et al., 2015). Likewise, activation of the proteasome or alleviation of its blockades when dealing with polyQ repeats in unfavorable contexts could be a promising direction in battling polyQ disorders (de Pril, 2004). Such approach was already indicated by the study in which overexpression of PA28 γ proteasome activator led to improvement in cell viability of striatal neurons that express mHTT and were exposed to pathological stressors (Seo et al., 2007).

Another possible or additional cause of 26S proteasome malfunction and consequently UPS impairment is the formation of IBs initiated by proteins with expanded polyQ repeats. This idea is based on the observation that the components of the 26S proteasome machinery are forming stable interactions with polyubiquitinated components of IBs but are resistant towards degradation (Verhoef et al., 2002; Waelter et al., 2001). Apart from containing different HTT and mHTT species (full-length mHTT, N-terminal fragment of mHTT and full-

length HTT), the IBs also entrap other cellular proteins that contain polyQ repeats in their native sequences like CREB and TATA box binding protein (Venkatraman et al., 2004). It was suggested that the constituents of IBs engaged with 26S proteasomes are getting kinetically trapped while being processed by the 26S proteasome and lead to depletion of free and active 26S proteasome species in cells (Holmberg et al., 2004). Although this theory proved to be true in the case of other types of protein aggregates like polyGlyAla aggregates, it did not seem to hold true for aggregates formed by proteins with expanded polyQ repeats (Guo et al., 2018). Several following studies showed that the 26S proteasome's engagement with polyQ IBs was dynamical and reversible (Holmberg et al., 2004; Schipper-Krom et al., 2014; Stenoien et al., 1999). Moreover, the 26S proteasome remained catalytically active and accessible to other cellular substrates since in the presence of IBs in the R6/2 mouse model of HD no accumulation of model proteasome substrate could be detected (Bett et al., 2009). However, when monitoring native UPS substrates in the same mouse model of HD another study did detect substrate accumulation (Maynard et al., 2009). The discrepancy among different studies was resolved when Ortega et al showed that UPS impairment indeed takes place but is transient and occurs only after acute expression of N-terminal fragment of mHTT. However, the UPS function is restored shortly after IB formation (Ortega et al., 2010). Surprisingly, these experiments attributed the protective role of IB formation towards UPS function as inhibition of IB formation in cellular and animal models prevented the observed restoration of UPS function (Ortega et al., 2010; Schipper-Krom et al., 2014). Despite their initial protective effect towards UPS function, the IBs, once large enough, can exert their toxic effect based solely on their size by disrupting membranes or acting as sequestration hubs for proteostasis components (Smith, 2018). Thus, it seems that similarly to the failure of UPS to handle the influx of monomeric polyQ expansion containing proteins, autophagy as the main pathway that can clear large protein aggregates fails to combat the formation and deleterious effects of IBs (Ciechanover and Kwon, 2015).

Apart from initially present monomeric species and IBs as a final product of monomer aggregation, a whole range of intermediate oligomeric species exist at the same time. These oligomers contain polyubiquitin tags and are also being shuttled to the 26S proteasome for degradation. Failure to process these oligomers results in their incorporation into IBs (Díaz-Hernández et al., 2006). Apart from resisting the degradation, polyubiquitinated oligomeric species purified from the R6/2 mouse model of HD had been shown to decrease 26S proteasome activity *in vitro* (Ortega et al., 2010). Similar effect was observed with oligomeric species of other proteins that cause neurodegeneration pathologies (Lindersson et al., 2004;

Smith, 2018). The observed decrease in 26S proteasome function is most likely a result of a competition between regular UPS substrates and oligomeric mHTT species. Although the oligomeric species are not affecting the proteasome activity itself, they interfere with the degradation rate of other substrates by occupying a certain portion of the 26S proteasomes in cells. In addition, low-oligomeric species of mHTT together with monomeric species are shown to be resistant against their clearance by autophagy, thus their removal would be strictly 26S proteasome-dependent (Harding and Tong, 2018).

Regardless of the individual effects exerted on the 26S proteasome's function, localization, and conformational state by different mHTT species, the therapeutic approach with the broadest implications in battling these deleterious effects should aim to increase 26S proteasome degradation capacity against monomeric species. This view is supported by the fact that the HD pathology is dependent on the constant influx of mHTT in cells (Waelter et al., 2001). Upon stopping of mHTT expression in HD inducible mouse model, the reversal of pathology was dependent on the 26S proteasome function as treatment with proteasome inhibitors abolishing recovery (Ortega and Lucas, 2014).

1.4.4. 26S proteasome as a therapeutic target

The 26S proteasome therapeutic value has increased dramatically in the last few years because of a decade's worth of research regarding its cellular levels and activities. It became evident that the 26S proteasome is not simply degrading targeted proteins but itself represents a final control checkpoint of protein degradation fine-tuned by a vast number of regulatory mechanisms. The adaptability of these mechanisms enables tolerance of adjustments in proteasome activity without globally impacting cellular regulation and survival (Schmidt and Finley, 2014). Targeting the 26S proteasome's function as means of disease treatment can include both, inhibition and activation of the 26S proteasome, depending on the nature of the disease.

Inhibition of the 26S proteasome has proven as a successful therapy in treating several types of cancers such as refractory multiple myeloma, non-small cell lung cancer, mantle cell lymphomas, and pancreatic cancer due to higher sensitivity for cancer cells compared to non-cancer cells to proteasome inhibition (Ding et al., 2014; Frankland-Searby and Bhaumik, 2012). Furthermore, since the 26S proteasome activity is the major source of antigen peptides, proteasome inhibition is a promising strategy in battling immune-related diseases like different

autoimmune disorders, graft-versus-host disease (GVHD), arthritis, colitis, systemic lupus erythematosus, myasthenia gravis, and allograft rejection (Verbrugge et al., 2015). Currently, three FDA-approved proteasome inhibitors are in clinical use. Bortezomib and ixazomib are reversible inhibitors and carfilzomib is an irreversible inhibitor of the proteasomes' chymotryptic activity (Kim, 2021).

In the field of neurodegeneration research, more emphasis is directed towards exploiting the UPS in removing misfolded pathological proteins to delay the disease onset or mitigate the symptoms (Myeku and Duff, 2018). One of the approaches would be to directly activate the 26S proteasome's function. This could be achieved using different mechanisms based on either gate opening to increase general substrate flux or allosteric regulation of the 26S proteasome which results in higher processivity by enhancing substrate binding and/or degradation. Several different approaches of 26S proteasome activation have been successfully applied in cellular and mouse models of neurodegenerative diseases. The 26S activation can be achieved using small-molecule modulators that can regulate posttranslational modifications on the proteasome subunits known to have activation effect. Alternatively, the activation can be achieved by using USP14 inhibitor that eliminates the effect of reduced substrate flux through the proteasome due to earlier substrate deubiquitination. In addition, genetic manipulation was tested in cellular models where overexpression of proteasomal subunits, activation of Nrf2, overexpression of proteasome activators or generation of open-gate mutants resulted in upregulated 26S proteasome activity producing similar protective effects. (Njomen and Tepe, 2019).

Though very encouraging, these therapeutic approaches also contain few caveats and unexplored avenues. In the case of the application of proteasome inhibitors in cancer treatment, it is already evident that certain cancer types can employ resistance mechanisms that are still not entirely understood (Kim, 2021). Furthermore, there is still a substantial lack of defined *in vitro* and *in vivo* selectivity and potency of small molecule modulators of 26S proteasome activity for their target proteins and an incomplete understanding of their mechanism of action. These factors can largely influence the physiological outcome of using proteasome activation as a therapeutic approach (Njomen and Tepe, 2019). Moreover, it is known that different pathological substrates with varying domain compositions and biophysical properties influence the rate of their degradation. Hence, the activation of 26S proteasome function by the same means can have a vastly different effects on eliminating various pathological targets from different neurodegenerative disorders. Better understanding of the regulatory mechanisms employed upon 26S proteasome malfunction would not only allow a much deeper

understanding of disease mechanisms but could also provide a better understanding and possibly broader application of 26S proteasome activation as a therapeutic approach in neurodegenerative diseases.

1.5. Regulation of 26S proteasome under malfunctioning conditions

1.5.1. Potential rescue mechanisms of malfunctioning 26S proteasomes

In addition to the homeostatic 26S proteasome regulation, the regulatory mechanisms employed under conditions that lead to impaired 26S proteasome function such as exposure to proteotoxic agents or encounter with individual toxic proteins discussed in Section 1.4.1 are of particular importance. Several potential modes involved in the rescue of the 26S proteasome's function, or its adaptation have been identified. However, the underlying mechanisms and their limitations are still poorly understood despite their possible application in disease treatment (Chondrogianni et al., 2015).

One of the adaptation mechanisms of the 26S proteasome function to increased substrate flux is a dynamic exchange and redistribution of proteasome activator complexes observed upon inhibition of proteasome activity (Shibatani et al., 2006). In particular, it was suggested that recruitment of PA28 activators to the 26S proteasome and formation of the so-called hybrid proteasome might serve as a cellular response to compromised proteasome function (Welk et al., 2016). In hybrid proteasome complexes, the PA28 activator is bound to the free end of 20S CP in the 26S proteasome complex. PA28 binding is thought to allosterically regulate catalytic activity and/or induce gate opening for more efficient product release when the 26S proteasome could get clogged (Kopp et al., 2001; Welk et al., 2016). Several other studies also implicate dynamic interchange of proteasome activators as a mechanism to counteract 26S proteasome impairment under harsh cellular conditions (Guo et al., 2018; Tsvetkov et al., 2015; Wang et al., 2017).

One of the proposed rescue factors of the 26S proteasome is the E3 ligase UBE3C, a 126 kDa protein that was shown to bind the 26S proteasome and assemble Lys29 and Lys48 linked polyubiquitin chains. UBE3C's activity, even under non-stress conditions, is crucial for the degradation of a particular set of proteins that are inherently challenging to degrade. This challenge can stem from protein's high folding energy, bulkiness or another biophysical characteristic that impedes proteasomal function. In the absence of UBE3C, the proteasomal

degradation of such stable proteins was only partial and yielded truncated degradation products (Aviram and Kornitzer, 2010). It was also observed that cells lacking UBE3C show decreased fitness in comparison to wild-type cells upon treatment with an inhibitor of molecular chaperone Hsp90. Such treatment causes an increase in proteasomal substrate load due to a higher rate of protein misfolding. These findings implicated UBE3C in the maintenance of 26S proteasome function to meet the degradation demands (Chu et al., 2013). Initially, it was hypothesized that either UBE3C ubiquitination activity is used for substrate retargeting to the proteasome in order for a substrate to get fully degraded or, alternatively, the constant addition of polyubiquitin chains on the substrate influences its overall stability and renders it more degradable (Carroll et al., 2021; Chu et al., 2013). Moreover, UBE3C was found to be extensively recruited to the functionally impaired 26S proteasome upon proteasome inhibition, heat stress or arsenite intoxication and it selectively modifies Rpn13 subunit of the 26S proteasome (Besche et al., 2014). Another study confirmed this finding and additionally assigned UBE3C a sensor role of acute protein unfolding in cells (Gottlieb et al., 2019). Taking it all together, Besche et al. suggested that UBE3C performs two distinct roles depending on whether it is bound to the 26S proteasome under normal or stress conditions. Under normal conditions, 26S-bound UBE3C promotes degradation by the proteasome. However, when bound to functionally impaired 26S proteasome, UBE3C catalyzes Rpn13 polyubiquitination to halt further substrate binding to the 26S proteasomes impaired by stalled substrates. This prevents engagement with multiple substrates, which might be even more toxic for the proteasome and ultimately for the cell (Besche et al., 2014).

Valosin-containing protein (VCP) or p97 (Cdc48 in yeast) is another component of the UPS implicated in the rescue of malfunctioning 26S proteasome. VCP subunits belong to the same family of AAA⁺ ATPases as Rpt subunits of the 19S RP and in a similar fashion form a hexameric ring. In a complex with its heterodimeric cofactor Ufd1/Npl4, VCP recruits polyubiquitinated substrates to extract them from membranes or molecular complexes to facilitate their subsequent degradation (Bodnar and Rapoport, 2017). Likewise, it was proposed that VCP can exert its segregation activity to pull out misfolded substrates stuck in the translocation channel of the 26S proteasome. VCP was also shown to act upstream of the proteasome and prepare stable substrates for degradation by exposing unstructured regions required for engagement with the ATPase motor of the 19S RP (Isakov and Stanhill, 2011; Olszewski et al., 2019). Whether VCP contribution in substrate processing by the 26S proteasome is a result of direct interaction or factor-mediated interaction or proximity-based

or combination of those is still not entirely understood due to discrepancies among different studies (Besche et al., 2009; Isakov and Stanhill, 2011; Olszewski et al., 2019).

Lastly, posttranslational modifications of some of the proteasome subunits have been shown to increase the degradation capacity of the 26S proteasome against misfolded disease-related proteins. The 19S RP subunit Rpn6 was found to be phosphorylated on serine residue at position 14 (Rpn6S14) by the cAMP-PKA pathway (VerPlank et al., 2020). The 26S proteasomes with phosphorylated or phosphomimetic Rpn6S14 have enhanced peptide and ATP hydrolysis rates, which results in an increased degradation of preexistent regulatory proteins and also of misfolded proteins that are the hallmarks of neurodegenerative diseases such as mutant tau, SOD1, and FUS (VerPlank et al., 2020). Apart from its effect on the activity of the 26S proteasome, Rpn6S14 phosphorylation also increases the abundance and stability of 26S proteasome complexes. Similarly, the Rpt6 subunit of the ATPase motor was found to be phosphorylated at a position S119 (Rpt6S119) in cells that were exposed to various proteotoxic conditions. The presence of phosphorylated or phosphomimetic Rpt6S119 in the 26S proteasomes mitigates the aggregate formation of mHTT103Q when compared to cells containing 26S proteasomes with Rpt6S119A mutation preventing phosphorylation at this residue (Marquez-Lona et al., 2017). These findings indicated that this modification might also play a role in relieving impaired 26S proteasome function (Marquez-Lona et al., 2017).

1.5.2. 26S proteasome regulation by ZFAND protein family

Among different eukaryotic organisms, a group of proteins possessing zinc finger domain of AN1 type (Zf-AN1) has been identified to interact with the 26S proteasome. Their role in the regulation of the 26S proteasome function under conditions where high protein turnover is required or in the presence of proteotoxic agents have been investigated by numerous studies (Glinka et al., 2013; Hassan et al., 2009; Lee et al., 2018; Sok et al., 2001; Turakhiya et al., 2018). In humans, four different Zf-AN1 domain (ZFAND) proteins that associate with the 26S proteasome have been identified, namely ZFAND5, ZFAND1 (Cuz1 in yeast), ZFAND2a and ZFAND2b (AIP-1 in *Caenorhabditis elegans*). All human ZFAND proteins, and their homologs in other organisms, contain at least one copy of the Zf-AN1 domain that is predominantly positioned at the N-terminus of the protein. Zf-AN1 domain contains six cysteine residues and two histidine residues that could coordinate two zinc atoms (Linnen et al., 1993). The C-terminal region of ZFAND proteins has diverged and can contain

different domains which attribute distinct regulatory functions to individual ZFAND proteins (**Figure 1.12**).

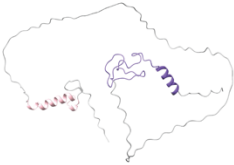
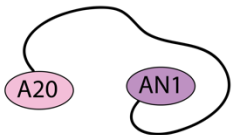
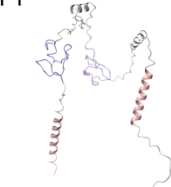
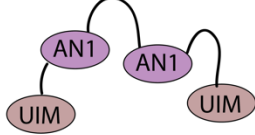
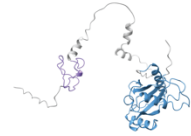
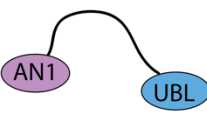
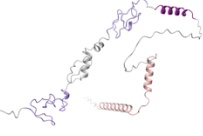
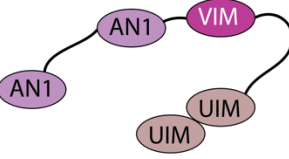
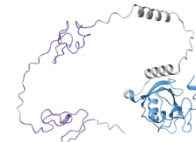
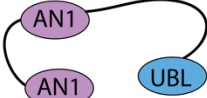
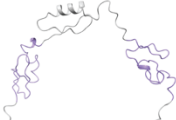

Predicted structure	Domain schematic	Predicted structure	Domain schematic
hZFAND5 		cAIP1 	
yCuz1 		hZFAND2b 	
hZFAND1 		hZFAND2a 	

Figure 1.12. AlphaFold structure prediction of ZFAND proteins and schematic representation of assigned domains. AN1 – zinc finger AN1 domain, A20 – zinc finger A20 domain, UBL – ubiquitin-like domain, UIM – ubiquitin- interacting motif, VIM – VCP-interacting motif, h – human, y - yeast, c – *Caenorhabditis elegans*.

The ZFAND5 protein is normally expressed in the eye, heart, and brain. It was also found to be induced in skeletal muscles undergoing atrophy caused by denervation or fasting. Consequently, mice with deleted ZFAND5 were resistant to muscle atrophy induced by denervation and showed increased accumulation of ubiquitinated proteins (Hishiya et al., 2006). ZFAND5 contains two zinc finger domains, N-terminal Zf-A20 and C-terminal Zf-AN1 domain connected by a very long flexible linker region (**Figure 1.12**). Zf-A20 domain is essential for binding to ubiquitin conjugates whereas full-length protein is required for ZFAND5 interaction with the 26S proteasome and observed functional changes. Upon binding, ZFAND5 enhances several different activities of the proteasome complex. Interaction through the Zf-AN1 domain stimulates all three peptidase activities. Moreover, interaction with the Zf-A20 domain elevates ATP hydrolysis and is essential for the increased protein degradation by the ZFAND5-bound 26S proteasome (Lee et al., 2018). Unlike other inducible ZFAND

proteins, ZFAND5 is not induced under proteotoxic conditions. Hence, it was suggested that ZFAND5 plays a role in the enhancement of overall protein turnover through direct interaction and activation of the 26S proteasome in cells with increased need of proteolysis, and not under conditions where toxic proteins accumulate.

Two parallel studies identified a protein in yeast that directly interacted with both components of the UPS, the 26S proteasome and Cdc48 (VCP in mammals). They named this protein Cuz1 (Cdc48-associated UBL/zinc finger protein-1) (Hanna et al., 2014; Sá-Moura et al., 2013). Though Cuz1 is not essential for growth under normal conditions and causes an only mild defect in UPS function when deleted, it was indispensable for cell survival upon treatment with certain proteotoxic agents, such as metalloids that induce protein misfolding (Hanna et al., 2014). Cuz1 contains an N-terminal Zf-AN1 domain, a short and disordered linker region, and a C-terminal ubiquitin-like (UBL) domain. The Zf-AN1 domain together with the linker region was shown to be sufficient for binding to the 26S proteasome and the UBL domain was shown to be required for binding to the Cdc48 (**Figure 1.12**) (Sá-Moura et al., 2013). Both studies suggested that Cuz1 plays a role in the removal of accumulated misfolded proteins under arsenite intoxication through its interaction with Cdc48 and the 26S proteasome. Whether this is achieved through substrate delivery by Cuz1 to either of the two complexes, by integrating the function of Cdc48 and 26S proteasome (by shuttling unfolded substrates from Cdc48 to the 26S proteasome) or by promoting substrate release from Cdc48 and/or 26S proteasome, is still undefined. The human homolog of Cuz1, called ZFAND1, contains one more additional Zf-AN1 domain when compared to Cuz1 (**Figure 1.12**) and it was also shown to interact with VCP and 26S proteasome upon arsenite intoxication (Turakhiya et al., 2018). ZFAND1 is essential for 26S and VCP recruitment to the stress granules to promote their efficient clearance during recovery from proteotoxic stress inferred by arsenite treatment. When ZFAND1 failed to bind and recruit either of the two complexes or was unable to interact with the stress granules; consequently, the formed stress granules persisted much longer. These granules contained additional protein load such as defective ribosomal products and could only be resolved by autophagy (Turakhiya et al., 2018). Interestingly, a nonsense mutation in ZFAND1 (ZFAND1-R130*) resulting in truncated ZFAND1 missing UBL domain was identified in ovarian, prostate, lung, and colorectal cancers. Truncated ZFAND1-R130* showed a similar defect in clearance of stress granules, providing an insight into the underlying mechanism of cancer development caused by ZFAND1 mutations (Lavalée et al., 2021; Turakhiya et al., 2018). As for Cuz1, the exact mechanisms employed by ZFAND1 to

coordinate and co-localize VCP and 26S proteasome functions to efficiently battle challenged UPS are still largely uninvestigated.

In *C. elegans*, protein termed AIP-1 (Arsenite Inducible Protein 1) was identified as an important factor in the regulation of proteasomal adaptation to proteotoxic stress and in the maintenance of animal life span (Yun et al., 2008). AIP-1 contains ubiquitin-interacting motif (UIM) at both of its termini connected via two Zf-AN1 domains (**Figure 1.12**). It is assumed, based on interaction studies with other Zf-AN1 proteins that AIP-1 interacts with the 26S proteasome through its Zf-AN1 domain, while UIMs bind polyubiquitinated substrates. AIP-1 is a constitutively expressed protein, albeit at lower levels under normal conditions and the expression is increased under proteotoxic conditions. Thus, AIP-1 is assumed to have a function similar to shuttle ubiquitin receptors Rad23b and Dsk2. AIP-1 most likely delivers substrates to the proteasome and by introducing more conformational flexibility in substrate accommodation, enables more efficient protein degradation (Yun et al., 2008). Indeed, AIP-1 overexpression enhances degradation of model proteasome substrate and the degradation of toxic and poorly degradable proteins such as A β ₄₂ peptide and polyQ fusion proteins, hallmarks of Alzheimer's and Huntington's disease, respectively. AIP-1's ability to increase general protein degradation attenuates and delays symptoms of neurodegeneration in *C. elegans* Alzheimer's disease model (Hassan et al., 2009).

In mammals, *aip-1* gene has diverged into two separate genes encoding an inducible ZFAND2a (also called AIRAP, Arsenite-Inducible RNA-Associated Protein) and a constitutively expressed ZFAND2b (also called AIRAPL, Arsenite-Inducible RNA-Associated Protein-Like) (Yun et al., 2008). ZFAND2a contains two Zf-AN1 domains connected with a flexible linker region and has lost additional binding modules, whereas ZFAND2b contains two Zf-AN1 domains at its N-terminus and two UIMs at its C-terminus (**Figure 1.12**). In addition, ZFAND2b contains a VCP-interacting motif (VIM) positioned in between Zf-AN1 and UIM motifs. Both, ZFAND2a and ZFAND2b have been implicated in the maintenance of folding capacity and regulation of protein degradation under proteotoxic conditions (Glinka et al., 2013; Rossi et al., 2010).

Interaction studies regarding ZFAND2b role in UPS have shown that ZFAND2b interacts with polyubiquitinated substrates through UIMs, with VCP N-terminal domains through VIM and it associates with the 26S proteasome upon proteotoxic conditions (Glinka et al., 2013; Rahighi et al., 2016; Yun et al., 2008). Such an interaction network highly resembles the one of ZFAND1. It is unknown if ZFAND1 and ZFAND2b bind the 26S proteasome simultaneous or mutually exclusive or whether they perform partially redundant or

completely individual roles. ZFAND1 function is implicated in later stages of proteotoxic response in removing stress granules and ZFAND2b seems to operate on a level of individual misfolded protein substrates. An observation that functionally impaired ZFAND2b leads to accelerated aging and protein aggregation was important for the discovery of a more constitutive role of ZFAND2b in the delivery of misfolded proteins that failed to get translocated into the ER to VCP and subsequently promoting their removal by the 26S proteasome (Braunstein et al., 2015).

Of all the ZFAND proteins, ZFAND2a's role is the most uncharacterized and hardest to speculate because it only contains two Zf-AN1 domains that mediate 26S proteasome binding and none of the other functional domains. Zfand2a gene is a canonical heat shock gene under the control of the HSF-1 transcription factor (Rossi et al., 2010). Apart from its expression upon heat shock, ZFAND2a is induced upon treating the cells with proteotoxic agents such as arsenite or proteasome inhibitors (Rossi et al., 2014; Scomazzon et al., 2019; Stanhill et al., 2006). In multiple myeloma cancer cells, ZFAND2a downregulation sensitizes cells to bortezomib-induced cell death, whereas ZFAND2a overexpression contributes to cell resistance towards the drug (Scomazzon et al., 2019). In mouse fibroblasts transiently treated with arsenite, polyubiquitinated substrates accumulate until the point of ZFAND2a induction after which their levels are maintained constant and upon recovery, they decline. In contrast to wild-type cells, ZFAND2a knockout cells accumulated much more polyubiquitinated substrates and required more time to recover after arsenite removal. The observed phenotype in ZFAND2a knockout cells was reversed when ectopic expression of ZFAND2a was introduced (Stanhill et al., 2006). These observations support ZFAND2a's direct role in regulating the removal of misfolded and toxic proteins by the 26S proteasome. The same study also found that the majority of expressed ZFAND2a was in a complex with the 26S proteasome, mapping the interaction to the Rpn1 subunit of the 19S RP. However, only a minority of proteasomes purified from arsenite treated cells contained ZFAND2a indicating that the interaction is most likely transient and the levels of ZFAND2a are tightly regulated in response to the extent of proteotoxic insult (Stanhill et al., 2006). Since proteasomes purified from arsenite treated ZFAND2a knockout mouse fibroblasts were found to be associated with more and not less polyubiquitinated substrates, the authors argued against ZFAND2a's role in substrate delivery. Recently published work suggested a rather specific role for ZFAND2a in rescuing arsenite-inhibited Rpn11 through zinc atom donation and exchange for Rpn11-bound arsenite since Rpn11 DUB requires Zn^{2+} for its activity (Suknik et al., 2021).

In summary, findings point towards ZFAND2a's role in the regulation of proteasome function under proteotoxic conditions (arsenite intoxication, heat stress) or direct proteasome impairment (proteasome inhibition). However, there is neither clear evidence regarding which functional aspect (substrate recruitment, accommodation, unfolding and/or degradation) does this regulation addresses nor how is this regulation achieved mechanistically. It is thus necessary to envision a broad range of plausible regulatory roles that ZFAND2a might perform upon its binding to 26S proteasome based on current knowledge and a general understanding of the 26S proteasome structure, function, and regulation (**Figure 1.13**).

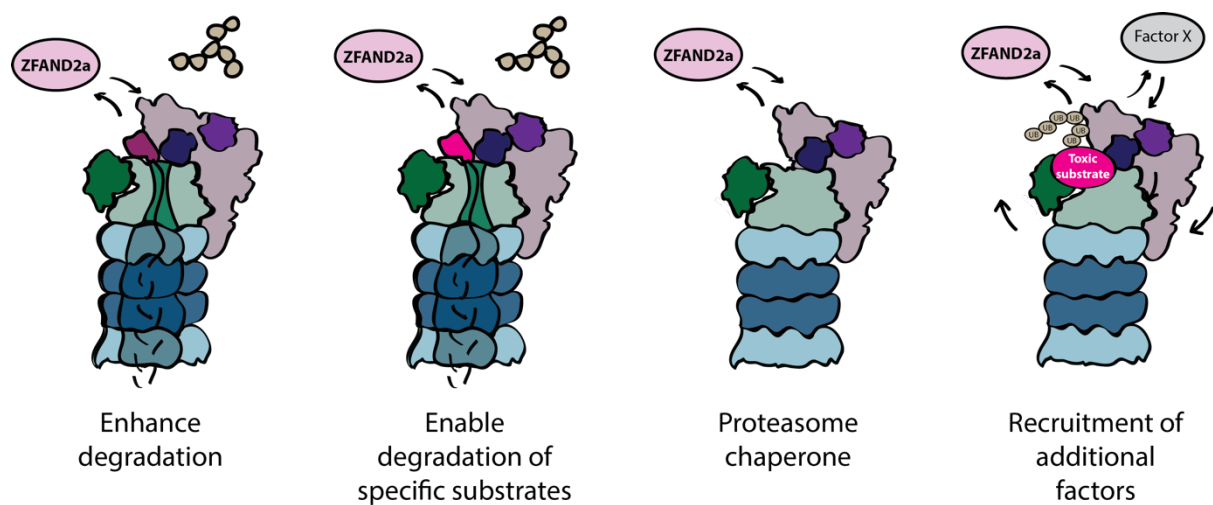


Figure 1.13 Hypothesized roles of ZFAND2a in rescuing malfunctioning 26S proteasomes.

ZFAND2a induced expression and binding to the malfunctioning 26S proteasome could either play an active role in the regulation of the degradation of toxic proteins (by enhancing overall protein turnover or enabling degradation of specific toxic substrates) or its binding would have a more structure-based role (by maintaining complex stability under harsh conditions or recruiting other PIPs).

The 19S RP oversees the rate-limiting steps during substrate degradation and is also a platform to which many regulatory proteins bind to ensure selective degradation. Thus, ZFAND2a binding through Rpn1 subunit might serve a functional role and ensure more rapid degradation of proteins overall or allow processing of specific, hard-to-degrade substrates whose accumulation in cells is otherwise toxic. This could be achieved by introducing preferential conformational states of the proteasome such as stabilizing substrate processing states or open-gate state that ensures more rapid or efficient processing. This idea is supported by the observation that when the proteasome degrades a substrate that contains a more stable

domain that causes slippage of ATPase motor, the proteasome revisits S_A state more frequently. The revisiting of S_A state might cause a delay or even a complete termination of degradation and result in release of partial and toxic intermediate degradation products (Jonsson et al., 2021). If the revisiting of S_A state would be prevented or at least decreased in frequency, such-hard-to degrade substrates might have higher chance of getting completely degraded. Alternatively, ZFAND2a binding could play a more passive, structural role such as chaperoning and providing stability and integrity to the 26S proteasome complex under harsh conditions since the equilibrium of different proteasome complexes seems to play an important role in battling proteotoxicity (Guo et al., 2018). Furthermore, it could be a combination of the functional and structural role in a way that ZFAND2a binding prefers a certain conformational state of the 19S RP which is more likely to recruit other regulatory proteins such as E3 ligases. It could also be the other way around and ZFAND2a binding could disable binding or lead to dissociation of already bound regulatory proteins such as DUBs. This type of selectivity towards a certain profile of bound regulatory proteins on the 19S RP could eventually result in more efficient degradation of all or specific substrate proteins.

While scarce functional information on the ZFAND2a-bound 26S proteasome complex exists, the structural data is completely missing. Due to the implication of *C. elegans* ZFAND2a homolog AIP-1 in providing greater ability to handle toxic proteins related to neurodegenerative disorders, the elucidation of all aspects of ZFAND2a regulatory role in adapting 26S proteasome function would potentially provide new avenues in applications that use the 26S proteasome as a therapeutic target.

2. Aims of the study

The main aim of this study was to characterize the regulation of the human 26S proteasome by Zinc-finger AN1-domain 2a (ZFAND2a) protein. Published work has shown that ZFAND2a directly binds the 26S proteasome under proteotoxic conditions, whereas ZFAND2a homolog in *C.elegans* AIP-1 enabled more efficient removal of toxic, disease-related proteins such as A β peptide and polyQ-containing proteins and delayed disease onset. Based on the previous findings, I set out to investigate the possibility of ZFAND2a's rescue role in adapting the 26S proteasome function when encountered with toxic substrates that impair its function thus jeopardizing or preventing their own and degradation of other cellular proteins.

To reach this aim, I set the goals to determine both functional and structural characteristics of the 26S proteasome complex in the presence of ZFAND2a. With the functional investigation, I aimed to test whether ZFAND2a binding to the 26S proteasome would increase overall protein degradation using *in vitro* degradation assay with non-toxic control substrate lacking the impairment element. Moreover, I aimed to test if ZFAND2a binding can enable the 26S proteasome to completely degrade toxic substrate proteins that contain impairment element. The impairment element used in this study contained long polyQ stretch found in proteins whose accumulation and inefficient removal causes several neurodegenerative disorders. By using the polyQ as an impairment element, the results obtained in this study could provide a potential therapeutic benefit; besides, contributing to a general advancement in the understanding of 26S proteasome regulation mechanisms.

There is no available structural information on the ZFAND2a-bound 26S proteasome complex. Hence, I set out to structurally characterize the ZFAND2a-bound 26S proteasome complex in the presence of a toxic substrate. I aimed to determine ZFAND2a binding site on the 26S proteasome and its effect on the 26S conformational state. Due to the large size and high flexibility of the complex, I decided to use single-particle cryo-EM approach for structure determination. This analysis would allow me to gain insights into the underlying molecular mechanisms of potential ZFAND2a rescue role when the 26S proteasome encounters a toxic substrate. Alternatively, it could provide information about any other potential roles behind ZFAND2a binding to the 26S proteasome apart from direct influence on substrate processing.

3. Materials and Methods

3.1. Materials

3.1.1. Standard chemicals

Adenosine 5'-triphosphate disodium salt (ATP) (*Roth*), agar (*Sigma Aldrich*), bis(2-hydroxyethyl)aminotris(hydroxymethyl)methane (BisTris) (*Sigma Aldrich*), bovine serum albumin (BSA) (*Sigma Aldrich*), dithiothreitol (DTT) (*Sigma Aldrich*), D-Maltose monohydrate (*Research Products International*), ethanol (*VWR Chemicals*), glycerol (*Sigma Aldrich*), kanamycin (Km) (*Sigma Aldrich*), L-glutathione reduced (GSH) (*Roth*), magnesium chloride (*Sigma Aldrich*), magnesium sulfate (*Sigma Aldrich*), phenylmethylsulfonyl fluoride (*PMSF*), polyethylene glycol (PEG) (*Sigma Aldrich*), potassium chloride (*Sigma Aldrich*), sodium chloride (*Sigma Aldrich*), sodium dodecyl sulfate (SDS) (*Sigma Aldrich*), Sterile MonoQ (*Molecular biology service, IMP*), sucrose (*Sigma Aldrich*), tris-(hydroxymethyl)-amino-methane (Tris) (*Sigma Aldrich*), Tween 20 (*Sigma Aldrich*).

3.1.2. Stains and reagents

Bromophenol blue (*Sigma Aldrich*), SafeBlue (*Molecular Biology Service, IMP*), Protein Assay Dye Reagent Concentrate 5x (*Bio-Rad*), SYBR™ Safe DNA Gel Stain (*Invitrogen*).

3.1.3. Standards, commercial kits, and enzymes

PageRuler prestained protein ladder 180 kDa (*Thermo Scientific*), PageRuler unstained protein ladder 200 kDa (*Thermo Scientific*), Precision plus protein standards 250 kDa (*Bio-Rad*), MiniPex 3in1 kit (*Molecular Biology Service, IMP*), benzonase nuclease (*Molecular Biology Service, IMP*), FastDigest DpnI (*ThermoScientific*), Q5® HotStart High-Fidelity (*New England BioLabs*).

3.1.4. *Escherichia coli* strains, mammalian cell lines and expression plasmids

***E. coli* strains:** BL21 (DE3), Rosetta 2, Arctic Express

Mammalian cell lines: HeLa, HEK293GP

Expression plasmids: pETM44, pETM33

3.1.5. Bacterial and cell culture media

Medium	Component
Autoinduction medium (<i>Molecular biology service, IMP</i>)	ZY medium (10 g/L tryptone and 5 g/L yeast extract) P (25 mmol/L (NH ₄) ₂ SO ₄ , 100 mmol/L KH ₂ PO ₄ , 100 mmol/L Na ₂ HPO ₄) 5052 (0.5% (v/v) glycerol, 0.05% (w/v) glucose, 0.2% (w/v) α-lactose) 1 mmol/L MgSO ₄ 0.05 mg/L Km
1000x Trace Metal Mix	50 μmol/L FeCl ₃ , 20 μmol/L CaCl ₂ , 10 μmol/L MnCl ₃ , 10 μmol/L ZnSO ₄ , 2 μmol/L CoCl ₂ , 2 μmol/L CuCl ₂ , 2 μmol/L NiCl ₂ , 2 μmol/L Na ₂ MoO ₄ , 2 μmol/L Na ₂ SeO ₃ , 2 μmol/L H ₃ BO ₃
Lysogeny broth (LB) liquid and solid medium (<i>Media kitchen, IMP</i>)	5 g/L yeast extract, 10 g/L tryptone, 10 g/L NaCl, 0.05 g/L Km, (+ 15 g/L agar for solid LB medium)
Super optimal broth (SOC) (<i>Media Kitchen, IMBA</i>)	5 g/L yeast extract, 20 g/L tryptone, 10 mmol/L NaCl, 2.5 mmol/L KCl, 10 mmol/L MgCl ₂ , 10 mmol/L MgSO ₄ , 20 mmol/L glucose
Cell culture medium for HEK293GP cells	Gibco™ FreeStyle™ 293 Expression Medium

3.2. Methods

3.2.1. Molecular cloning

3.2.1.1. Polymerase chain reaction (PCR)

Polymerase Chain Reaction (PCR) was used to amplify desired DNA constructs, vector backbones, or inserts. The total volume of the reaction was 50 μL. The PCR reaction mixture contained template DNA (20-50 ng) added with 1 μL from the stock, forward and reverse

primer (0.5 $\mu\text{mol/L}$ each) (*Microsynth*) from a 100 $\mu\text{mol/L}$ stock, 25 μL of 2x Q5[®] HotStart High-Fidelity 2X MM (*New England BioLabs*) and 23 μL of Sterile MonoQ H₂O (*Media Kitchen, VBC*). The PCR reaction was run using C1000 Touch Thermal Cycler (*Bio-Rad*) with the following program: 1 cycle of initial denaturation at 95 °C for 3 min, 30 cycles consisting of denaturation step at 95 °C for 15 s, an annealing step at varying temperatures (55-72 °C) depending on the primer's annealing region for 15 s and an extension step at 72 °C for varying time (12 s – 1.5 min) depending on the size of the DNA template. The program was ended with a final extension step at 72 °C for 10 min. The PCR reactions were held at 4 °C until the PCR products were purified.

3.2.1.2. Agarose gel electrophoresis

PCR products were analyzed on a 1% (w/v) agarose gel prepared by mixing the corresponding amount of agarose (*SigmaAldrich*) with 1xTAE buffer and dissolving the agarose by heating the mixture in the microwave. After cooling the mixture to sub-boiling temperature, 5 μL of SYBR[™] Safe DNA Gel Stain (*Invitrogen*) was added, and the solution was poured into Mupid-One Electrophoresis system (*Genetics*) with pre-inserted comb and let to solidify. Once the gel solidified, the comb was taken out. The PCR samples were prepared by mixing 5 μL of PCR product with 1 μL of Gel Loading Dye Purple 6x (*BioLabs*) and loaded into the gel wells. Electrophoresis was run at room temperature and 100 V for 30 min. The gel was imaged on a ChemiDoc MP Imaging System (*Bio-Rad*), using the SYBR Safe channel to detect resolved DNA bands.

1xTAE buffer: 40 mmol/L Tris/HCl pH 8.0, 1 mmol/L EDTA, 20 mmol/L acetic acid

3.2.1.3. PCR product purification

Plasmids and PCR products were purified using the MiniPex 3in1 kit (*Molecular Biology Service, IMP*) according to the manual's instructions. For PCR product purification 5 volumes of Buffer B were added and the sample was applied onto a binding column. The columns were centrifuged at 21,130 $\times g$ at 4 °C for 1 min. The flowthrough was discarded, and a column wash was performed by applying 750 μL of Buffer W and centrifuged at 21,130 $\times g$ at 4 °C for 1 min. Flowthrough was again discarded, and the columns were additionally

centrifuged at 21,130×g at 4 °C for 1 min to remove residual Buffer W. The columns were transferred to clean 1.5 mL microcentrifuge tubes and 30 µL of Sterile MonoQ H₂O (*Media Kitchen, IMBA*) was added onto the column resin and incubated for 1 min. The plasmid was eluted by centrifugation at 21,130×g at 4 °C for 1 min. DNA concentration was determined using Nanodrop DS-11 FX + Spectrophotometer (*DeNovix*).

3.2.1.4. Gibson assembly

A Gibson assembly reaction was used to incorporate desired fragments of DNA inside vectors to obtain affinity-tagged variants of proteins of interest. The input to the Gibson assembly reaction was vector backbone (100 ng) and the insert was added in 10x molar excess to the vector. The total volume of the reaction was 20 µL. The reaction contained the corresponding volumes of vector backbone and insert (usually around 1 µL from the stock), 10 µL of Gibson Master mix 2x (*Molecular Biology Service, IMP*), and 8 µL Sterile MonoQ H₂O (*Media Kitchen, IMBA*). The mixture was incubated for 1 h at 50 °C and transferred on ice. Then the template DNA was digested by addition of 1 µL FastDigest *DpnI* (*ThermoScientific*) and 2 µL 10x FastDigest buffer (*ThermoScientific*) and the sample was incubated for 1 h at 37 °C. The Gibson assembly reaction was directly used to transform DH5α *E. coli* cells.

3.2.1.5. Transformation of chemically competent DH5α *E. coli* cells

Gibson assembly products or purified recombinant DNA were introduced into DH5α cells for vector propagation. 4 µL of a Gibson assembly reaction or 100 ng of the finalized vector was mixed with 50 µL of competent cells on ice. The cells were incubated for 15 min on ice followed by a heat shock for 1 min at 42 °C in a ThermoMixer (*Eppendorf*) and immediately transferred back on ice. 250 µL SOC media (*Media kitchen, IMBA*) was added to the cells, and the cells were grown for 1 h at 37 °C. 100 µL of cells was plated onto an agar plate (LB solid medium, *Media Kitchen, IMBA*) supplemented with ampicillin or kanamycin antibiotic. The colonies were grown overnight at 37 °C.

3.2.1.6. Miniprep and sequencing

Single colonies were inoculated in 5 mL LB liquid media (*Media Kitchen, IMBA*) supplemented with ampicillin (0.1 mg/mL) or kanamycin (0.05 mg/mL). The cultures were grown overnight at 37 °C and 180 rpm. The next day cells were pelleted by centrifugation at 4,186×g at 4 °C for 10 min. The supernatant was removed, and the plasmids were purified using the MiniPex 3in1 kit (*Molecular Biology Service, IMP*) according to the manual's instructions. The cell pellet was resuspended in 250 µL ice-cold Buffer R1 and transferred to microcentrifuge tubes. 250 µL of Buffer L2 was added and the tube was inverted 4 times. 350 µL Buffer N3 was added, and the tubes were again inverted 4 times. The sample was centrifuged at 21,130×g at 4 °C for 10 min. Supernatants were collected and applied onto a binding column. The columns were centrifuged at 21,130×g at 4 °C for 1 min and the flowthrough was discarded. Columns were washed by applying 750 µL of Buffer W, centrifuged at 21,130×g at 4 °C for 1 min and flowthrough was discarded. Additional centrifugation at 21,130×g at 4 °C for 1 min was performed to remove residual Buffer W. Columns were transferred into clean 1.5 mL microcentrifuge tubes, 30 µL of Sterile MonoQ H₂O (*Media kitchen, IMBA*) was applied onto a column, and plasmids were eluted by centrifugation at 21,130×g at 4 °C for 1 min. DNA concentration was determined using Nanodrop DS-11 FX + Spectrophotometer (*DeNovix*). Purified plasmid sequences were verified using an in-house Sanger sequencing service (*Molecular Biology Service, IMP*). Plasmids were stored at -20 °C.

3.2.2. Biochemical methods

3.2.2.1. Sodium dodecyl sulfate polyacrylamide gel electrophoresis (SDS-PAGE)

Samples for analysis on SDS-PAGE were prepared by mixing the sample with 5x SDS-PAGE loading dye. For the analysis of proteins with polyQ stretches 2 mol/L urea was added to 5x SDS-PAGE loading dye to ensure complete protein denaturation. Denaturation by incubation at 95 °C was not possible due to its effect on diminishing EGFP fluorescence. Prepared samples were loaded in the wells of a 4-15% or 4-20% precast gel (Criterion TGX Stain-free Precast gel, *Bio-Rad*) positioned inside Criterion™ Vertical Electrophoresis Cell (*Bio-Rad*) filled with 1x SDS-PAGE running buffer (*Media Kitchen, IMBA*). For detection of

individual protein band molecular weights, 5 μ L of PageRuler prestained protein-ladder (180 kDa) (*Thermo Scientific*) and/or PageRuler unstained protein ladder (200 kDa) (*Thermo Scientific*) was also loaded. The gel was run for 35 min at room temperature at 200 V using the PowerPac Basic Power Supply (*Bio-Rad*). The gels were imaged in a ChemiDoc MP Imaging System (*Bio-Rad*) using a StainFree channel that visualizes Tryptophan fluorescence or Fluorescein channel that visualizes EGFP fluorescence. In addition, the gels on which time points of degradation assays were analyzed were stained overnight in 20 mL SafeBlue solution (*Molecular Biology Service, IMP*), de-stained in MonoQ H₂O for 1 h, and imaged in a ChemiDoc MP Imaging System (*Bio-Rad*) with a Coomassie channel.

1x SDS-PAGE Running buffer: 30% (w/v) Tris base, 14.4% (w/v) glycine, 1% (w/v) SDS
5x SDS-PAGE loading dye: 250 mmol/L Tris-HCl pH 6.8, 10% (w/v) SDS, 50% (w/v) glycerol, 0.5 mol/L DTT, 0.25% (w/v) bromophenol blue
SafeBlue solution: 8.5% (w/v) Coomassie Brilliant Blue G-250, 6.6% (v/v) ethanol, 4% (v/v) ortho-phosphoric acid, 0.55% (w/v) beta-cyclodextrin

3.2.2.2. Western blot

Western blot analysis was performed using Nitrocellulose Membrane 0.45 μ L (*Bio-Rad*). The protein transfer was performed using Trans-Blot Turbo Transfer System (*Bio-Rad*) with following settings: 1.3 A, 25 V for 7 min. The membrane was blocked for 10 min in 10 mL EveryBlot Blocking Buffer (*Bio-Rad*). Corresponding primary and secondary antibodies were diluted according to the manufacturer's instructions in 10 mL EveryBlot Blocking Buffer (*Bio-Rad*). Membrane washes were performed 3x10 min in 20 mL 1xTBS-T at room temperature after blocking and incubation with antibodies. Incubation with antibodies was carried out for 1 h. All incubation and wash steps were performed on a seesaw shaker at room temperature. Chemiluminescence was visualized on a ChemiDoc MP Imaging System (*Bio-Rad*) using ClarityTM Western ECL Substrate mixture (*Bio-Rad*) and Chemiluminescence channel.

TBS-T - 1xTBS (*Molecular Biology Service, IMP*), 1% Tween 20

Primary antibodies: Strep II Tag Mouse monoclonal antibody MB2017 (*Lucerna-Chem*),
GST Tag Monoclonal Antibody (8-326) HRP (*Thermo Fisher Scientific*)

Secondary antibodies: Goat anti-Mouse IgG (H+L) Secondary Antibody, HRP 31430 (*Thermo Fisher Scientific*)

3.2.2.3. Analytical size exclusion chromatography

Frozen 55 μ L aliquots of ubiquitination reactions were thawed in hands and centrifuged in an Eppendorf™ 5424 Microcentrifuge (*Eppendorf*) at 21,113 \times g and 4 °C for 1 min. Complete volume of 55 μ L was injected on a Superdex 200 5/150G (*Cytiva*) analytical size-exclusion column preequilibrated with 1 CV of Analytical SEC buffer. The sample was eluted with 1.2 CV isocratic elution with Analytical SEC buffer at a flow rate of 0.12 mL/min and 50 μ L fractions were collected after the void volume of the column. 8 μ L of selected fractions were mixed with 2 μ L of 5x SDS-PAGE loading dye to prepare samples for subsequent SDS-PAGE analysis. Fractions containing the majority of polyubiquitinated substrate separated from the non-ubiquitinated substrate protein were pooled and immediately used in subsequent degradation or reconstitution assays.

Analytical SEC buffer: 25 mmol/L BisTris, 50 mmol/L KCl, 5 mmol/L MgCl₂, 5% glycerol, 0.5 mmol/L TCEP, 150 mmol/L NaCl

3.2.2.4. Determination of protein concentration

Depending on the sample, the protein concentration was determined using one of the three methods: Bradford assay, Fluoro-Standard assay, or absorbance at 280 nm.

Protein concentration measurement using Bradford assay was performed using a standard curve prepared by mixing Bovine serum albumin (BSA) solution at known concentrations (2, 4, 6, 8, 10, 12, 14 and 16 μ g/mL) with 1 mL of Protein Assay Dye Reagent Concentrate 1x (*Bio-Rad*). Samples whose concentration was being measured were prepared by mixing 2 μ L of protein sample with 1 mL of Protein Assay Dye Reagent Concentrate 1x (*Bio-Rad*). The sample-reagent mixture was incubated for 2-3 min at room temperature and then absorbance was measured at 595 nm on the BioPhotometer Plus (*Eppendorf*). The absorbance values measured with BSA standard were plotted against known used concentrations to create a standard curve. The concentration of the protein sample was subsequently calculated from the standard curve based on the measured absorbance.

The Fluoro-Standard assay was performed by preparing standard curve with protein standard solutions containing EGFP protein with known concentrations (0, 0.625, 1.25, 2.5, 5, 10, 20, 40 $\mu\text{g/mL}$). The standard curve was created using DS-11 FX + Spectrophotometer (*DeNovix*) by measuring the EGFP emission of standard solutions. Subsequently, the sample for measuring was diluted 1:200 in 50 mmol/L HEPES pH 7.3, 300 mmol/L NaCl, 0.5 mmol/L TCEP, 10 mmol/L glutathione (the same buffer in which standards were prepared). Using the created standard curve, protein concentration was determined by measuring EGFP emission using DS-11 FX + Spectrophotometer (*DeNovix*).

Absorbance at 280 nm (A_{280}) was used to measure protein concentrations when the molar extinction coefficient ($\epsilon[\text{L mol}^{-1} \text{cm}^{-1}]$) for the protein could be calculated (single protein samples). The mass concentration (g/L) was determined by measuring the A_{280} for 1% (1 g/L) protein mixture using a DS-11 FX + Spectrophotometer (*DeNovix*) and calculated using the provided molar extinction coefficient ($\epsilon^{1\%}[\text{L mol}^{-1} \text{cm}^{-1}]$) that was estimated using Exspasy's ProtParam tool (Gasteiger et al., 2005).

3.2.2.5. Sucrose density gradient ultracentrifugation

Continuous 10-30% sucrose gradients were prepared from 10% (w/v) and 30% (w/v) sucrose solutions prepared in 25 mmol/L BisTris, 50 mmol/L KCl, 5 mmol/L MgCl_2 , 4 mmol/L ATP or ADP and 1 mmol/L DTT. The solutions were added with a syringe and a thin needle (*BBraun/BD*) into the SW60 tubes (*Seton*) and the sucrose gradient was made using the Gradient master 108 (*Biocomp*). 200 μL volume was removed from the top of the gradient and replaced with 200 μL of the sample. The gradients were then ultracentrifuged at $100,000\times g$ and 4°C for 16 h using Optima XE-90 Ultracentrifuge, SW60Ti rotor (*Beckman Coulter*). The gradients were manually fractionated into 200 μL fractions in the 96-deep-well plate (*Biocompare*). 12 μL of each or every second fraction was mixed with 3 μL of 5x SDS-PAGE loading dye and subsequently analyzed on SDS-PAGE.

3.2.3. Recombinant protein expression and purification

3.2.3.1. Transformation of chemically competent *E. coli* cells

Purified and sequence-verified plasmid DNA was introduced into BL21(DE3) cells for expression of ZFAND2a-MBP-His construct or into Arctic Express and Rosetta2 cells for expression of control substrate and stalling substrate constructs. Plasmid DNA (100 ng) was mixed with 50 μ l of competent cells and the following transformation protocol was identical to the one described in Section 2.2.1.5.

3.2.3.2. Protein expression in autoinduction media

Single colonies containing DNA constructs of interest were inoculated in 25 mL of LB liquid media (*Media kitchen, IMBA*) supplemented with ampicillin (0.1 mg/mL) or kanamycin (0.05 mg/mL). The cultures were grown overnight at 37 °C and 180 rpm. The autoinduction media was prepared by mixing 2 L of ZY media, 100 mL 20xP, 40 mL 50x52 and supplementing with ampicillin (0.1 mg/mL) or kanamycin (0.05 mg/mL) (Fw, 2005). For ZFAND2a-MBP-His expression 2 mL of 1000x Trace metal-mix was added. 12.5 mL of overnight culture was inoculated into 2 L of prepared autoinduction media, and the culture was initially grown for 5.5 h at 37 °C at 180 rpm and then switched to overnight growth at 18 °C at 180 rpm. The cell pellets were collected the next day by centrifugation at 4,000 \times g for 20 min at 4 °C and the supernatant was discarded. The cell pellets were collected in a plastic bag, flash-frozen in liquid nitrogen, and stored in a -69 °C freezer.

3.2.3.3. Cell lysis

The frozen cell pellet was thawed on ice and resuspended on a magnetic stirrer (*IKA® WERKE*) in the cold room (4 °C) in the Lysis buffer in 1:1 ratio for cell lysis using the sonicator or 1:3 ratio using the French press. Resuspended cells expressing ZFAND2a-MBP-His were lysed using the Constant cell Disruption System (*I&L Biosystems*) operating at 1.4 kbar pressure whereas cells expressing control substrate and stalling substrates were lysed using the Branson Digital Sonifier® (*Marshall Scientific*) with the following settings: 60% amplitude, 1 s on, and 1 s off for 6 min in 1.5-min intervals and 3-min break between intervals. Lysed cells were centrifuged in Sorvall LYNX 6000 centrifuge, rotor F9-6x1000 (*Thermo Scientific*)

for 45 min at 18,500×g at 4 °C. The supernatant was collected as cleared cell lysate and filtrated once through miracloth.

MBP Trap Lysis buffer (ZFAND2a-MBP-His purification): 50 mmol/L HEPES pH 8, 300 mmol/L NaCl, 0.5 mmol/L TCEP, 2x protease inhibitor cocktail tablet, 2x benzonase, 1 mmol/L PMSF

GST Trap Lysis buffer (substrate protein purification): 50 mmol/L HEPES pH 7.3, 500 mmol/L NaCl, 0.5 mmol/L TCEP, 5% glycerol, 2x protease inhibitor cocktail tablet, 2x benzonase, 1 mmol/L PMSF

3.2.3.4. MBPTrap affinity chromatography

MBPTrap affinity chromatography was used as a first step to purify the ZFAND2a-MBP-His construct. The MBP Trap column (*Cytiva*) was equilibrated with 2 CV H₂O followed by 5 CV MBPTrap Binding buffer with a flow rate of 5 mL/min. Cleared cell lysate was applied onto the column using a sample pump with a flow rate of 2.5 mL/min. After sample application, the column was washed with 25 CV MBPTrap Binding buffer. The protein was eluted from the column in two steps: the first step was a gradient elution from 0% to 100% MBP Trap Elution buffer with 10 CV, followed by a step with fill 100% MBPTrap Elution buffer with 5 CV. Elution was fractionated into 1.5 mL fractions using a fraction collector. Fractions showing a peak in 280 nm UV absorbance were analyzed on SDS-PAGE and fractions containing the protein of interest were pooled and concentrated using Amicon Ultra-4 concentrators with 10 kDa cutoff (*Merck*) to 10 mL.

MBPTrap Binding buffer: 50 mmol/L HEPES pH 8, 300 mmol/L NaCl, 0.5 mmol/L TCEP

MBPTrap Elution buffer: 50 mmol/L HEPES pH 8, 150 mmol/L NaCl, 0.5 mmol/L TCEP, 10 mmol/L D-maltose

3.2.3.5. MagneGST Glutathione Particles affinity purification

MagneGST Glutathione Particles were used to purify GST-tagged substrate proteins. 1.5 mL of settled magnetic beads were washed three times using 10 mL of MagneGST Binding buffer. The beads were then resuspended in the final volume of 5 mL of MagneGST Binding

buffer and added to the cleared cell lysate (approximately 1.5 mL of settled beads was used for 140 mL of cleared cell lysate). The beads were then incubated overnight with the cleared cell lysate on a RCT basic rotating platform (*Denley*) in the cold room at 4 °C. The next morning, the beads were settled down by centrifugation at 1,000×g for 5 min at 4 °C and the flowthrough fraction was collected. The beads were then washed three times with 20 mL of MagneGST Binding buffer by incubating the beads on a RCT basic rotating platform (*Denley*) for 10 min at 4 °C and repeating the beads settling using centrifugation at 1,000×g for 5 min at 4 °C and collecting wash fractions. The protein was eluted by incubating the beads three times with 3 mL MagneGST Elution buffer and collecting the elution fractions by settling down the beads using centrifugation at 1,000×g for 5 min at 4 °C. All collected fractions were analyzed on SDS-PAGE and good fractions were frozen in LN₂ and stored in a -69 °C freezer.

MagneGST Binding buffer: 50 mmol/L HEPES pH 7.3, 500 mmol/L NaCl, 0.5 mmol/L TCEP, 5% glycerol

MagneGST Elution buffer: 50 mmol/L HEPES pH 7.3, 300 mmol/L NaCl, 0.5 mmol/L TCEP, 5% glycerol, 10 mmol/L L-Glutathione

3.2.3.6. Ion-exchange chromatography

Ion-exchange chromatography was used as a second step in ZFAND2a-MBP-His purification. A Resource MonoQ 5/50 GL 1 mL column (GE Healthcare) was equilibrated with 1 CV H₂O and 5 CV IEX Binding buffer. The sample from the MBP Trap affinity purification step was diluted to 50 mmol/L NaCl and applied using sample pump onto the column with a flow rate of 3 mL/min. The column was washed with 5 CV IEX Binding buffer. The protein was eluted from the column using linear elution from 0-37% with 20 CV IEX Elution buffer followed by 5 CV elution wash with 100% IEX Elution buffer. 1.5 mL fractions were collected and fractions with the peak at 280 nm UV were analyzed on SDS-PAGE. Fractions containing the protein were pooled for the next purification step.

IEX Binding buffer: 50 mmol/L HEPES pH 8.0, 50 mmol/L NaCl, 0.5 mmol/L TCEP

IEX Elution buffer: 50 mmol/L HEPES pH 8.0, 2 mol/L NaCl, 0.5 mmol/L TCEP

3.2.3.7. Size-exclusion chromatography

Size-exclusion chromatography was used as a third purification step in ZFAND2a-MBP-His purification to further increase the sample purity. For this purpose, a Superdex™ 75 16/600 column (*GE Healthcare*) was equilibrated with 1 CV H₂O followed by 1 CV of SEC Buffer 1. The concentrated protein sample from ion-exchange chromatography (10 mL) was applied using a sample pump at a flow rate of 1 mL/min and the protein was eluted using the isocratic elution of 1.2 CV. 1.5 mL fractions were collected after 0.2 CV has passed through the column and fractions with the peak at 280 nm UV were analyzed on SDS-PAGE. Fractions containing the protein were pooled, protein concentration was measured, the protein was aliquoted, frozen in LN₂, and stored in a -69 °C freezer.

SEC Buffer 1: 50 mmol/L HEPES pH 8.0, 200 mmol/L NaCl, 0.5 mmol/L TCEP

3.2.4. Purification of human 26S proteasomes

3.2.4.1. Purification from HeLa cytoplasmic extracts using GST-UBL method

HeLa cytoplasmic extract provided from H. Stark lab (*MPI Göttingen*) was used for purifying HeLa 26S proteasomes. Before thawing, the extract was supplemented with 1 mmol/L DTT, 4 mmol/L ATP, 0.1 mmol/L PMSF, and 1x benzonase and thawed in water bath (*ThermoScientific*) at 37 °C. The extract was placed in a cold room on a magnetic stirrer and drop-by-drop a solution of 50% (w/v) PEG 8,000 was added to a final concentration of 4% (w/v) and the extract was incubated for 15 min. The extract was centrifuged in Sorvall LYNX 6000 centrifuge, rotor F9-6x1000 (*Thermo Scientific*) at 16,000×g and 4 °C for 15 min after which the supernatant was collected, and the pellet discarded. The supernatant was placed in the cold room on a magnetic stirrer and drop-by-drop a solution of 50% (w/v) PEG 8,000 was added to a final concentration of 20% (w/v) and the supernatant was incubated for 15 min. The supernatant was centrifuged at 12,000×g and 4 °C for 15 min. After the centrifugation, the supernatant was discarded and a short centrifugation for 1 min at 12,000×g and 4 °C was done to remove any residual liquid. The remaining liquid was removed, and the pellet was dissolved in 1x work buffer supplemented with 10% glycerol, 4 mmol/L ATP, and 1 mmol/L DTT. Into dissolved cell extract 5 mg of GST-UBL (purified by *I. Grishkovskaya*) and 1 mL of settled

MagneGST Glutathione beads (*Promega*) were added. The extract, GST-UBL, and beads were incubated overnight in the cold room at 4 °C on a RCT basic rotating platform (*Denley*) to allow UBL binding to the 26S proteasome and GST binding to the beads. The next day the beads were settled using centrifugation at 1,000×g at 4 °C for 5 min and flowthrough was collected. The beads were washed three times with 40 mL 1x work buffer supplemented with 10% glycerol, 4 mmol/L ATP, and 1 mmol/L DTT in the cold room at 4 °C on RCT basic rotating platform (*Denley*). After collecting the last wash, bound protein complexes were eluted with 2x5 mL of 2 mg/mL hHisUIM (purified by *I. Grishkovskaya*) in 1x work buffer supplemented with 10% glycerol, 4 mmol/L ATP, and 1 mmol/L DTT. The elution was carried out in the ThermoMixer (*Eppendorf*) at 8 °C and 500 rpm for 1.5 hour. After the second elution the beads were washed once more with 5 mL 1x work buffer supplemented with 10% glycerol, 4 mmol/L ATP, and 1 mmol/L DTT. hHisUIM competes with 26S proteasome for GST-UBL binding hence collected flowthrough contained free 26S and excess hHisUIM while GST-UBL – hHisUIM complex remained bound to the beads. Beads were additionally eluted with 4 mL GSH elution buffer for 10 min at 8 °C and 500 rpm on ThermoMixer (*Eppendorf*). HisTrap Excel 1 mL column (*GE Healthcare*) was washed with 1 CV water and equilibrated with 5 mL 1x work buffer supplemented with 10% glycerol, 4 mmol/L ATP, and 1 mmol/L DTT. Separate runs were performed for two elution samples with hHisUIM and one wash sample after hHisUIM elutions. The samples were applied onto a column using a sample loop at a flow rate of 0.5 mL/min and 1.5 mL flowthrough fractions were collected. The column was washed with 5 CV 1x work buffer supplemented with 10% glycerol, 4 mmol/L ATP, and 1 mmol/L DTT between sample runs. hHisUIM was eluted from the column with Step fill 100% 10 CV HisTrap Elution Buffer.

1x work buffer: 25 mmol/L Bis-Tris pH 6.5, 50 mmol/L KCl, 5 mmol/L MgCl₂

HisTrap Elution Buffer: 25 mmol/L Tris pH 7.4, 150 mmol/L NaCl, 500 mmol/L imidazole

3.2.4.2. Purification from HEK293GP cells using Streptavidin affinity chromatography

The stable HEK293GP cell line expressing hRpn11-HTBH (His-TEV-Biotin-His) (gift from Dr. Daniel Finley's lab, *Harvard Medical School*) were grown in Gibco™ FreeStyle™ 293 Expression Medium (*Thermo Scientific*) to a density of 2×10⁶ cells/mL. The suspension

culture was centrifuged at 15,000×g and 4 °C for 20 min. The supernatant was discarded, and the cell pellet was resuspended in ice-cold 1xPBS (100 mL of 1xPBS was used per 2 L of centrifuged suspension culture). Resuspended cells were subjected to an additional round of centrifugation at 4,000×g and 4 °C for 15 min. The supernatant was discarded, and the cell pellet was collected in 50 mL falcon, resuspended in 1:1 volume ratio in Lysis buffer, frozen in LN₂, and stored in a -69 °C freezer until used. For affinity purification of the 26S proteasomes, fresh 4 mmol/L ATP, 1 mmol/L DTT, 0.1 mmol/L PMSF, protease inhibitor cocktail tablet, and 1x benzonase were added to still frozen resuspended cells. The cells were then thawed in water bath (*Thermo Scientific*) prewarmed at 37 °C. Cells were lysed using Dounce homogenizer by first pressing 15x with the type A and then 15x with the type B pestle. The lysate was incubated on ice for 15 min and cell debris was subsequently removed by ultracentrifugation at 100,000×g and 4 °C for 1 h. The cleared supernatant was filtered through a double layer of miracloth and 0.45 µm filter and applied with 0.2 mL/min flow rate onto a 1 mL HP Streptavidin column (*GE Healthcare*) equilibrated with 10 CV Wash buffer. The column was then washed with 10 CV Wash buffer 1, 10 CV Wash buffer 2, and again 10 CV of Wash buffer 1. Using the loop, 2 mL of Elution buffer 1 containing GST-TEV protease (*Molecular Biology Service, IMP*) was applied onto a column and the column was incubated overnight at 4 °C. GSTrap FF 1 mL column (*Cytiva*) was equilibrated with 10 CV Wash buffer 1 and attached below HP Streptavidin column. Cleaved 26S proteasome complexes and GST-TEV were eluted from the column using isocratic elution with 10 CV Wash buffer 1 with a flow rate of 0.2 mL/min. GST-TEV protease remained bound to the attached GSTrap FF column, while the 26S proteasomes were collected in 1.5 mL fractions. GSTrap FF column was eluted with 10 CV Elution buffer 2 and 1.5 mL fractions were collected. All collected fractions were analyzed on SDS-PAGE. Fractions containing proteasomes were pooled and protein concentration was measured using Bradford assay. Purified 26S proteasomes were frozen in 50 µl aliquots and stored in a -69 °C freezer.

Lysis buffer: 25 mmol/L BisTris pH 6.5, 50 mmol/L KCl, 5 mmol/L MgCl₂, 10% glycerol, 0.1% NP-40 (freshly added 4 mmol/L ATP, 1 mmol/L DTT, 0.1 mmol/L PMSF, 1x protease inhibitor cocktail tablet, 1x benzonase).

Wash buffer 1: 25 mmol/L BisTris pH 6.5, 50 mmol/L KCl, 5 mmol/L MgCl₂, 10% glycerol, 4 mmol/L ATP, 1 mmol/L DTT

Wash buffer 2: 25 mmol/L BisTris pH 6.5, 50 mmol/L KCl, 5 mmol/L MgCl₂, 10% glycerol, 4 mmol/L ATP, 1 mmol/L DTT, 150 mmol/L NaCl

Elution buffer 1: 25 mmol/L BisTris pH 6.5, 50 mmol/L KCl, 5 mmol/L MgCl₂, 10% glycerol, 4 mmol/L ATP, 1 mmol/L DTT, 3.3 mg GST-TEV

Elution buffer 2: 25 mmol/L BisTris pH 6.5, 50 mmol/L KCl, 5 mmol/L MgCl₂, 10% glycerol, 10 mmol/L L-Glutathione reduced

3.2.5. *In vitro* assays

3.2.5.1. Ubiquitination assay

A large-scale ubiquitination reaction of model proteasome substrates was performed using two different combinations of E2/E3 enzymes to prepare K11/K63-type and K48-type polyubiquitinated model proteasome substrates. Reactions were performed in 1 mL volume using 20 mmol/L HEPES pH 7.3 as a ligase buffer supplemented with 50 mmol/L NaCl for the reaction with SuperE2 and 200 mmol/L NaCl for the reaction with the APC/C.

For the synthesis of K48-type ubiquitin chains, the reaction contained E1 Uba1 (1.5 µmol/L) (purified by *I.Grishkovskaya*), Super E2 (2 µmol/L) (purified by *S.J.Amann*), ATP (10 mmol/L), free ubiquitin (0.2 mmol/L) (purified by *H.L.Brunner*), and a model proteasome substrate protein (10 µmol/L). All reaction components, apart from substrate, were premixed on ice and the ubiquitination enzymes were primed by incubating the substrate-free enzyme mixture for 15 min at 30 °C in a ThermoMixer (*Eppendorf*). The substrate was added after priming, the reaction was gently resuspended with a pipette to ensure proper mixing of components and placed in a ThermoMixer (*Eppendorf*) preheated at 30 °C for 22 h.

For the synthesis of K11/K63-type ubiquitin chains the reaction contained E1 Uba1 (1 µmol/L) (purified by *I.Grishkovskaya*), E2 Ubch10 (1 µmol/L), APC/C E3 (100 nmol/L), Cdh1 activator (0.66 µmol/L), ATP (10 mmol/L), free ubiquitin (0.25 mmol/L) and a model proteasome substrate protein (2 µmol/L). Ubch10, APC/C and Cdh1 were purified and provided by N.G.Brown's lab (*UNC School of Medicine*). All reaction components were mixed on ice with ubiquitin being added last to start the ubiquitination reaction. The reaction was gently resuspended with a pipette to ensure proper mixing of components and placed in a ThermoMixer (*Eppendorf*) preheated at 30 °C for 22 h.

For both ubiquitination reactions, control reactions with omitted ATP or substrate were set. The reaction progress was monitored by taking 8 µL aliquots at chosen time points and quenched with 2 µL of 5X SDS-PAGE loading dye. The taken time points were analyzed on

SDS-PAGE. Successful ubiquitination reactions were transferred on the ice after 22 h, aliquoted into 55 μ L aliquots, frozen in LN₂, and stored in a -69 °C freezer.

3.2.5.2. Degradation assay

In vitro degradation of model proteasome substrates was performed in 20 μ L or 110 μ L volume using Activity buffer. The Eppendorf tubes used in the activity assay were blocked with 150 μ L Activity assay buffer for 1 h at 37 °C.

Initial degradation assay screen was performed with ubiquitination reaction as input for a substrate. HeLa 26S proteasomes (25 nmol/L) were mixed with 10 μ L of ubiquitination reaction and Activity buffer was added to a final volume of 20 μ L. Control reaction without proteasomes was performed by mixing 10 μ L Activity assay buffer with 10 μ L ubiquitination reaction. Reaction with USP21 deubiquitinating enzyme was set by mixing 10 μ L ubiquitination reaction with USP21 (2.5 μ mol/L) and Activity assay buffer was added to a final volume of 20 μ L. Reactions were incubated for 24 h at 37 °C in a ThermoMixer (*Eppendorf*) at 300 rpm. At time points 0 and 24 h, 7 μ L aliquots were taken and the reaction was quenched with 3 μ L 5X SDS-PAGE loading dye.

Degradation assay with ZFAND2a was performed by mixing HEK293GP 26S proteasomes (50 nmol/L) with polyubiquitinated model proteasome substrate (<5 nmol/L) after analytical size exclusion (36 μ L of a chosen fraction), ZFAND2a (1 μ mol/L) and Activity assay buffer was added to a final volume of 110 μ L. Reaction without ZFAND2a was performed by mixing HEK293GP 26S proteasomes (50 nmol/L) with polyubiquitinated model proteasome substrate (<5 nmol/L) after analytical size exclusion (36 μ L of a chosen fraction) and the Activity buffer was added to a final volume of 110 μ L. A master mix containing appropriate concentrations of 26S proteasomes and polyubiquitinated model proteasome substrate was prepared and equally distributed to reaction with and without ZFAND2a to ensure more equal enzyme/substrate input. Control reaction containing only polyubiquitinated model proteasome substrate (<5 nmol/L) and Activity buffer was also set. Reactions were incubated at 37 °C in a ThermoMixer (*Eppendorf*). At chosen timepoints 8 μ L aliquots were taken and the reaction was quenched with 2 μ L 5X SDS-PAGE loading dye supplemented with 2 mol/L urea.

Collected timepoints were analyzed on SDS-PAGE. The gel was imaged using ChemiDoc MP Imaging System (*Bio-Rad*) with StainFree and Fluorescein channels. The gel was also stained with SafeBlue solution.

Activity buffer: 25 mmol/L Tris pH 7.5, 5 mmol/L MgCl₂, 5% glycerol, 10 mmol/L ATP, 1 mmol/L DTT, 2 mg/mL BSA

3.2.5.3. Reconstitution assay

Reconstitution reactions were performed in ~200 μ L volume using Reconstitution buffer. The control reconstitution reaction contained polyubiquitinated model proteasome substrate (<5 nmol/L) after analytical size exclusion (40 μ L of a chosen fraction) and ZFAND2a (9 μ mol/L) and the Reconstitution buffer was added to a final volume of 200 μ L. The reconstitution reaction without ZFAND2a contained HEK293GP 26S proteasomes (150 nmol/L), polyubiquitinated model proteasome substrate (<5 nmol/L) after analytical size exclusion (48 μ L of a chosen fraction) and ATP (4 mmol/L). Reconstitution reaction with ZFAND2a contained HEK293GP 26S proteasomes (150 nmol/L), polyubiquitinated model proteasome substrate (<5 nmol/L) after analytical size exclusion (30 μ L of a chosen fraction), ZFAND2a (6.7 μ mol/L), ADP (4 mmol/L), D-Glucose (20 mmol/L) and hexokinase (10 mU). After combining all components on ice, reactions were incubated for 35 min at 37 °C in ThermoMixer (*Eppendorf*). After incubation, the complete volume of reconstitution reaction was applied on a 10-30% continuous sucrose gradient and the sample was processed further as described in Section 3.2.2.5. of Materials and Methods.

Reconstitution buffer: 25 mmol/L BisTris, 50 mmol/L KCl, 5 mmol/L MgCl₂, 10% glycerol

3.2.6. Cryo-electron microscopy

3.2.6.1. Sample preparation

Sucrose gradient fractions containing the ZFAND2a-bound 26S proteasome complex in the presence of stalling model proteasome substrate were buffer exchanged into a sucrose-free desalting buffer using a ZebaTM Spin Desalting columns, 7K MWCO, 0.5 mL (*Thermo*

Scientific). The storage buffer in the desalting column was removed by centrifugation at $1,500\times g$ and $4\text{ }^{\circ}\text{C}$ for 1 min. The desalting column was then equilibrated with $4\times 300\text{ }\mu\text{L}$ of a desalting buffer by centrifugation at $1,500\times g$ and $4\text{ }^{\circ}\text{C}$ for 1 min. The desalting column was placed in a clean 1.5 mL Eppendorf tube, $150\text{ }\mu\text{L}$ of sucrose gradient fraction was applied on the top of the desalting column and centrifuged at $1,500\times g$ and $4\text{ }^{\circ}\text{C}$ for 2 min.

Quantifoil® R3.5/1 grids (*Electron Microscopy Sciences*) with holey carbon film were glow-discharged for 60 s at 20 mA in SCD 005 Sputter Coater (*Bal-Tec*) with holey carbon surface facing up. Around $33\text{ }\mu\text{L}$ of the buffer exchanged sample was placed in a small hole of an ice-cold metal holder in a way to achieve a perfectly flat surface. A small piece of additional 2 nm thick layer of continuous carbon film was placed on the surface of the sample and the glow-discharged grid was added on top of the carbon film with a holey carbon surface facing down. Grids were incubated with the sample for times ranging from 10–20 min. Sample vitrification was performed using a Leica EM GP grid plunger (*Leica Microsystems*). After incubation, grids were picked up with forceps and attached to a freezing device. $4\text{ }\mu\text{L}$ droplet of double distilled H_2O was added on the carbon film side of the grid, blotted for 2 s against a Whatman No.1 paper at $4\text{ }^{\circ}\text{C}$ and with 80% humidity. After blotting, the grids were instantaneously plunged frozen in liquid ethane. Vitrified grids were stored in an LN_2 tank until further processing.

Desalting buffer: 25 mmol/L BisTris pH 6.5, 50 mmol/L KCl, 5 mmol/L MgCl_2 , 10% glycerol, 4 mmol/L ATP or 4 mmol/L ADP, 1 mmol/L DTT

3.2.6.2. Grid screening and data collection

Vitrified grids were clipped inside autogrids (*Thermo Scientific*) to be screened with ThermoScientific™ Glacios™ Cryo-TEM Microscope (*VBC Electron Microscopy Core Facility, Vienna*) at an acceleration voltage of 200 kV. Glacios Cryo-TEM microscope is equipped with a high-brightness field emission gun (X-FEG) as an electron source and a Falcon3 Direct Electron Detector for imaging. Each grid was screened to assess the ice quality and particle concentration and quality with the purpose to identify the best grid for the collection of a large data set. Images were taken at 2-3 different regions of the grid using a total dose of $50\text{ e}^- \text{ \AA}^{-2}$ with an exposure time of 1.99 s and a magnification of $155,000\times$ corresponding to a pixel size of $0.98\text{ \AA}/\text{pxl}$.

The best grid was used for the collection of data set on FEI Titan Krios G2 (*FEI*) Cryo-TEM Microscope (*eBIC, Thermo Fisher Scientific and Diamond Light Source*) at an acceleration voltage of 300 kV using Bio Quantum K3 detector and Gatan energy filter slit width set at 20 nm. In each chosen grid hole 14 movies were collected using a total dose of $48.76 \text{ e}^- \text{ \AA}^{-2}$, fractionated into 50 frames with an exposure time of 4 s at varying defocus range from -1.3 to -2.1 μm in 0.2 μm steps at a magnification of $81,000 \times$ corresponding to a pixel size of 1.06 $\text{\AA}/\text{pxl}$. In total 10,070 movies were collected.

3.2.6.3. Movie preprocessing and 2D image processing

Initial movie preprocessing and subsequent 2D image processing were performed using CryoSPARC v3.3.1 (Punjani et al., 2017). Movies were imported and motion correction was performed using Patch Motion and CTF parameters were estimated using Patch CTF estimation (multi). During patch motion correction, the individual movie frames of the same imaged area are combined into a micrograph by aligning smaller regions of each frame to correct for beam-induced motion and movements of the sample holder during the data acquisition (Li et al., 2013). After alignment and before the final micrograph is constructed, a dose weighting is performed to account for the radiation damage accumulated in later frames in a way that high-frequency information of the final micrograph is derived mostly from the earlier frames. Since the data acquisition is done with a user-defined defocus to assure enough contrast in the micrographs, the micrographs suffer from signal aberrations and delocalization (Wade, 1992). CTF estimation models these aberrations to correct them later during 3D processing.

Around 1,000 particles were manually selected from several different micrographs, extracted and 2D classification was performed. During 2D classification randomly oriented selected particles are in a reference-free manner aligned and compared to be grouped in user-defined number of 2D class averages based on their similarities. The resulting 2D class averages have a much better signal-to-noise ratio when compared to the individual particle images. 2D class averages representing different orientations of the 26S proteasome were selected and used as 2D templates for the Template picker to, in an automated manner, identify as many as possible 26S proteasome particles in all 10,070 micrographs. Using Inspect Picks option, NCC score and power threshold sliders were used to optimize picking coordinates to eliminate false positives. Selected particles were extracted from micrographs with a box size of 600 pxl and subsequently Fourier cropped to a box size of 480 pxl to decrease the

computational load. Extracted particles were subjected to two rounds of 2D classification. After each round of 2D classification, 2D class averages that showed nice and clear features of 26S proteasome in different orientations were selected for further 3D processing. Before 3D processing, the selected particles were re-extracted with a box size of 600 pxl and subsequently Fourier cropped to a box size of 440 pxl.

3.2.6.4. 3D processing

A subset of particles from selected good 2D class averages was used to calculate the *ab initio* model of the 26S proteasome in CryoSPARC v3.3.1 (Punjani et al., 2017). CryoSPARC uses Stochastic gradient descent algorithm to perform unsupervised *ab initio* 3D classification for which it does not require any prior structural knowledge to determine low-resolution 3D states of a complex. The *ab initio* model is required for subsequent 3D refinement of all particle images to obtain a 3D reconstruction of the complex of interest at a higher resolution. This is achieved through an iterative projection-matching approach in which 2D particle projections are matched to 3D projections generated from an input reference model. Throughout 3D refinement, the particles are assigned to two shift values and three Euler angles that describe their relative 3D orientations (Agard et al., 2014).

All selected and re-extracted particles and calculated *ab initio* model were exported from CryoSPARC to Relion v4.0 (Kimanius et al., 2021). Using 3D-Autorefine, a cryo-EM map of the 26S complex was calculated. ZFAND2a masks of varying sizes were created using Chimera (Pettersen et al., 2004) and Mask Create option in Relion and used in multiple rounds of focused 3D classifications to separate ZFAND2a-bound and ZFAND2a-free 26S proteasome particles. Particles belonging to the ZFAND2a-bound 26S proteasome stack were further sorted for conformational heterogeneity using CryoDRGN v0.3.3/4 (Zhong et al., 2021) and additional focused 3D classification with ZFAND2a mask was performed in Relion (Kimanius et al., 2021). A single 3D class containing ZFAND2a density was selected and 3D-Autorefine was performed to obtain the final cryo-EM map of ZFAND2a-bound 26S proteasome. Local resolution estimation of final cryo-EM maps was obtained in CryoSPARC using the Local Resolution option. The average resolution of the final structures was estimated by Fourier shell correlation (FSC) which measures the correlation between two independently refined half-sets of particles as a function of spatial frequencies. The final resolution of the map is estimated at an FSC curve value of 0.143 (Rosenthal and Henderson, 2003).

4. Results & Discussion

4.1. *In vitro* approach for investigation of ZFAND2a-bound 26S proteasome complex

The 26S proteasome complex contains all the necessary structural and enzymatic requirements to carry out the degradation of polyubiquitinated proteins in cells and in an *in vitro* setup. However, to face the challenge of more than a thousand structurally different substrates and varying degradation demands in cells, the 26S proteasome binds different regulatory proteins that contribute to its overall processivity. One such factor, ZFAND2a, was found to be induced and directly bind the 26S proteasome under proteotoxic conditions when a higher degradation rate is required and when the 26S proteasome function might be impaired. This implicates ZFAND2a in the regulation of malfunctioning 26S proteasomes. However, there is no evidence of which aspect of the 26S proteasome activity ZFAND2a influences and how this regulation is achieved mechanistically. Therefore, I aimed to investigate the potential rescue role of ZFAND2a binding to the 26S proteasome under malfunctioning conditions. For this purpose, I chose an *in vitro* approach to address functional and structural aspects of this biological question. The required preparation steps included affinity purification of ZFAND2a and 26S proteasome complex; in addition to the generation of model proteasome substrate with and without a structural element that causes 26S proteasome malfunction.

4.1.1. Affinity purification of human 26S proteasome complexes

The proteasome complexes have been routinely purified for many years by several different groups. Hence, the established purification protocols are proven to be reproducible across labs and if executed properly result in yields high enough for *in vitro* activity assays and structural analysis by single particle cryo-EM. For the purposes of this study, I purified human 26S proteasome complexes from two different cell lines using two different protocols since the availability of the required cell material varied throughout the duration of the study.

In the first approach, 26S proteasomes were affinity purified from a stable HEK293GP suspension cell line that expresses a tagged hRpn11-HTBH (His-TEV-Biotin-His) subunit, which is one of the constitutive subunits of the 19S RP subcomplex. Cells and purification protocol were kindly provided by the Finley lab (*Harvard Medical School*) and adapted according to the experience in proteasome purification in the Haselbach lab. The general

outline of the affinity purification procedure is depicted in **Figure 4.1 A.** and described in Section 3.2.4.2 of Materials and Methods. The purification contained a wash step with NaCl (150 mmol/L) to remove the bound proteasome interacting proteins (PIPs) such as deubiquitinating enzymes, E3 ligases, and extrinsic ubiquitin receptor proteins. This is possible since their interaction with the 26S proteasome was shown to be sensitive to higher salt concentrations (Besche et al., 2009). I introduced this step to obtain a homogenous 26S proteasome sample and remove additional regulatory proteins that could influence the 26S proteasome activity. All steps during the purification were analyzed on SDS-PAGE (**Figure 4.1 B).**

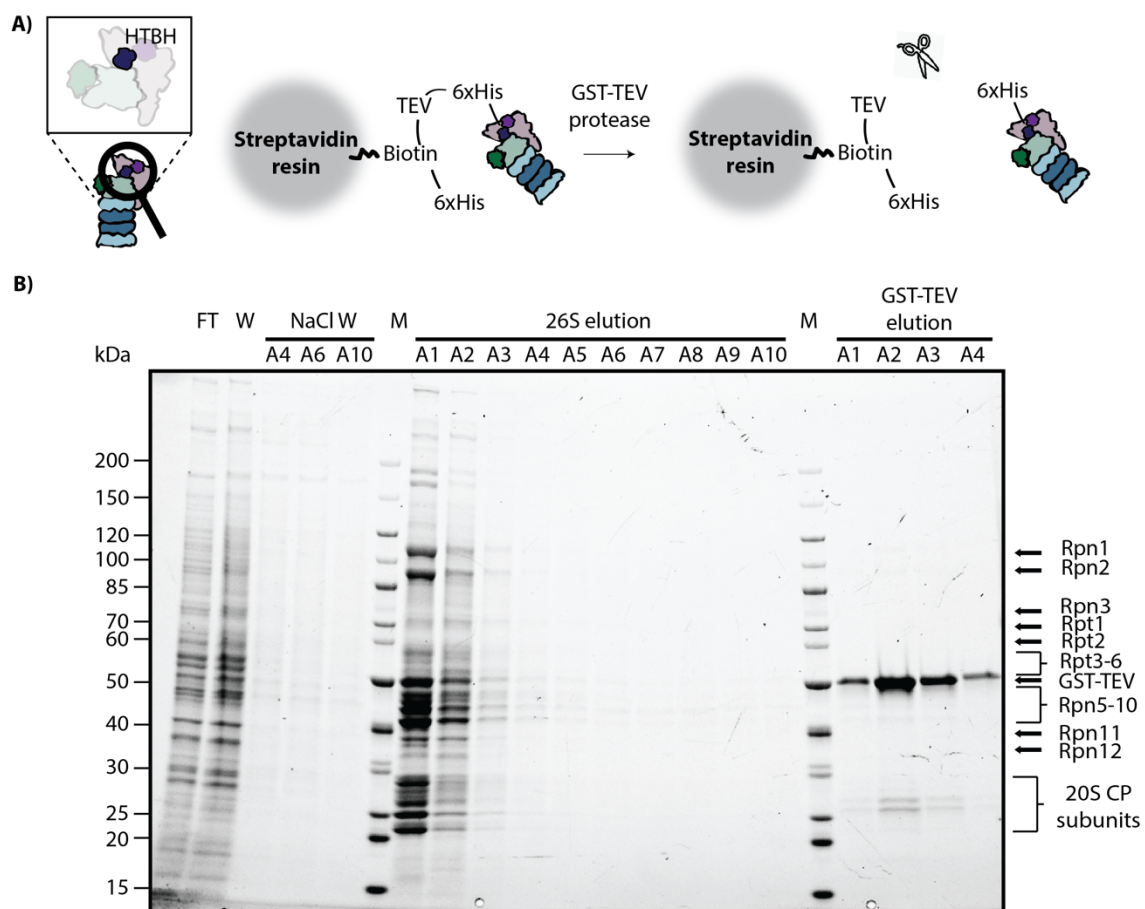


Figure 4.1. Affinity purification of hRpn11-HTBH 26S proteasome complexes from HEK293GP cells.

A) Schematic representation of affinity purification steps.

B) SDS-PAGE analysis of the purification. On the right, the positions of corresponding subcomplexes/subunits of the 26S proteasome complex and the position of GST-TEV protease are indicated. The image was taken using a Stain-free channel. FT – flowthrough, W – wash, M – PageRuler unstained protein ladder.

26S proteasomes were detected in the first three collected fractions after the cleavage (26S elution – A1-A3). Only fractions 26S elution – A1 and A2 were pooled together and stored, as fraction 26S elution – A3 contained a substantially lower amount of proteasomes. The protein concentration of pooled fractions was determined using the Bradford assay. On average, I obtained ~12 mg of HEK293GP 26S proteasomes from 30 mL of cell pellet. GST-TEV protease was efficiently removed from the final 26S proteasome sample and eluted separately in fractions GST-TEV elution - A1-A4. The fraction 26S elution - A3 was submitted for mass spectrometry analysis (K. Mechtler lab, *Protein Chemistry facility, IMBA, Vienna Austria*). Protein identification analysis confirmed the presence of all constitutive 26S proteasome subunits and their relative abundance was much higher compared to all other detected proteins (**Supplementary Table 1**). Even though, the NaCl wash removed large amount of PIPs, the final sample still contained in sub-stoichiometric amounts extrinsic ubiquitin receptors RAD23A and RAD23B, deubiquitinating enzymes USP14 and UCHL5, E3 ubiquitin ligase UBE3A, and in trace amounts adaptor protein ECM29 and VCP complex (**Supplementary Table 1**). Having a 26S proteasome sample completely depleted of the PIPs, would have been better to eliminate their effects on the 26S proteasome degradation assays, but this requires the use of higher NaCl concentration. However, higher salt wash could compromise the stability of the 26S proteasome, as it was shown that under high salt concentrations the 26S proteasome complex disassembles into 19S RP and 20S CP (Leggett et al., 2002; Sonn-Segev et al., 2020).

In the second approach, the 26S proteasomes were purified from cytoplasmic HeLa cell extracts (kindly provided by H. Stark lab, *MPI Göttingen*) using the protocol adapted from (Besche and Goldberg, 2012). The general outline of the affinity purification procedure is depicted in **Figure 4.2 A**. and described in Section 3.2.4.1 of Materials and Methods. In this protocol, the bait protein GST-UBL was used to affinity purify 26S proteasomes. The UBL domain of the bait protein corresponds to Ubiquitin Like Domain derived from the human RAD23B, an extrinsic ubiquitin receptor that binds Rpn10 subunit of the 19S RP. The elution of the 26S proteasomes was done with hHisUIM that contains human Rpn10's Ubiquitin Interacting Motif (UIM) that competes with Rpn10 for UBL binding. All the purification steps were analyzed on SDS-PAGE (**Figure 4.2 B**). The band pattern of the 26S proteasome complex can be seen in fraction hHisUIM elution and in fractions HisTrap FT - A2-A6. The fractions containing proteasomes after HisTrap were pooled together, and protein concentration was measured using the Bradford assay. On average, I obtained ~1 mg of HeLa 26S proteasomes from 50 mL of cytoplasmic extract.

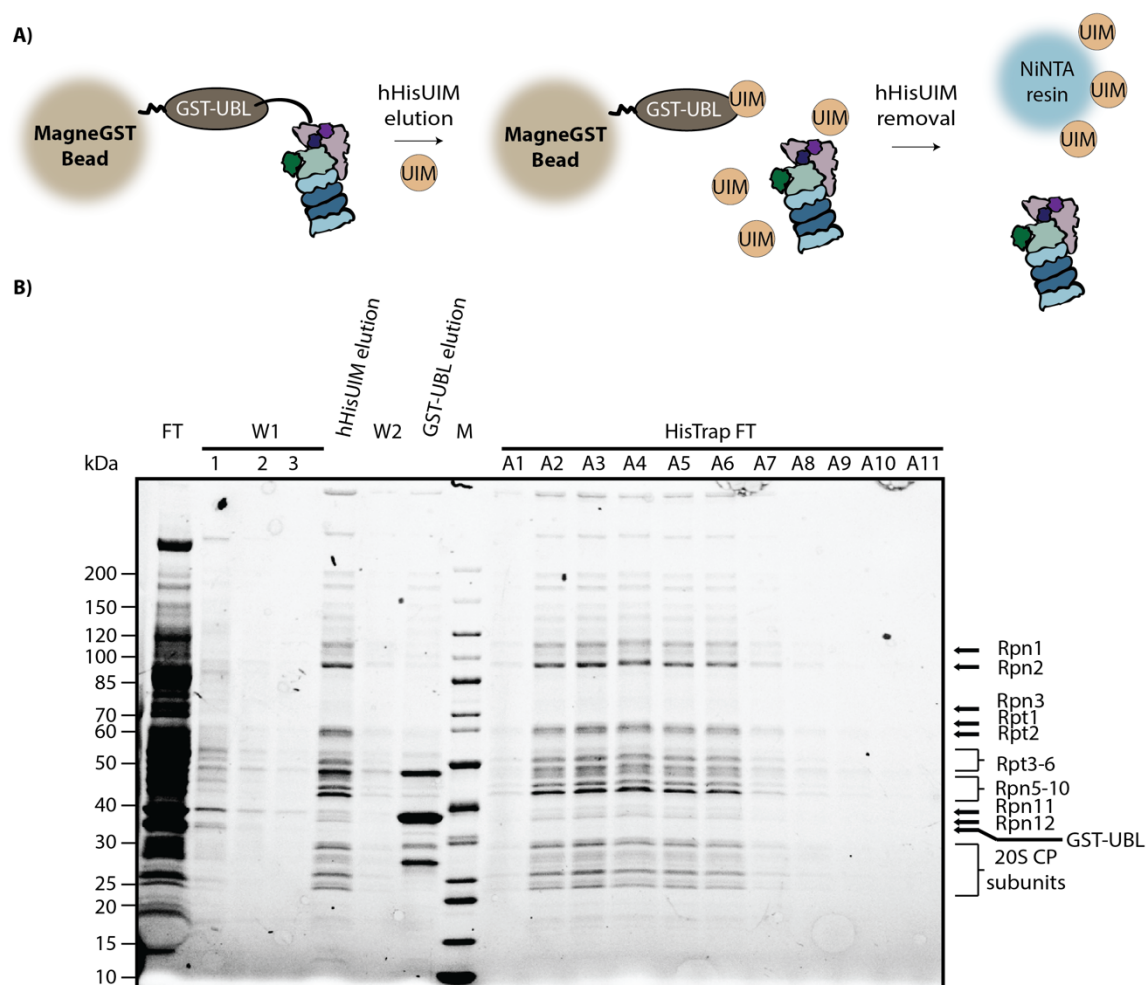


Figure 4.2 Affinity purification of 26S proteasome complexes from HeLa cells.

A) Schematic representation of affinity purification steps.

B) SDS-PAGE analysis of the purification. On the right, the positions of corresponding subcomplexes/subunits of the 26S proteasome complex are indicated. After the elution of 26S proteasomes from GST-UBL, GST-UBL itself was eluted using GSH containing buffer and the position of corresponding GST-UBL band is indicated with the arrow on the right. W1 lanes represent the wash after GST-UBL + 26S proteasome binding and W2 lane represents the wash done after hHisUIM elution of 26S proteasomes from GST-UBL in order to collect the remaining 26S proteasomes. The image was taken using a Stain-free channel. FT – flowthrough, W – wash, M – PageRuler unstained protein ladder.

The fraction HisTrap FT - A2 was submitted for mass spectrometry analysis (K. Mechtler lab, *Protein Chemistry facility, IMBA, Vienna Austria*). As for 26S proteasome sample from HEK293GP cells, all constitutive 26S proteasome subunits were identified with their relative abundance being higher compared to identified PIPs (**Supplementary Table 2**).

The detected PIPs were the same to the ones found in the sample from HEK293GP cells and in addition, TXNL1, HASPB1 and PAAF1 were also detected (**Supplementary Table 2**).

4.1.2. Purification of recombinant ZFAND2a-MBP-6xHis protein

Human ZFAND2a protein is a small protein with a molecular mass of ~20 kDa predicted to contain two terminal Zinc finger-AN1 domains connected via a flexible linker. Due to its small size and previously published work with recombinant ZFAND2a, I chose the *E.coli* expression system to recombinantly produce the ZFAND2a protein which I then used for functional and structural analysis with the 26S proteasome. Hence, human ZFAND2a protein was cloned with a C-terminal double affinity tag consisting of a Maltose binding protein (MBP) derived from *E.coli* followed by a polyhistidine tag (6xHis tag). A 3C cleavage site was introduced between the C-terminal end of ZFAND2a protein and the double-affinity tag (**Figure 4.3 A**). The affinity tag was placed at the C-terminus because it was reported that the N-terminal tag on ZFAND2a can obstruct proteasome binding (Stanhill et al., 2006).

Recombinant ZFAND2a-MBP-6xHis was purified in a three-step protocol described in detail in Section 3.2.3 of Materials and Methods. After each step, collected fractions were analyzed on SDS-PAGE (**Figure 4.3 B, C and D**). After the first purification step the protein was detected in a broad range of fractions (**Figure 4.3 B**). After the second purification step, the protein was detected in a fewer number of fractions compared to the elution profile from the previous step (**Figure 4.3 C**). However, the protein concentration in a single fraction seemed to be in the same range, assessed by the visual inspection of band intensities, thus indicating a loss in protein yield. Moreover, the second step did not significantly improve the overall sample purity. To improve the purity of the protein, a third purification step was performed (**Figure 1.3 D**). Similar to the previous step, the protein concentration in a single fraction seemed to be in the same range, assessed by visual inspection of the band intensities, thus indicating an additional loss in protein yield. Again, the overall sample purity did not seem to have improved significantly. Nevertheless, the fractions contained ZFAND2a-MBP-6xHis purified to >70% purity were pooled together, the protein was concentrated, and final protein concentration was measured based on the absorbance at 280 nm (A_{280}). On average, I was able to obtain 0.6 mg of protein from 44 g of bacterial cell pellet.

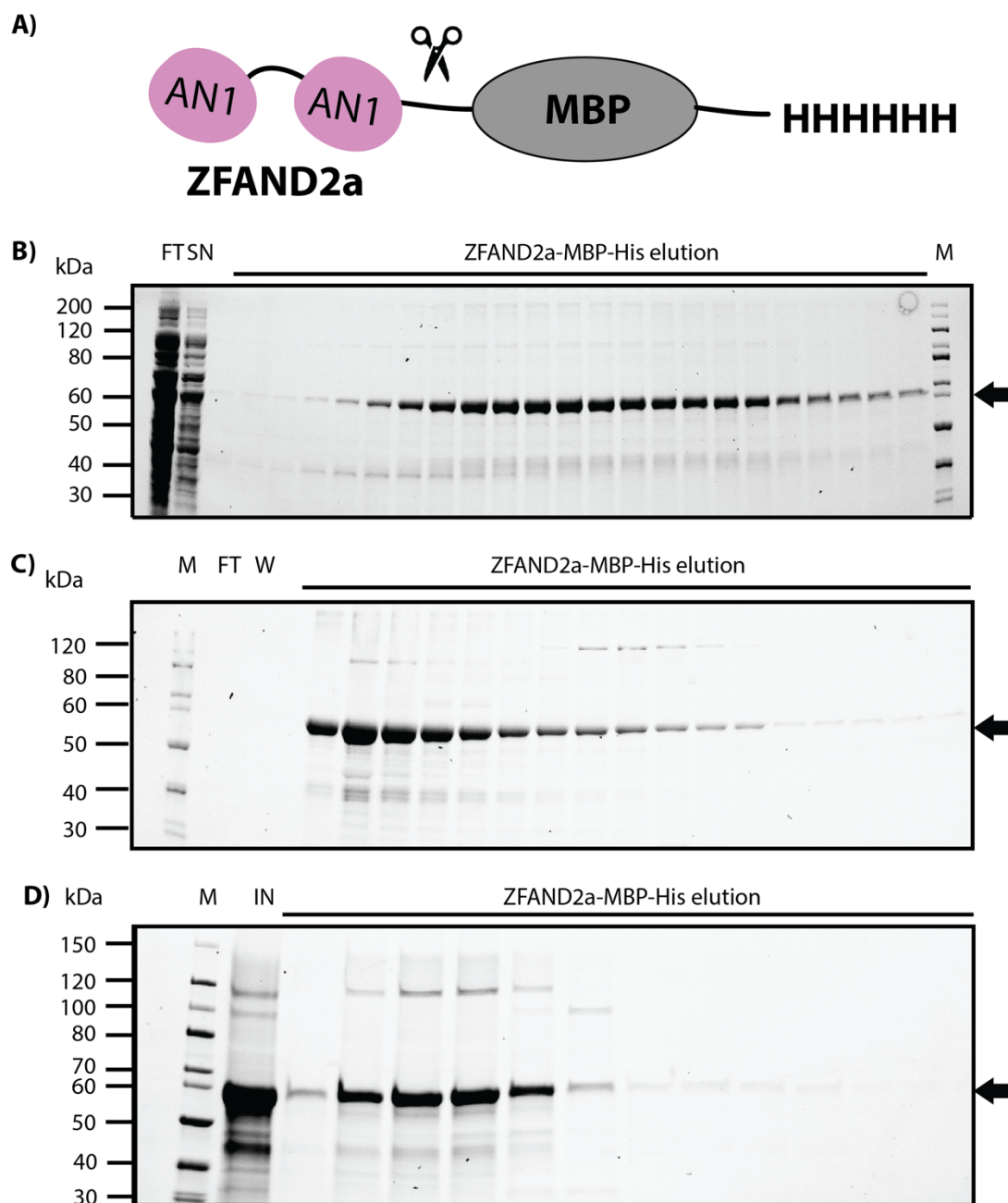


Figure 4.3. Purification of recombinant ZFAND2a-MBP-6xHis

A) Illustration of ZFAND2a construct. Cartoon scissors represent the 3C protease cleavage site. AN1 – Zinc Finger AN1 domain, MBP – Maltose Binding Protein, HHHHHH - 6xHis.

B) SDS-PAGE analysis of immobilized metal affinity chromatography (IMAC) purification step.

C) SDS-PAGE analysis of ion-exchange chromatography (IEX) purification step.

D) SDS-PAGE analysis of size-exclusion chromatography (SEC) purification step.

On the right, the position of the band corresponding to the monomeric ZFAND2a-MBP-6xHis protein (62.6 kDa) is indicated by the arrow. FT- flowthrough, W - wash, SN – supernatant, M - PageRuler unstained protein ladder, IN – input.

Although I introduced a cleavage site in the construct to obtain tag-less ZFAND2a, I could not produce a ZFAND2a protein without MBP-6xHis tag. A possible reason could be the formation of soluble protein aggregates at high protein concentrations potentially obstructing the 3C-protease cleavage site. Hence, for all experiments containing ZFAND2a, I used the tagged protein version.

4.1.3. Generation of proteasomal substrates

General requirements for a protein to be successfully degraded by the 26S proteasome have been characterized by many studies (Amici et al., 2004; Bragança and Kraut, 2020; Kahana et al., 2005; Martinez-Fonts et al., 2020; Petroski and Deshaies, 2003). These studies used a wide range of “model” proteasomal substrates. Nevertheless, the design of the substrates was highly influenced by the overall aim of those studies. Model proteasomal substrates usually contain at least three common elements: an unstructured initiation region, a proteasome targeting signal, and a stably folded domain. The unstructured initiation region is often arbitrarily chosen, or it is derived from known proteasomal substrates and often varies in length and sequence among different studies (Prakash et al., 2004). For the targeting signal, the substrate protein is usually expressed in-frame with a linear tetraubiquitin or a single ubiquitin which serves as an acceptor ubiquitin in ubiquitination reaction to build different types of polyubiquitin chains (Petroski and Deshaies, 2003). Alternatively, proteasome binding domains such as the UBL domain derived from RAD23B can be fused to deliver substrates to the 26S proteasome (Martinez-Fonts et al., 2020). Among folded protein domains, the most popular choice is the enzyme dihydrofolate reductase (DHFR) because it is possible to monitor its degradation by measuring an enzymatic activity or to manipulate its degradability through stabilization with substrate analog methotrexate (Johnston et al., 1995). Other commonly used model substrate is green fluorescent protein (GFP) or its variants, enhanced GFP (EGFP) or circular permutant GFP (cpGFP). They can be used as direct reporters of 26S proteasome activity using fluorescence measurement (Bragança and Kraut, 2020). Guided by the sum of knowledge from the above-mentioned studies, I designed different versions of model proteasomal substrates that should cause 26S proteasome malfunction through the introduction of a polyQ element assumed to stall 26S proteasome degradation. I also designed a control version that is efficiently degraded because it does not contain stalling element.

4.1.3.1. Strategy in substrate protein design

I have designed a total of seven different substrate proteins as potential candidates for investigating ZFAND2a's influence on 26S proteasome degradation (**Figure 4.4**). Each substrate protein contained the following domains listed from N- to C-terminus with their respective molecular weights indicated in brackets: first 95 amino acids derived from human Cyclin B (CycB(N95), 10.5 kDa), human dihydrofolate reductase (DHFR, 21.5 kDa), enhanced green fluorescent protein (EGFP, 26.9 kDa) and human ubiquitin (UB, 8 kDa) (**Figure 4.4**). CycB(N95) contains destruction box motif recognized by E3 ligase APC/C^{Cdh1} complex and serves as an unstructured initiation region. DHFR represents stably folded protein domain that requires ATP-dependent proteasome unfolding to get degraded whereas EGFP is used for detection through fluorescence imaging. Finally, C-terminal ubiquitin serves as an acceptor for the building of polyubiquitin chains necessary for substrate delivery to the 26S proteasome. For protein purification and western blot purposes, the substrate proteins were tagged on both N- and C-terminus, respectively. His-GST affinity tag (26.6 kDa) was attached to the N-terminus followed by a 3C protease cleavage sequence (depicted with cartoon scissors in **Figure 4.4**) and TwinStrep affinity tag (3.3 kDa) was attached to the C-terminus.

To cause proteasome malfunction, I have decided to introduce a long polyQ stretch, previously indicated to stall the processive 26S proteasome degradation. It was previously shown that shorter, non-pathological, polyglutamine stretches (<35Q) do not cause proteasome stalling while longer, pathological stretches stall the proteasome and render it malfunctioning, thus causing premature termination of protein degradation (Holmberg et al., 2004).

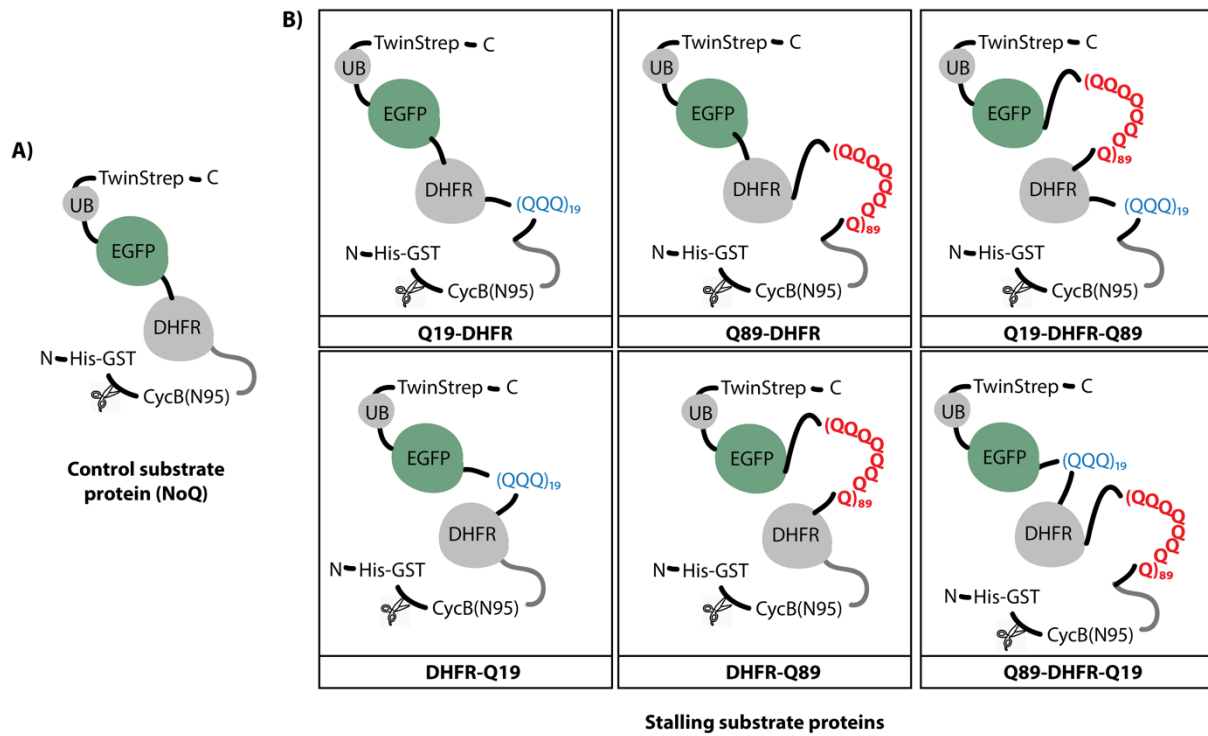


Figure 4.4. Schematic illustration of domain composition of designed substrate proteins.

A) Control substrate protein without an introduced polyQ stretch as proteasome stalling element.
B) Potential stalling substrate proteins that contain varying sizes and positions of introduced polyQ stretches as proteasome stalling elements.

The potential mechanism by which longer polyQ stretch causes the stalling of the 26S proteasome degradation is still not completely understood. One possibility could be that an encounter of a longer polyQ sequence with pore-1 loops of ATPase motor in charge of substrate translocation results in slippage or weaker pulling force by the proteasome's ATPase motor similar to the suggested stalling mechanism by glycine-alanine repeats (GAR) (Hoyt et al., 2006). This might render the 26S proteasome unable to unfold the protein domain following the longer polyQ stretch and terminate substrate processing. Alternatively, it is still a matter of debate whether the 26S proteasome stalling originates from inability of the proteasome to cleave inside a longer polyQ sequence (Pratt and Rechsteiner, 2008; Venkatraman et al., 2004). In case the 26S proteasome can only cleave at the border of a polyQ stretch, an uncleavable polyQ stretch, longer than 35 residues, that is already translocated inside the 20S CP, could potentially lead to clogging of the proteolytic chamber and halt further substrate processing.

In this study, I decided to introduce two sizes of polyQ stretches. A stretch of 19 (Q19) and/or 89 (Q89) glutamines were introduced into a sequence of substrate proteins in front of

and/or following the folded domain of DHFR (**Figure 4.4 B**). Hence, for model proteasome substrates designed in this study I expected that substrates containing Q19 (Q19-DHFR and DHFR-Q19) are, just like the control NoQ substrate, completely degradable by the 26S proteasome, while the degradation of substrates containing Q89 (Q89-DHFR, DHFRQ-Q89, Q19-DHFR-Q89, and Q89-DHFR-Q19) by the 26S proteasome is stalled and/or terminated at the position of where Q89 start. The size of degradation products after degradation of different substrates should be observed as a ~21 kDa difference when analyzed on SDS-PAGE, corresponding to the molecular size of DHFR domain that is either following or preceding the introduced Q89 stretch.

4.1.3.2. Purification of designed substrate proteins

Genes encoding for substrate proteins were ordered as synthetic genes, cloned, recombinantly expressed in *E.coli* cells and purified using affinity purification described in Section 3.2.3.5 of Materials and Methods. The steps during purification were analyzed on SDS-PAGE (**Figure 4.5**). All seven substrate proteins were successfully purified with varying yields as can be seen when comparing Elution 1 (E1) and Elution 2 (E2) lanes from different substrate proteins in **Figure 4.5**. Double bands are detected in Elution lanes due to EGFP taking on different folding states which have distinct migration properties in polyacrylamide gel because of only partial denaturation in SDS sample buffer (Martinez-Fonts et al., 2016). Since *E.coli* cells also express their endogenous GST, a strong band corresponding to the size of GST (22.8 kDa) is also detected in Elution lanes.

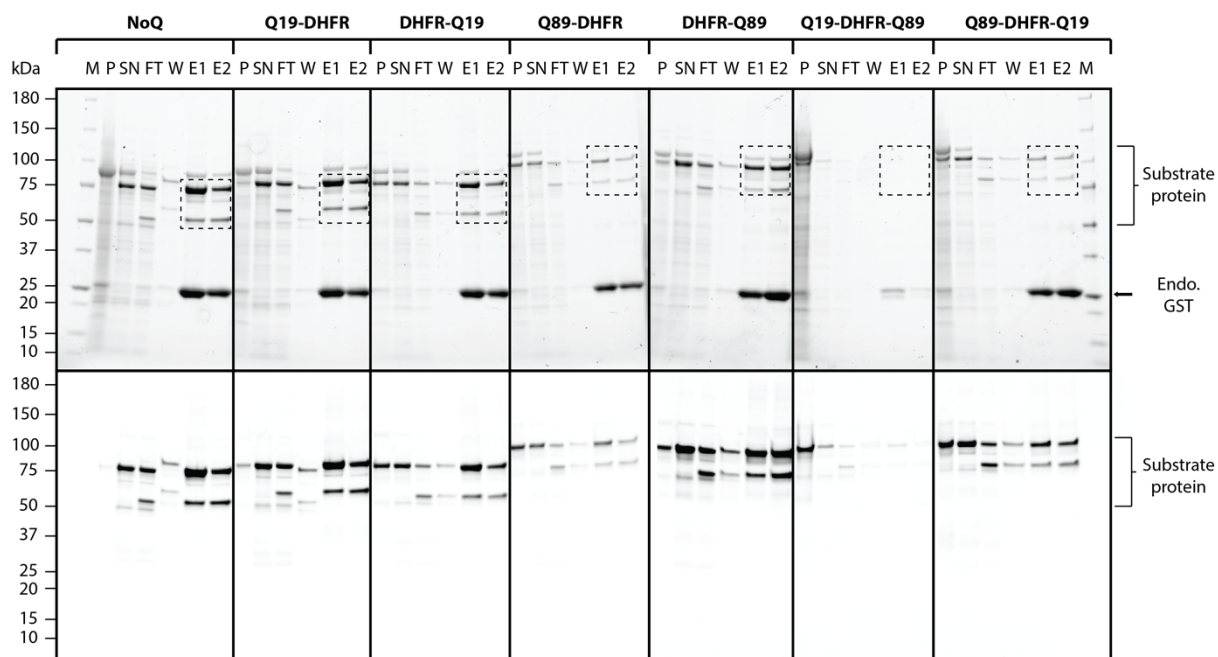


Figure 4.5. SDS-PAGE analysis of affinity purification of designed substrate proteins.

On the right the enclosing brackets and dashed squares on the gel image mark the positions of individual bands corresponding to substrate proteins and the arrow indicates the position of endogenous *E.coli* GST (Endo. GST) co-pulled with tagged protein. The upper panel represents a Stain-free image, and the lower panel represents an image of EGFP fluorescence. M – PageRuler unstained protein ladder, P – pellet, SN – supernatant, FT – flowthrough, W – wash, E – elution.

The purified proteins were concentrated, and the protein concentration was measured using EGFP fluorescence to avoid overestimation of protein concentration due to the presence of co-purified endogenous GST. In the shown purification example only Q19-DHFR-Q89 substrate protein was not purified in a measurable amount. However, subsequent repetition of the same purification yielded comparable amounts of this substrate protein compared to the others (**Supplementary Figure 2**). The purification yield varied among different substrate proteins and on average, I obtained 5-18 mg of protein from 25-30 g of bacterial cell pellet.

The proteasomal substrate proteins I designed in this study have a molecular weight between 90 and 112 kDa, the protein size considered to be challenging for the successful expression in *E.coli* cells (Rosano and Ceccarelli, 2014). Therefore, to make sure that the substrate proteins were expressed and purified as intact proteins, anti-GST western blot was performed against N-terminal GST tag in combination with anti-Strep western blot against C-terminal Twin-Strep tag (**Figure 4.6**). Western blot against either of the tags detected double

bands in Elution (E) lanes, as observed previously in the Fluorescence image of substrate protein purification (**Figure 4.5**). The same bands were detected using anti-GST and anti-Strep antibodies, albeit with different intensities mostly due to different binding and detection efficiencies of two antibodies. The detection of both termini being present confirmed that the substrate proteins were purified as full-length substrate proteins. In addition, anti-GST western blot confirmed that the strong band detected at ~25 kDa is indeed endogenous GST (**Figure 4.6**).

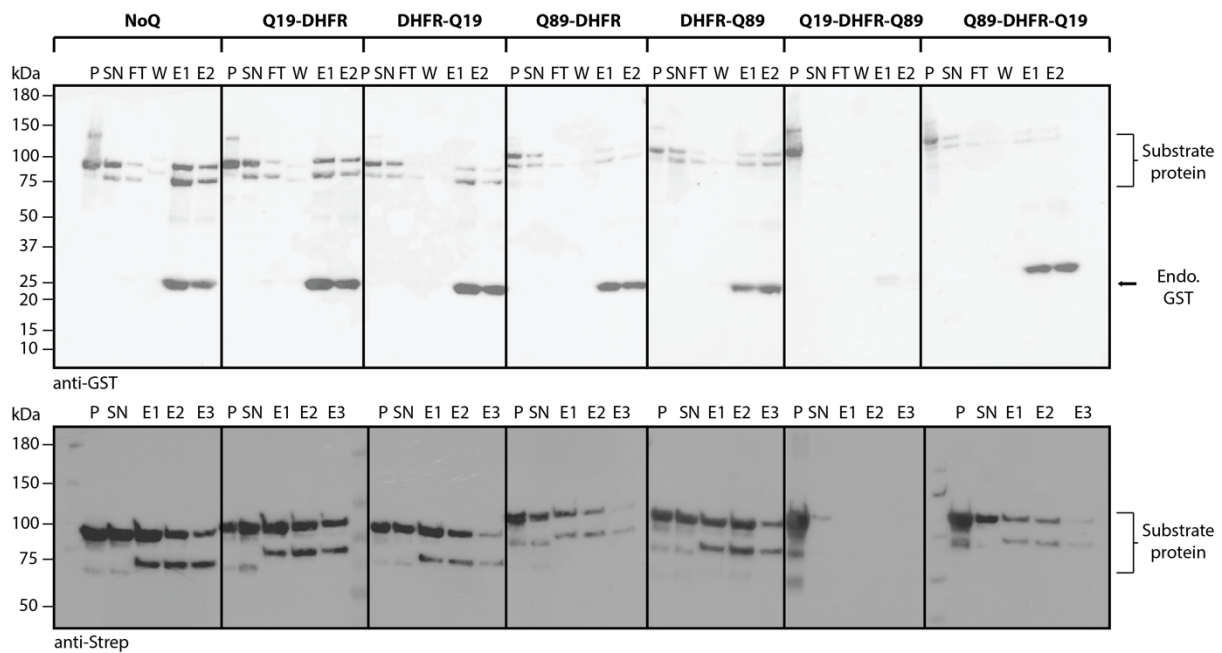


Figure 4.6. Western blot analysis of affinity purification of substrate proteins.

The upper panel represents anti-GST western blot, and the lower panel represents anti-Strep western blot. On the right, the position of endogenous *E.coli* GST (Endo. GST) co-pulled with tagged proteins is indicated together with double-band positions corresponding to substrate proteins. The nitrocellulose membranes were visualized using a Chemiluminescence channel. P – pellet, SN - supernatant, FT – flowthrough, W – wash, E – elution.

In addition to the western blot analysis, all resolved protein bands for the substrate proteins were excised from the polyacrylamide gels and submitted for mass spectrometry analysis (K. Mechtler lab, *Protein Chemistry facility, IMBA, Vienna Austria*). Peptide identification analysis showed the presence of peptides originating from full-length substrate proteins (**Supplementary Table S3**). This result further confirms that the substrate proteins

were expressed and purified as intact protein species and that both bands visualized on the SDS-PAGE correspond to full-length proteins.

4.1.3.3. Ubiquitination of substrate proteins

In cells, the protein needs to carry a degradation tag, most often in a form of a polyubiquitin chain, to be targeted to the 26S proteasome for degradation (Hershko et al., 1980). For this purpose, purified substrate proteins were polyubiquitinated using two different ubiquitination reactions. The reactions differed in the type and number of polyubiquitin chains added to the substrate protein as this can infer different degradation properties by the 26S proteasome (Martinez-Fonts et al., 2020).

The most common type of polyubiquitin chain that targets the proteins for degradation in cells is the K48-type ubiquitin chain (Gordon et al., 2003). To build K48-type ubiquitin chains, substrate proteins were polyubiquitinated in a reaction catalyzed by E1 enzyme Uba1 that activates ubiquitin in an ATP-dependent manner and E3-independent E2 enzyme SuperE2 that adds activated ubiquitin on an existing ubiquitin present at the C-terminus of substrate proteins. Consequently, substrate proteins were polyubiquitinated with a single linear K48-type polyubiquitin chain positioned at the protein's C-terminus (**Figure 4.7**). Different time points during ubiquitination reaction were analyzed on SDS-PAGE and substrate species were visualized using EGFP fluorescence to confirm that the reaction was indeed taking place (**Figure 4.7**). After 3 hours, the appearance of higher molecular weight bands (marked by Ubn-Sub) can be observed, indicating successful building of K48-type polyubiquitin chains. Due to the high molecular weight of substrates containing Q19/Q89, instead of individual bands, the polyubiquitinated species are observed as a smear above the non-ubiquitinated substrate protein (marked as Sub). As a control, if no ATP was added to the reaction, which is required for the ubiquitin activation by Uba1, there were no higher molecular weight species observed at the final time point.

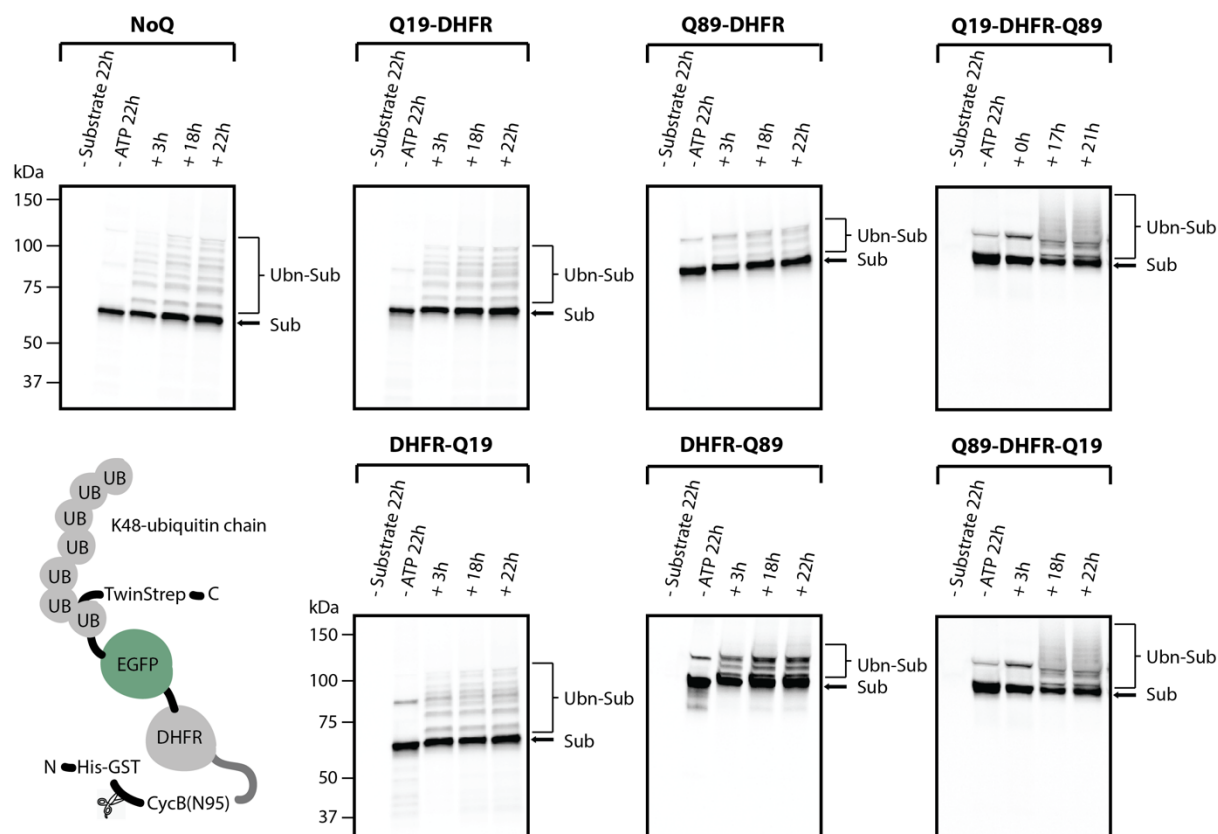


Figure 4.7. SDS-PAGE analysis of ubiquitination reaction of substrate proteins catalyzed by Uba1/SuperE2.

In the bottom left corner, a schematic of SuperE2 K48-polyubiquitinated control NoQ substrate is illustrated. On the right of each gel panel, the arrow indicates the band corresponding to substrate protein without any added ubiquitin moieties (Sub), while the enclosed brackets indicate the polyubiquitinated substrate species (Ubn-Sub). For control reactions, - Substrate and - ATP, only final time-points were analyzed on SDS-PAGE. The image was taken using the Fluorescein channel.

Although SuperE2-mediated substrate protein ubiquitination was overall successful, the reaction efficiency did not reach 100% which would correspond to complete polyubiquitination of all substrate protein species. The SuperE2-mediated substrate ubiquitination had very low efficiency, albeit sufficient to produce enough material required for performing degradation and reconstitution assays.

In addition to K48-type polyubiquitination, certain proteins in cells, such as important cell cycle regulators cyclin B and securin, can be targeted to the 26S proteasome by being marked with branched K11/K48-type ubiquitin chains (Meyer and Rape, 2014). This type of polyubiquitination is carried out by APC/C^{Cdh1} in conjunction with Ubch10/Ube2S E2 enzymes

(King et al., 1995). Both securin and cyclin B1 contain destruction box (D-box) sequence motif that is recognized by Cdh1 adaptor protein which brings together the enzymatic machinery to carry out the ubiquitination (Penas et al., 2012). In this study, designed substrate proteins contained on their N-terminus first 95 amino acids derived from human cyclin B1 with D-box motif. Since Ube2S was unintentionally omitted from the reaction, the substrate proteins were in the end K11/K63-polyubiquitinated on their N-terminus in a reaction catalyzed by Uba1, Ubch10, and APC/C^{Cdh1}. Later communication with N.G Brown lab (*UNC School of Medicine*) led to the realization that in APC/C^{Cdh1} mediated ubiquitination reaction a K11/K63-polyubiquitin chain on the C-terminal ubiquitin was also built due to the presence of a lysine residue nearby. Hence, APC/C^{Cdh1} K11/K63-polyubiquitinated substrate proteins contained branched polyubiquitin chains positioned at the N-terminal CycB(N95) and at the C-terminal ubiquitin. Only NoQ and DHFR-Q89 substrate proteins were used as inputs for APC/C^{Cdh1} ubiquitination assay. During ubiquitination reactions, aliquots were taken at different time points and analyzed on SDS-PAGE. Substrate species were visualized using EGFP fluorescence to confirm the reaction was indeed taking place (**Figure 4.8**). After 5 hours, polyubiquitination can be observed by the appearance of higher molecular weight species (marked with Ubn-Sec in lanes 5h and O/N). The APC/C^{Cdh1} polyubiquitinated species are only visualized as a smear instead of individual bands as was the case with K48-polyubiquitinated substrates. This is most likely due to the much longer polyubiquitin chains built by APC/C^{Cdh1}. For control purposes, the omittance of ATP in the same reaction, abolished ubiquitination reaction as no visible higher molecular weight species appeared even after an overnight incubation.

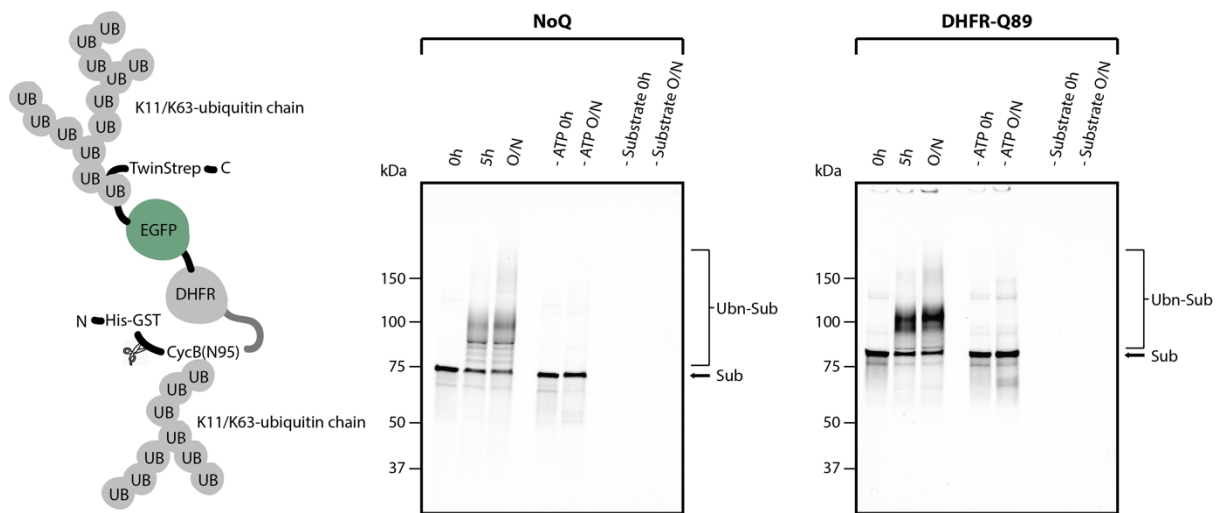


Figure 4.8. SDS-PAGE analysis of ubiquitination reaction of control NoQ and stalling DHFR-Q89 substrate proteins catalyzed by APC/C^{Cdh1}, Ubch10, and Uba1.

On the left, a schematic of APC/C^{Cdh1} K11/K63-polyubiquitinated control NoQ substrate is illustrated. On the right of each gel panel, the arrow indicates the band corresponding to substrate protein without any added ubiquitin moieties (Sub), while the enclosed brackets indicate the polyubiquitinated substrate species (Ubn-Sub). O/N – overnight. The image was taken using the Fluorescein channel.

Although slightly more efficient than E2-mediated ubiquitination reaction, the overall efficiency of APC/C^{Cdh1} mediated ubiquitination was still quite low, with approximately half of the initial amount of substrate protein (Sub) remaining without any polyubiquitin chain added. Nevertheless, the amount of polyubiquitinated substrate (UbnSub) was sufficient to carry out degradation assays.

The reasons for the low efficiency of both types of ubiquitination reactions most likely originate from input substrate proteins, as the same enzymes used under the same conditions and concentration ratios with different substrate proteins in the Haselbach lab resulted in much higher ubiquitination efficiency. It is probable that the elements required by ubiquitination machinery, C-terminal ubiquitin, and D-box in CycB(N95), were not easily accessible for ubiquitin conjugation either due to steric clashes with surrounding protein elements or more likely because of the partial aggregation of substrate proteins in solution.

4.1.3.4. Initial degradation screen with K48-polyubiquitinated substrates

First, I performed an initial degradation assay screen with K48-polyubiquitinated proteasomal substrates to test whether the control substrate was getting efficiently degraded by purified 26S proteasomes *in vitro* and which of the designed stalling substrates stalled proteasomal degradation and caused 26S proteasome malfunction. For this purpose, HeLa 26S proteasomes were added directly to the ubiquitination reaction together with additional ATP necessary for substrate unfolding and translocation into the 20S CP for degradation. In addition, a reaction with the deubiquitinating enzyme USP21 was carried out to depict the different outcomes when the proteasomal substrate is only deubiquitinated in comparison to when it is being deubiquitinated and degraded. The control reaction without any enzymes was performed to monitor the stability of EGFP fluorescence over time as the assay is performed overnight at 37°C. Initial and final timepoints were sampled and analyzed on SDS-PAGE (**Figure 4.9**). To focus the analysis on the fate of substrate protein, detection of EGFP fluorescence was used. Visualizing all proteins present in the reaction would interfere with distinguishing which bands correspond to the substrate protein and which correspond to components of ubiquitination machinery.

In control reaction without any enzymes (Sub Ctrl lanes) EGFP fluorescence only slightly faded over the time course of the reaction, and after 24h the bands of non-ubiquitinated (Sub) and polyubiquitinated species (Ubn-Sub) were still present (**Figure 4.9**). The appearance of higher molecular weight species after 24h in some of the Sub Ctrl lanes is probably a result of a partial protein aggregation over time. Due to a loading error, this control is absent in one of the reactions with Q89-DHFR-Q19. USP21 successfully deubiquitinated all substrate species as can be observed by the disappearance of Ubn-Sub bands in the USP21 24h lane compared to USP21 0h lane from USP21 reaction (**Figure 4.9**). The reactions containing 26S proteasomes also showed deubiquitination activity when comparing lanes 26S 0h and 26S 24h, albeit at a lower efficiency when compared to USP21 (compare lanes USP21 24h and 26S 24h) (**Figure 4.9**). More importantly, in the presence of 26S proteasomes after 24h protein bands with a molecular weight lower than the size of the full-length substrate protein accumulated (Deg-Sub). The accumulation of such bands is indicative of substrate degradation by the 26S proteasome.

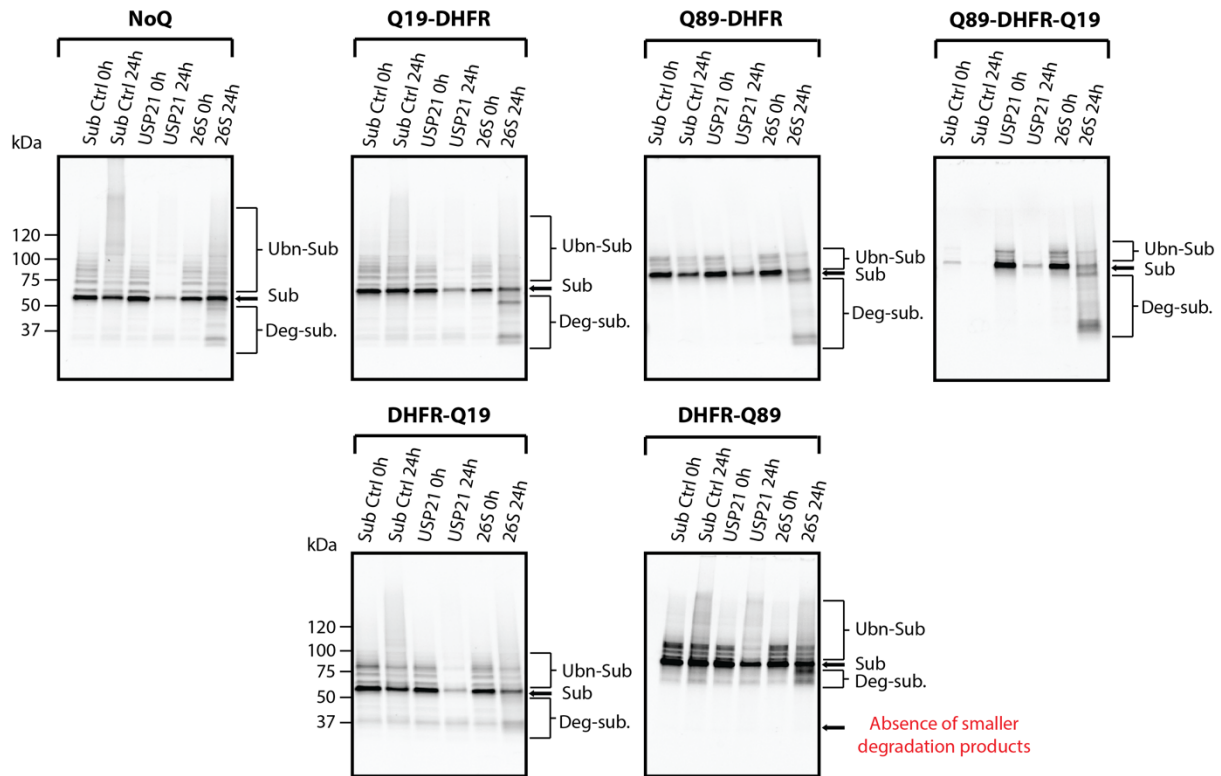


Figure 4.9. SDS-PAGE analysis of initial degradation assay with K48-polyubiquitinated substrates and HeLa 26S proteasomes.

On the right the arrow indicates the band corresponding to substrate protein without any added ubiquitin moieties (Sub), the enclosed brackets indicate the polyubiquitinated substrate species (Ubn-Sub), and the bands corresponding to degradation intermediates (Deg-Sub). The initial degradation assay screen did not involve Q19-DHFR-Q89 substrate because this substrate protein was not available at the time. I assumed that reaction with Q19-DHFR-Q89 substrate would give the same result as the reaction with DHFR-Q89 substrate. The image was taken using the Fluorescein channel.

The smallest accumulating degradation fragment detected has a molecular weight of ~37 kDa. Since this fragment shows a signal when detecting EGFP fluorescence and the degradation is assumed to be initiated from the N-terminal part of the substrate protein, this fragment corresponds to the size of the EGFP-Ub-TwinStrep region of the full-length substrate protein. This ~37 kDa degradation fragment is observed in almost all reactions, including reaction with control NoQ substrate, and is only not observed in the reaction with DHFR-Q89 substrate. These observations indicate that once the 26S proteasome reaches the EGFP part of the model proteasomal substrate designed in this study, EGFP is not getting degraded with 100% efficiency by the 26S proteasome *in vitro*. Moreover, the lower efficiency of EGFP

processing by the 26S proteasome is occurring regardless of the presence of polyQ stretches. This is evident since in reaction with control NoQ substrate the same EGFP-Ub-TwinStrep degradation fragment is detected as in reactions with substrates that do contain polyQ stretches (Q19-DHFR, DHFR-Q19, Q89-DHFR, Q89-DHFR-Q19) (**Figure 4.9**). These results are in agreement with previous observations made by others showing that different GFP variants have different susceptibility to getting degraded by the 26S proteasome *in vitro* due to differences in intrinsic protein stabilities (Bragança and Kraut, 2020). Among them, the EGFP was shown to be least efficiently degraded as it most likely represents the biggest unfolding challenge for the proteasomal ATPases due to its compact β -barrel structure (Bragança and Kraut, 2020).

The only exception to described degradation pattern was observed in the reaction with DHFR-Q89 substrate in which the smallest degradation fragment detected by the accumulation of intensity in this gel area has a size of ~55 kDa (**Figure 4.9**). This indicates that the degradation of this substrate protein was terminated earlier in the protein sequence compared to other substrate proteins. The fragment size comprising of Q89-EGFP-Ub-TwinStrep would have a mass of ~50 kDa which is close to the observed smallest degradation fragment size in the reaction with DHFR-Q89 substrate. Here it is important to note that long polyQ stretches in proteins can interfere with protein mobility in polyacrylamide gels (Holmberg et al., 2004). Hence, it is not entirely trustworthy to base conclusions solely upon the apparent protein size but to consider the relative position differences between the smallest fragments observed in reactions with other substrates and the ones observed in reaction with DHFR-Q89 substrate. In summary, the detection of ~55 kDa band as the smallest degradation fragment in reaction with DHFR-Q89 substrate indicates that most likely the Q89 stretch positioned upstream of EGFP leads to stalling and causes 26S proteasome malfunction.

Surprisingly, I did not observe stalling of proteasomal degradation when the Q89 is positioned in front of DHFR domain in Q89-DHFR and Q89-DHFR-Q19 substrates. This lack of stalling effect confirms that pathological polyQ stretches stall 26S proteasome degradation depending on the context in which they are present in the substrate in a similar fashion that was observed for GAR (Daskalogianni et al., 2008). In this case, I reason that DHFR unfolding is energetically less demanding than EGFP unfolding to allow translocation of the polypeptide inside the 20S CP for degradation. In other words, the steric influence of the introduced Q89 region inside the polypeptide chain on substrate unfolding and translocation is perhaps not severe enough for impeding DHFR unfolding by the ATPase motor and subsequent degradation. Moreover, in this study I did observe that the 26S proteasome was able to degrade through Q89 stretch present in Q89-DHFR and Q89-DHFR-Q19 substrates. This result speaks

against the clogging of the proteolytic chamber with a too long uncleavable protein stretch as an underlying mechanism of polyQ-mediated 26S proteasome malfunction as some studies suggest (Venkatraman et al., 2004).

4.1.3.5. Separation of polyubiquitinated from non-ubiquitinated substrate species

The initial degradation assay provided me with an insight into which of the potential stalling substrates indeed cause proteasome stalling by the introduced polyQ stretches. However, the input into the initial degradation reaction still contained enzymes of ubiquitination machinery and free ubiquitin chains and monomers. These components could potentially interfere with the kinetics of the substrate protein degradation. In particular, free ubiquitin chains were shown to compete with proteasomal substrates for binding to the 26S proteasome and slowing down their degradation *in vitro* (Thrower et al., 2000). To avoid this inhibitory effect while investigating 26S proteasome degradation of control and stalling substrate proteins in the presence or absence of ZFAND2a, the ubiquitination reaction was subjected to size-exclusion chromatography. This chromatography step removes the ubiquitination enzymes and free ubiquitin. Also, it allowed to a certain extent, the separation of polyubiquitinated from non-ubiquitinated proteasomal substrate proteins.

Ubiquitination reactions containing K48(NoQ) and K48(Q19-DHFR-Q89) substrates as well as K11/K63(NoQ) and K11/K63(DHFR-Q89) substrates were separated on an analytical size-exclusion chromatography column and collected fractions were analyzed on SDS-PAGE. Substrate bands were detected using EGFP fluorescence (**Figure 4.10** and **Figure 4.11**). The separation of K48(NoQ) substrate resulted in almost complete separation of polyubiquitinated from non-ubiquitinated species (lane 6, 7, and 8 in **Figure 4.10 A**), whereas separation of K48(Q19-DHFR-Q89) substrate resulted in a single fraction (lane 1 in **Figure 4.10 B**) that reached the level of separation similar to K48(NoQ) substrate. The separation of K11/K63(NoQ) and K11/K63(DHFR-Q89) substrates showed somewhat different behavior. A big portion of total protein input got eluted in the void volume or close to it (lanes 1, 2 and 3, **Figure 4.11 A and B**). This indicated that a large amount of the protein aggregated, either during the time course of ubiquitination reaction and/or upon freezing and thawing of ubiquitination reaction. The majority of non-ubiquitinated species and polyubiquitinated species with extremely long polyubiquitin chains (>200 kDa in molecular weight) but also one

portion of polyubiquitinated species with moderate chain length (120-150 kDa) was present in the void-volume fractions. I assume that the medium length (>9 ubiquitin moieties) polyubiquitin chains could have contributed to better solubility and attenuated complete aggregation of corresponding polyubiquitinated species. In contrast, the non-ubiquitinated substrate and the substrate with longer polyubiquitin chains had a higher propensity to aggregate. Indeed, it was previously shown in literature that very long polyubiquitin chains tend to lead to aggregation due to decrease in folding stability of the ubiquitin in longer chains (Morimoto et al., 2015). Despite the observed partial aggregation in the ubiquitination reactions, there was still enough amount of soluble polyubiquitinated protein (**Figure 4.11**, lanes 4-6 **A**) and lanes 5-10 **B**). The remaining soluble species were separated to a workable extent from non-ubiquitinated protein species. The fractions after SEC that contained soluble polyubiquitinated substrates were used as an input for *in vitro* degradation assay or *in vitro* reconstitution experiments.

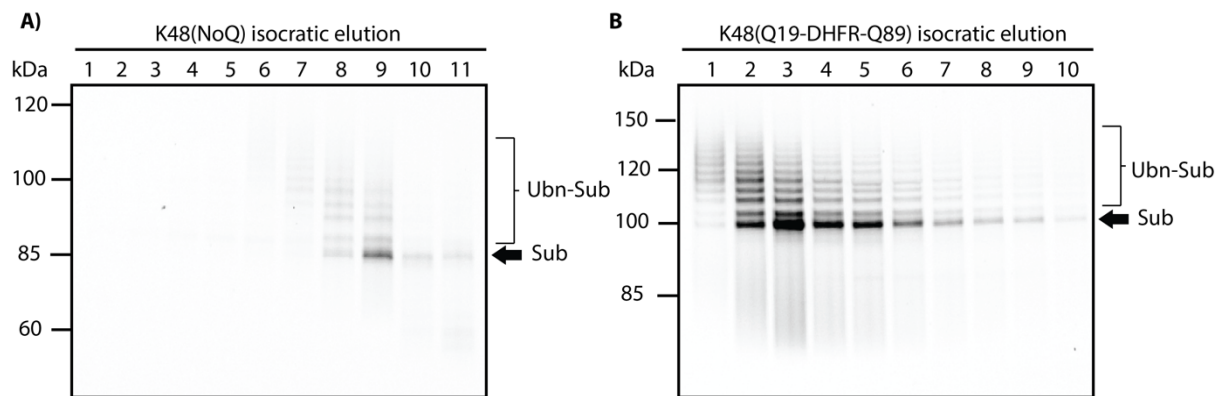


Figure 4.10. SDS-PAGE analysis of separation of K48-polyubiquitinated substrate species from non-ubiquitinated substrate species using size-exclusion chromatography. Fractions 7, 8, and 9 from K48(NoQ) substrate and fractions 1 and 2 from K48(Q19-DHFR-Q89) substrate were used in subsequent *in vitro* assays. The image was taken using the Fluorescein channel.

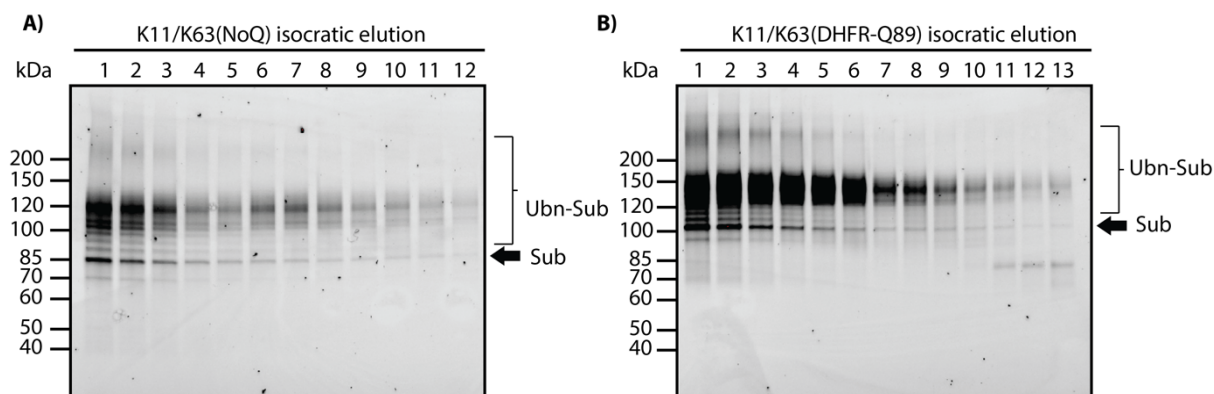


Figure 4.11. SDS-PAGE analysis of separation of K11/K63-polyubiquitinated substrate species from non-ubiquitinated substrate species using size-exclusion chromatography. Fractions 4-10 from K11/K63(NoQ) substrate and fractions 4-10 from K11/K63(DHFR-Q89) substrate were used in subsequent *in vitro* assays. The image was taken using the Fluorescein channel.

4.3. Functional analysis of ZFAND2a-bound 26S proteasome complex

Once I prepared all the necessary components and verified control and identified stalling proteasomal substrates, I set out to test if, in the system with minimal components, ZFAND2a binding to the 26S proteasome would potentially result in the overall enhancement of protein degradation by the 26S proteasome. I envision that increased 26S proteasome activity upon ZFAND2a binding could compensate for the observed insufficient handling of substrate load by the UPS due to proteotoxic stress or expression of mutant, disease-related proteins such as mHTT. Alternatively, I wanted to test the possibility that ZFAND2a might also directly bind the malfunctioning 26S proteasomes stalled by toxic substrate. I hypothesize that in such scenario, the ZFAND2a binding could energetically favor and enable coordinated conformational changes of proteasomal subunits to restore the 26S proteasome function. Consequently, the 26S proteasome conformational movements upon ZFAND2a binding would result in efficient processing of either misfolded proteins, or more specific, substrates with stalling elements like pathological polyQ stretches. To test these hypotheses, I used an established protocol for an *in vitro* degradation assay with purified components – 26S proteasomes, ZFAND2a-MBP-6xHis and control NoQ substrate or stalling DHFR-Q89 or Q19-DHFR-Q89 substrates carrying two different polyubiquitination signals.

4.3.1. SDS-PAGE analysis of degradation assay

In vitro degradation assays were set under single-turnover conditions. The assay with control K48(NoQ) or K11/K63(NoQ) substrate was performed to test if ZFAND2a binding would enhance overall activity of the 26S proteasome. The assay with stalling K48(Q19-DHFR-Q89) or K11/K63(DHFR-Q89) substrate was performed to investigate whether ZFAND2a binding could rescue malfunctioning 26S proteasomes and enable complete degradation of substrates with long polyQ stretches that otherwise stall the degradation. Substrates after analytical size exclusion were mixed with purified human HEK293GP 26S proteasomes in the presence or absence of ZFAND2a-MBP-6xHis in a stoichiometric ratio of 1:20 as described in Section 3.2.5.2 of Materials and Methods. Chosen time points throughout the assay were taken and analyzed on SDS-PAGE (**Figure 4.12** and **Figure 4.13**). In a similar fashion to the initial degradation assay, a control reaction containing only substrate was performed to control for the stability of EGFP fluorescence over time. In addition to imaging fluorescence, the gels were also stained with SafeBlue to detect ubiquitin released upon deubiquitination (**Figure 4.12** and **Figure 4.13**, bottom panel).

Efficient degradation of K48(NoQ) substrate by the 26S proteasome could be observed with the smallest degradation fragment having a molecular size of ~37 kDa (**Figure 4.12 A**). This was in accordance with the result obtained in the initial degradation assay (**Figure 4.9**). The same pattern of degradation fragments and extent of NoQ substrate degradation was identified in the presence and absence of ZFAND2a, which suggests that the ZFAND2a binding did not enhance the overall rate of protein degradation by the 26S proteasome. However, after a more thoughtful analysis I rendered this assay as inconclusive since the first sampled time point seemed to be taken after the degradation was already almost done.

In contrast to the control substrate K48(NoQ), only partial degradation of the stalling K48(Q19-DHFR-Q89) substrate was observed. The smallest degradation fragment corresponds to a molecular weight of ~55 kDa assessed by the end range of a smear below a band representing full-length non-ubiquitinated substrate protein (**Figure 4.12 B**). This outcome is also in agreement with the result of the initial degradation assay (**Figure 4.9**). Any apparent difference in smear length could not be identified between the reaction containing ZFAND2a and the one that doesn't contain ZFAND2a. However, if ZFAND2a binding to the 26S proteasome would have enabled uninterrupted processing through polyQ stretches by the 26S proteasome, I expected the smear length in the reaction containing ZFAND2a to appear lower in the gel than in the reaction with no present ZFAND2a. Hence, I concluded that in this

in vitro setup and with our designed stalling Q19-DHFR-Q89 substrate, ZFAND2a does not enable 26S proteasome processing of long polyQ stretches in (K48)-polyubiquitinated substrate.

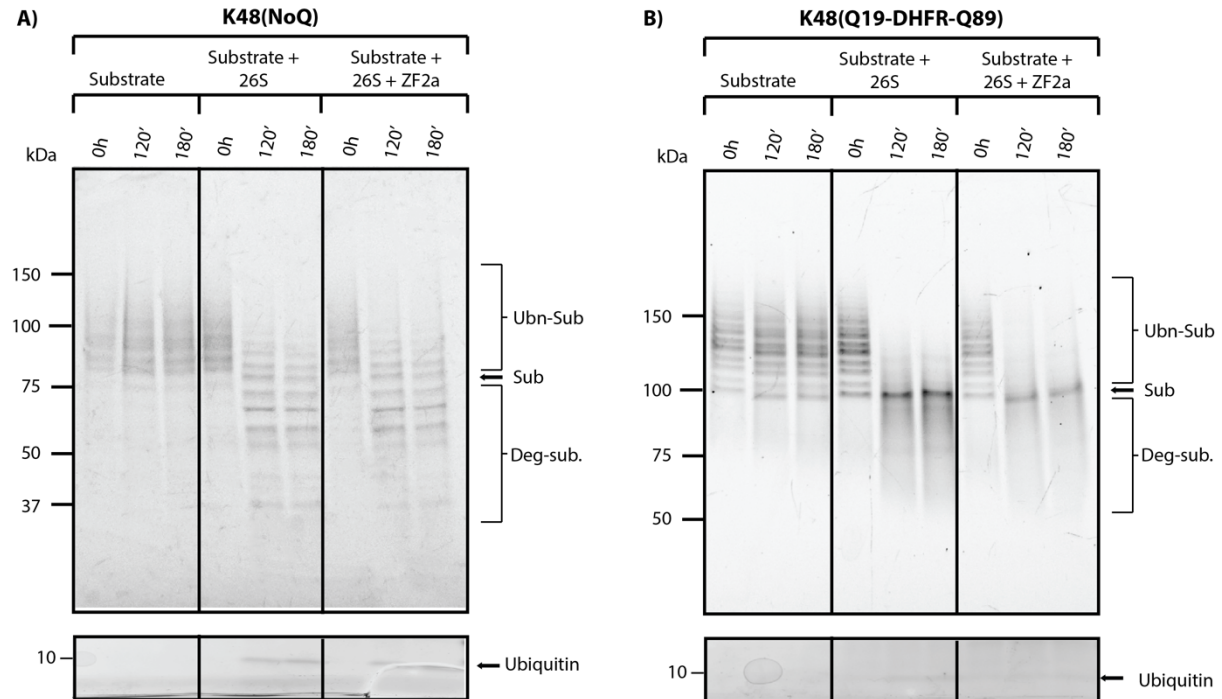


Figure 4.12. SDS-PAGE analysis of *in vitro* degradation assay with HEK293GP 26S proteasomes and control K48(NoQ) substrate or stalling K48(Q19-DHFR-Q89) substrate.

On the right side of the gel, the band position of non-ubiquitinated substrate (Sub) is indicated with an arrow, the band range representing polyubiquitinated substrate (Ubn-Sub) and degradation products (Deg-sub) is indicated with enclosing brackets. Ubiquitin band is indicated with an arrow in the lower panel. The upper image was taken using the Fluorescein channel. The bottom image was taken after overnight staining of the gel with SafeBlue and imaging with the Coomassie channel.

The same *in vitro* degradation assay was performed using control K11/K63(NoQ) substrate and stalling K11/K63(DHFR-Q89) substrate. By using differently polyubiquitinated substrates, I wanted to exclude the possibility that the type and number of polyubiquitin chains might influence the regulatory function of ZFAND2a when bound to the 26S proteasome. In this assay, I sampled more time points to avoid under-sampling as in the assay with K48-polyubiquitinated substrates.

Efficient degradation of the control K11/K63(NoQ) substrate can be observed up until the EGFP as again the smallest detected degradation fragment had a molecular weight of ~37 kDa (**Figure 4.13 A**). Contrary, the stalling K11/K63(DHFR-Q89) substrate was only degraded to the position of Q89 stretch preceding EGFP as the smallest detected degradation fragment had a molecular weight of ~55 kDa (**Figure 4.13 B**). A slight decrease in the overall rate of substrate deubiquitination was observed in the presence of ZFAND2a for both reactions. However, experiments with increasing ZFAND2a concentrations showed that this effect could be due to unspecific ZFAND2a-substrate interactions since when lower ZFAND2a concentrations were used the effect was no longer observed (**Figure S2**). Hence, I assume that the cause of decreased deubiquitination rate is probably due to unspecific interactions between much longer, aggregation-prone polyubiquitin chains on K11/K63-ubiquitinated substrates and ZFAND2a soluble aggregates present at higher ZFAND2a concentrations. These interactions most likely interfere with substrate binding and/or accommodation on the 26S proteasome.

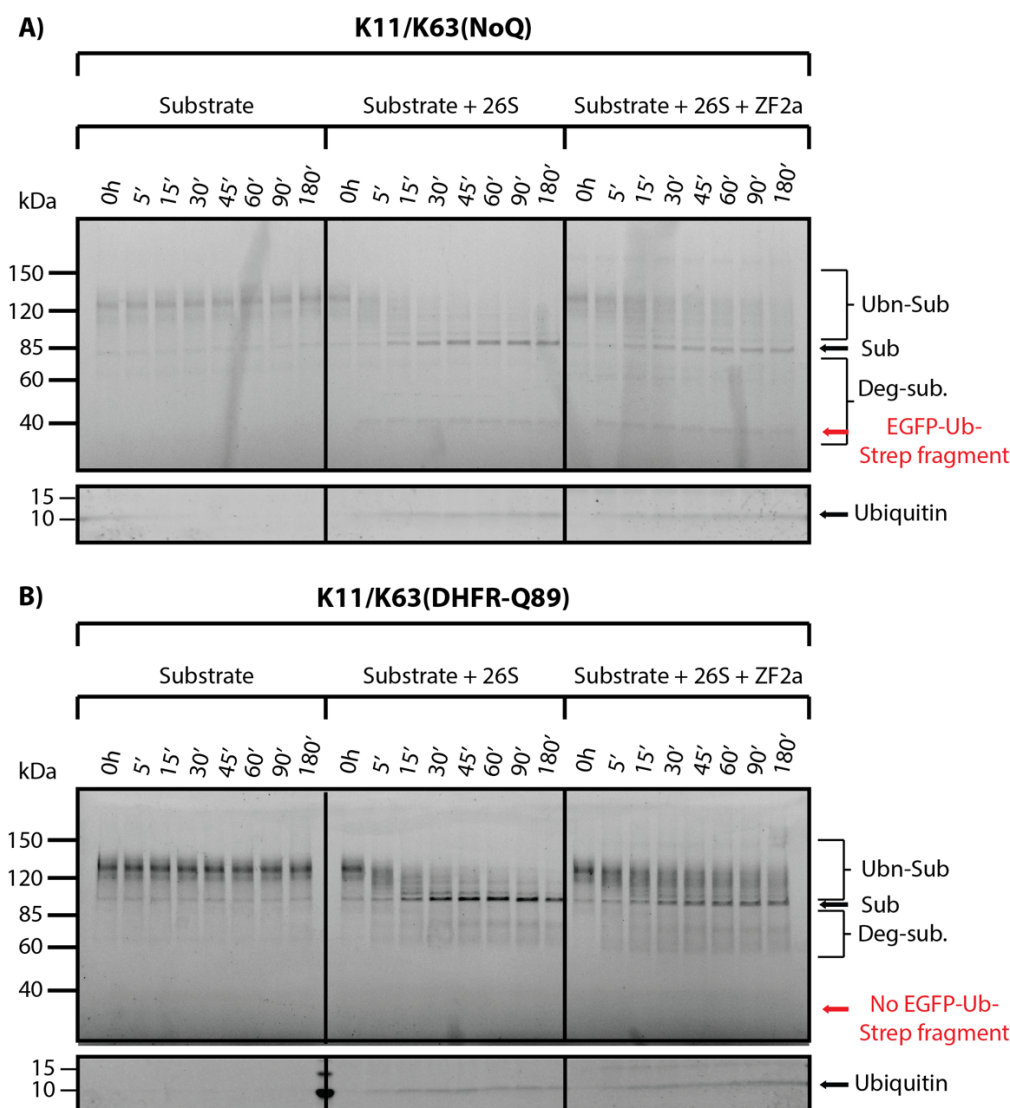


Figure 4.13. SDS-PAGE analysis of *in vitro* degradation assay with HEK293GP 26S proteasomes and K11/K63(NoQ) or K11/K63(DHFR-Q89) substrate.

On the right side of the gel, the band position of non-ubiquitinated substrate (Sub) is indicated with an arrow, the band range representing polyubiquitinated substrate (Ubn-Sub) and degradation products (Deg-sub) is indicated with enclosing brackets. The position of smallest degradation fragment EGFP-Ub-Strep is indicated with an arrow. Ubiquitin band is indicated with an arrow in the lower panel. The upper image was taken using the Fluorescein channel. The bottom image was taken after overnight staining of the gel with SafeBlue and imaging with the Coomassie channel.

The results I report in this study from the *in vitro* degradation assay with K11/K63(NoQ), also when repeated with decreased ZFAND2a concentrations to minimize the inhibitory effect of unspecific interactions, suggest that ZFAND2a binding to the 26S

proteasome in a minimal component system does not result in an increased rate of protein degradation. This is in accordance with another study where they also did not observe an increase in the degradation of tetraubiquitin-fused DHFR in the presence of N-terminally His-tagged ZFAND2a (Lee et al., 2018). However, these results were interpreted with caution since another study showed that N-terminally tagged ZFAND2a is not able to bind the 26S proteasome (Stanhill et al., 2006). Furthermore, the results of the *in vitro* degradation assay with stalling K11/K63(DHFR-Q89) substrate I reported in this study agree with our observations made with stalling K48(Q19-DHFR-Q89) substrate, that the 26S proteasome is not able to process Q89 stretch positioned upstream from EGFP. The inability to process these substrates was not influenced by different type of polyubiquitin chains or ZFAND2a presence. Based on these assays, I concluded that ZFAND2a binding does not seem to influence 26S proteasome to process substrates with long polyQ stretches in a minimal component system.

4.4. Structural analysis of ZFAND2a-bound 26S proteasome complex

In the second part of this work, I aimed to provide structural characterization of the ZFAND2a-bound 26S proteasome complex. Firstly, I wanted to identify the exact ZFAND2a binding site on the 19S RP. Secondly, I searched for additional clues regarding the regulatory nature and molecular mechanisms behind ZFAND2a binding to the 26S proteasome under conditions that compromise its function and the potential role in rescuing the stalled system.

The information about the exact ZFAND2a binding site on the 19S RP is fairly scarce and there is, to my knowledge, no available structural data on ZFAND2a-bound 26S proteasome complex. A study from 2006 identified Rpn1 in an immunoprecipitation experiment as the most likely subunit through which interaction between ZFAND2a and 26S proteasome is established (Stanhill et al., 2006). The same study attempted to structurally characterize the ZFAND2a-bound 26S proteasome complex by using negative stain single-particle transmission electron microscopy (nsTEM). In this method, a sample containing a complex of interest is applied onto an EM grid and is then embedded into a layer of a heavy metal salt solution, the excess of which is removed by blotting to a thin filter paper, and the grid is left to dry. Since the macromolecular complexes are then visualized based on the exclusion of the electron-dense stain, the method was termed negative staining (Ohi et al., 2004). This method allows quick and simple sample preparation to provide initial structural

insights. However, its drawbacks in limited achievable resolution and a high chance of macromolecular complex disintegration and architectural distortion restricts the quality of attainable information. Therefore, the aforementioned analysis of ZFAND2a-bound 26S proteasome complex by nsTEM was not high quality to discern individual subunits of the 19S RP, and ZFAND2a binding site (Stanhill et al., 2006).

Since then, another method named single-particle cryo-EM has been rapidly developed and optimized. This method does not suffer from the same consequences and limitations of nsTEM; besides, it can reach a higher resolution. In single-particle cryo-EM, the sample is not embedded in stain, but is rather vitrified in a very thin ice on an EM grid. Such sample preparation allows preservation of native macromolecular structures and, in an ideal case, does not cause severe damage to the specimen (Frank, 2002). These advantages of single-particle cryo-EM made it the method of choice for structural work during my doctorate studies.

4.4.1. Reconstitution of ZFAND2a-bound 26S proteasome complex

For structural analysis by single-particle cryo-EM, I used an *in vitro* reconstitution approach to obtain ZFAND2a-bound 26S proteasome complex in the presence of stalling substrate from individually purified components. Pull-down experiments in earlier studies reported that binding of ZFAND proteins, namely ZFAND2a and ZFAND1, to the 26S proteasome is compromised under ATP conditions and is enriched under ADP conditions (Stanhill et al., 2006, Turakhiya et al., 2018). Initially, I reasoned that perhaps ADP nucleotide condition favors certain 26S proteasome conformation that is preferably recognized and bound by ZFAND2a. However, data reported in the literature do not suggest that ADP condition results in a preference towards any particular 26S proteasome state under *in vitro* conditions, but it only slightly alters conformational equilibrium when compared to ATP nucleotide condition (Bard et al., 2018). It is also questionable whether a parallel can be drawn between *in vitro* observations and pull-down experiments performed from a cellular environment which contains all the other components of the UPS. One could imagine that one portion of the 26S proteasomes from cell extracts is actively engaged with a substrate. A sudden depletion of the ATP needed to actively translocate the substrate by conversion to ADP could potentially result in the substrate “stalling” in the translocation channel. Such an event might reflect the 26S proteasome stalling by toxic proteins or when treated with proteasome inhibitors, both conditions are known to induce ZFAND2a expression and binding to the 26S proteasome

(Stanhill et al., 2006). However, complete elimination of ATP from all steps during *in vitro* reconstitution reaction would impose a challenge in this study since the 26S proteasome requires ATP to initiate substrate unfolding and translocation prior to stalling. The ATP to ADP exchange most likely would not compromise the stability of the complex since ADP alone is sufficient for maintaining stable association of the 19S RP and the 20S CP. Taking all the aforementioned information, I reasoned that the presence of stalling substrate designed in this study, which mimics proteotoxicity, even under initial ATP conditions, might also push the 26S conformational equilibrium towards the state recognized and bound by ZFAND2a.

Finally, the reconstitution reaction contained HEK293GP 26S proteasomes and an excess of ZFAND2a-MBP-6xHis in the presence of low-nanomolar concentration of stalling K48(Q19-DHFR-Q89) substrate. As controls, reactions containing stalling substrate together with only ZFAND2a-MBP-6xHis or only 26S proteasomes were prepared (**Figure 4.14 A**). The input sample containing HEK293GP proteasomes that was used already contained ATP originating from the purification protocol described in Section 3.2.4.2 of Materials and Methods. As discussed, the presence of ATP at the beginning of the reaction allowed initial substrate engagement and translocation. After 10 min incubation on ice, the nucleotide equilibrium was shifted towards ADP conditions by adding hexokinase and D-glucose upon which hexokinase catalyzes the phosphorylation of D-glucose and converts ATP to ADP. ADP conditions ensured complete halt of 26S processing and could simultaneously stabilize ZFAND2a-bound 26S proteasome complex. Following the incubation and overnight ultracentrifugation on a sucrose gradient, different molecular complexes from each reaction were separated based on their densities. The gradients were manually fractionated and either all fractions or fractions assumed to contain a complex of interest were analyzed on SDS-PAGE (**Figure 4.14**).

In the gradient containing stalling K48(Q19-DHFR-Q89) substrate and ZFAND2a-MBP-6xHis reaction, ZFAND2a-MBP-6xHis was identified in fractions throughout the whole gradient with the major peak being in fractions 5-9 (**Figure 4.14 B**). According to ZFAND2a construct's molecular weight of ~62 kDa, ZFAND2a-MBP-6xHis was expected to remain at the top of the sucrose gradient. However, my previous assumption that ZFAND2a-MBP-6xHis forms soluble aggregates at higher concentrations due to its disordered nature was confirmed by its rather broad distribution in the first half of the gradient. The stalling K48(Q19-DHFR-Q89) substrate was similarly spread in the first half of the gradient. This was expected since individual substrate monomers have different polyubiquitin chain lengths attached and hence different densities. Throughout the gradient an additional subtle separation between non-

ubiquitinated substrate and polyubiquitinated substrate was achieved (**Figure 4.14 B**). The majority of non-ubiquitinated substrate remained in the first three gradient fractions, while the polyubiquitinated substrate was present in gradient fractions 4-15. Trace amounts of the non-ubiquitinated substrate could also be in fact detected throughout the whole gradient. I assume that this is most likely because the substrate protein aggregated during freeze/thaw cycles or simply over time due to the presence of aggregation-prone polyQ stretch.

In the gradient containing the reaction with all three components - the stalling K48(Q19-DHFR-Q89) substrate, the ZFAND2a-MBP-6xHis, and the 26S proteasome - the 26S proteasome characteristic band pattern was detected in fractions 11-13 (**Figure 4.14 C**). The protein peaks for ZFAND2a-MBP-6xHis and stalling substrate K48(Q19-DHFR-Q89) coincided with the 26S proteasome peak in fractions 11-13 and are slightly shifted towards the second half of the gradient when compared to the control gradient (**Figure 4.14 B**). Thus, I predicted that fractions 11-13 contained ZFAND2a-bound 26S proteasome complex and the stalling K48(Q19-DHFR-Q89) substrate. The presence of the 26S proteasome in the reconstitution reaction resulted in a narrower distribution of polyubiquitinated substrate species across the gradient. Since the 26S proteasome concentration is 10x the substrate concentration, all polyubiquitinated substrate species were expected to be at least bound to, if not engaged with the 26S proteasome. Moreover, the 26S proteasome species were expected to be in only few gradient fractions. Consequently, the polyubiquitinated substrate species are detected only in fractions that also contain the 26S proteasome complexes (**Figure 4.14 C and D**).

In the gradients that contained stalling K48(Q19-DHFR-Q89) substrate and 26S proteasome with or without ZFAND2a-MBP-6xHis, additional bands are detected in the gradient fractions 1-4 with an estimated molecular weight of ~75 kDa and ~60 kDa (**Figure 4.14 C and D**). This band size can be correlated with the size of degradation fragments I observed previously in SDS-PAGE analysis of the *in vitro* degradation assay. This indicates that the initial ATP conditions allowed engagement and partial processing of one portion of polyubiquitinated substrates. Partial processing of all the stalling K48(Q19-DHFR-Q89) substrate species was most likely prevented by depletion of ATP in the reconstitution reaction and by the fact that the sucrose gradient was supplemented with ADP. The ADP condition allowed the substrate species to remain bound or engaged with the intact 26S proteasome during the overnight experiment before making the cryo-EM grid with final sample preparation.

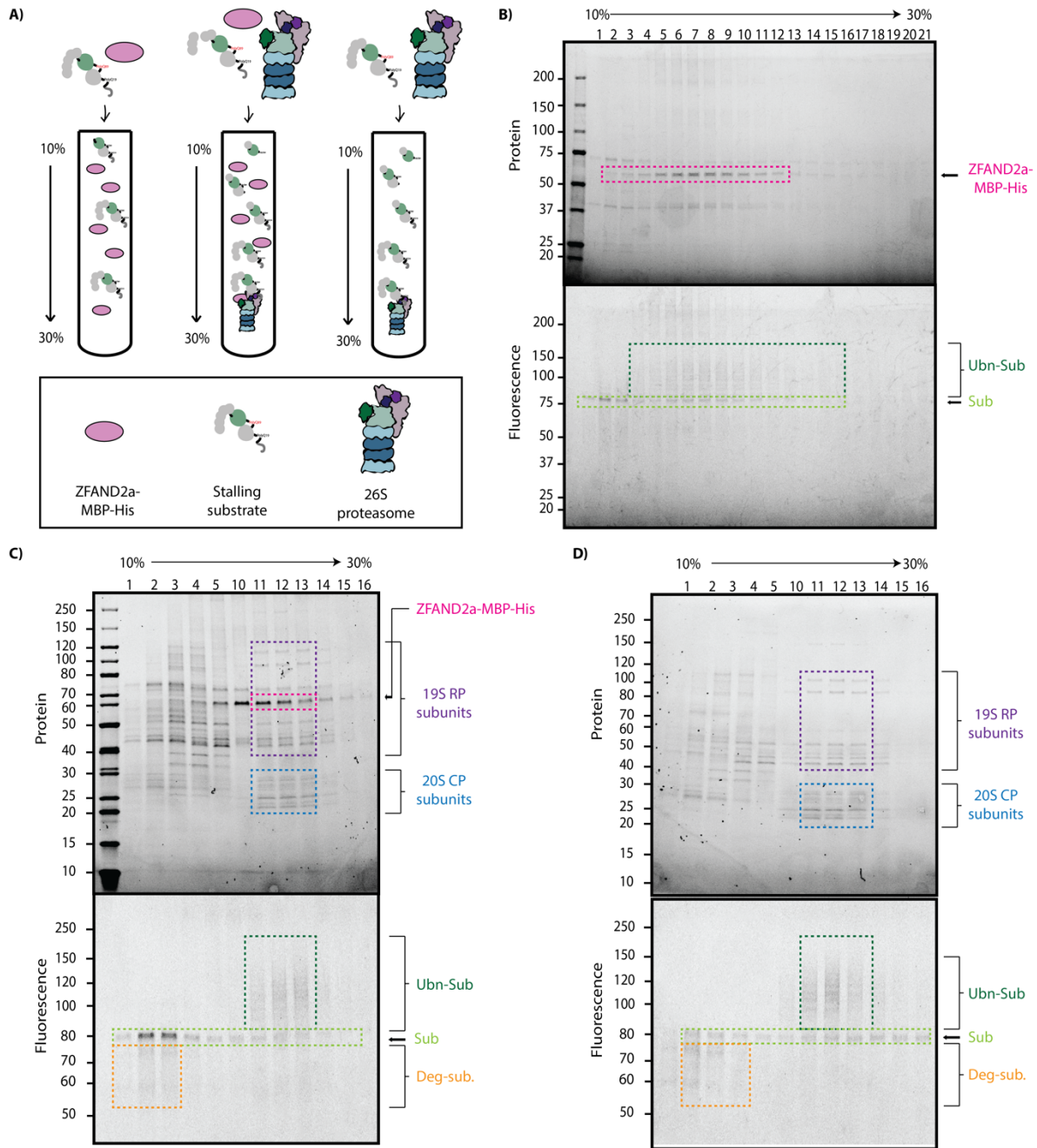


Figure 4.14. SDS-PAGE analysis of *in vitro* reconstitution reaction separation on a sucrose density gradient ultracentrifugation.

A) Schematic representation of different *in vitro* reconstitution reactions and the separation of individual components and complexes in a sucrose density gradient.

B) Control *in vitro* reconstitution with stalling K48(Q19-DHFR-Q89) substrate and ZFAND2a-MBP-6xHis.

C) *In vitro* reconstitution with 26S proteasome, ZFAND2a-MBP-6xHis, and stalling K48(Q19-DHFR-Q89) substrate.

D) *In vitro* reconstitution with 26S proteasome and stalling K48(Q19-DHFR-Q89) substrate.

On the right side of the Stain-free image, the positions of subunits of 26S proteasome subcomplexes are indicated with enclosed brackets and the position of ZFAND2a-MBP-6xHis is indicated with an arrow. On the right of the fluorescence image, the positions of polyubiquitinated (Ub-Sub), non-ubiquitinated substrate (Sub) as well as degradation products (Deg-Sub) are indicated. The bands of interest are enclosed with dashed squares on gel images. The gel was imaged with the Stain-free channel and the Fluorescein channel.

It was hypothesized that the long polyQ stretches permanently inhibit the 26S proteasome by staying stuck in the central channel; thus, inhibiting further binding and degradation of other cellular proteins. In such scenario, the potential rescue mechanism would include extraction of stalled substrates from the 26S proteasome, the role previously suggested for the VCP segregase (Isakov and Stanhill, 2011). However, results obtained during my doctorate studies suggest that the long polyQ stretch do not stay permanently stuck on the 26S proteasome once their degradation is stalled. This is supported by the detection of degradation intermediates in a separate fraction from 26S proteasomes indicating that upon the stalling of degradation at the polyQ stretch, the partially processed stalling K48(Q19-DHFR-Q89) substrate is being released from the 26S proteasomes, thus not leading to absolute and irreversible 26S proteasome inhibition (**Figure 4.14 C and D**). When contrary would be the case, I would expect the degradation intermediate bands to be detected in the same fraction with the 26S proteasomes. Furthermore, the release of stalled K48(Q19-DHFR-Q89) substrate took place regardless of whether the ZFAND2a-MBP-6xHis was present or not, arguing against the possibility that ZFAND2a binding enabled the release of partially processed and stalled substrates from the 26S proteasome central processing channel.

4.4.2. Cryo-EM analysis of ZFAND2a-bound 26S proteasome complex

The advantages of single-particle cryo-EM application made it a preferable method of choice for the investigation of the ZFAND2a-bound 26S proteasome complex structural features. For this purpose, fractions 12 and 13 from sucrose gradient with reconstitution reaction containing 26S proteasome, ZFAND2a-MBP-6xHis, and stalling K48(Q19DHFRQ89) substrate (**Figure 4.14 B**) were subjected to buffer exchange to remove sucrose and cryo-grids were frozen. After initial grid screening, the best grid was chosen for data collection. The details and theory regarding data acquisition and processing steps are described in Section 3.2.5 of Materials and Methods.

In a single collection on a Titan Krios cryo-TEM microscope 10,070 micrographs were collected (**Figure 4.15 A**) and imported in CryoSPARC software (Punjani et al., 2017) for initial preprocessing. After Motion correction and CTF estimation, 1,115 particles were manually picked from several randomly chosen micrographs and subjected to 2D classification. The resulting 2D class averages were manually inspected, and representative averages (**Figure 4.15 A**) were selected as input for automated template-based particle picking. Initially, 2,019,271 particles were picked (**Figure 4.15 C**). After filtering and extraction 1,527,949 particles were subjected to 2D classification. This step removed most of the false-positive picks containing empty micrograph regions, broken, aggregated or misfolded particles, or ice contaminations. After two rounds of 2D classification, selected 2D class averages contained 648,037 particles (**Figure 4.15 D**). Most particles represented the 26S proteasome, with a minor percentage of particles containing an additional 19S RP, thus representing the 30S proteasome. A subset of selected particles was used to calculate the *ab initio* model of 26S proteasome (**Figure 4.15 E**). The *ab initio* model is required as a reference for any further 3D processing.

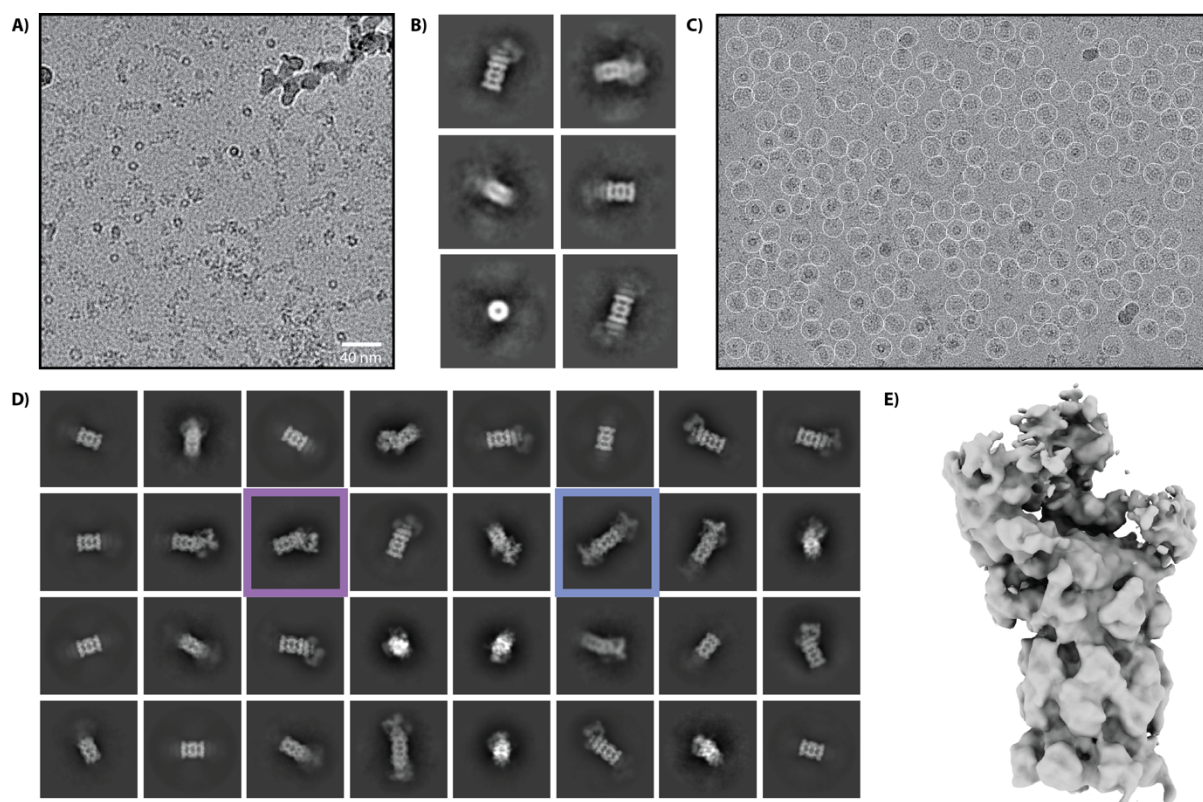


Figure 4.15. Initial cryo-EM preprocessing, particle localization, and calculation of *ab initio* model in CryoSPARC.

A) Representative cryo-EM raw micrograph after Motion correction.

B) 2D class averages used as templates for automated particle picking (template matching).

C) Representative micrograph with indicated picked particle locations after applying NCC Score Threshold and Local Power filters.

D) Representative 2D class averages containing particles used in further 3D processing steps. An example of a 2D class average representing the 26S proteasome is indicated with a purple box, and an example of a 2D class average representing the 30S proteasome is indicated with a blue box.

E) *Ab initio* model calculated from a subset of selected particles.

After initial preprocessing and 2D processing in CryoSPARC, the 3D processing was performed in Relion (Kimanius et al., 2021). Selected particle locations in CryoSPARC were re-extracted and after two rounds of repeated 2D classification to ensure that the extraction produced similar particle images, 636,315 particles were exported for 3D processing. First 3D refinement performed in Relion yielded a cryo-EM map of the mainly 26S proteasome complex, though at lower thresholds; moreover, a density for the second 19S RP also appears (**Figure 4.16. A**). Since this density was much weaker than the one on the other side of the 20S

CP, it was cut off from the figures. The overall complex architecture was identical to other cryo-EM maps of the 26S proteasome (Dong et al., 2018). However, an additional density was identified in the region of the 19S RP when comparing the 26S cryo-EM map shown in **Figure 4.16. A** with the ones reported in the literature. This type of density was never observed before, neither in cryo-EM analyses of 26S proteasome alone, nor in the presence of polyubiquitinated substrate. The identified additional density connects Rpn1 subunit with Rpn3 and Rpn7 subunits. Previous report that ZFAND2a interacts with the Rpn1 subunit of the 26S proteasome (Stanhill et al., 2006) led me to assume that this density might represent the ZFAND2a bound to the 26S proteasome. Hence, from here after, I will refer to the described additional density as the ZFAND2a density. The ZFAND2a density contained a very weak signal in comparison to other proteasomal subunits. This was most likely because not all 26S proteasome particles contained bound ZFAND2a in the calculated cryo-EM map, but rather had partial occupancy.

In the next processing step, a mask surrounding the ZFAND2a density and partially neighboring proteasomal subunits Rpn1, Rpn2, and Rpn3, was created and used in focused 3D classification (**Figure 4.16 B**). With this step I aimed to identify and separate particles that have ZFAND2a bound from particles that do not contain ZFAND2a bound. This is achieved by limiting the 3D class average calculation only on the part of the map surrounded by a provided mask. The resulting 3D classes were visually inspected in ChimeraX (Pettersen et al., 2021) (**Figure 4.16 B**) and particles belonging to the classes containing ZFAND2a density were separated from particles belonging to classes that did not contain ZFAND2a density. Subsequently, particles with ZFAND2a density and particles without ZFAND2a density were further refined separately (**Figure 4. 16 C**). After 3D refinement of both classes, the class with ZFAND2a density contained better-defined features of ZFAND2a density and binding regions on the 26S proteasome than the previous cryo-EM map shown in **Figure 4.16 A**. 3D refinement of particles with no ZFAND2a density yielded, as expected, the 26S proteasome map without ZFAND2a density. Subsequently, a second mask surrounding now better-defined ZFAND2a density and a very small portion of proteasomal subunits Rpn1 and Rpn7 was created and used in another round of focused 3D classification to further separate any remaining particles that do not contain ZFAND2a signal (**Figure 4.16 D**). This step resulted in only two out of ten 3D classes showing the signal of ZFAND2a density in the region occupied by the mask (**Figure 4. 16 D**). These two classes were again subjected to 3D refinement separately after which only one class still showed clear ZFAND2a density (**Figure 4.16 E**). However, the overall map quality did not improve after removing more of particles without bound ZFAND2a by focused 3D classification procedure.

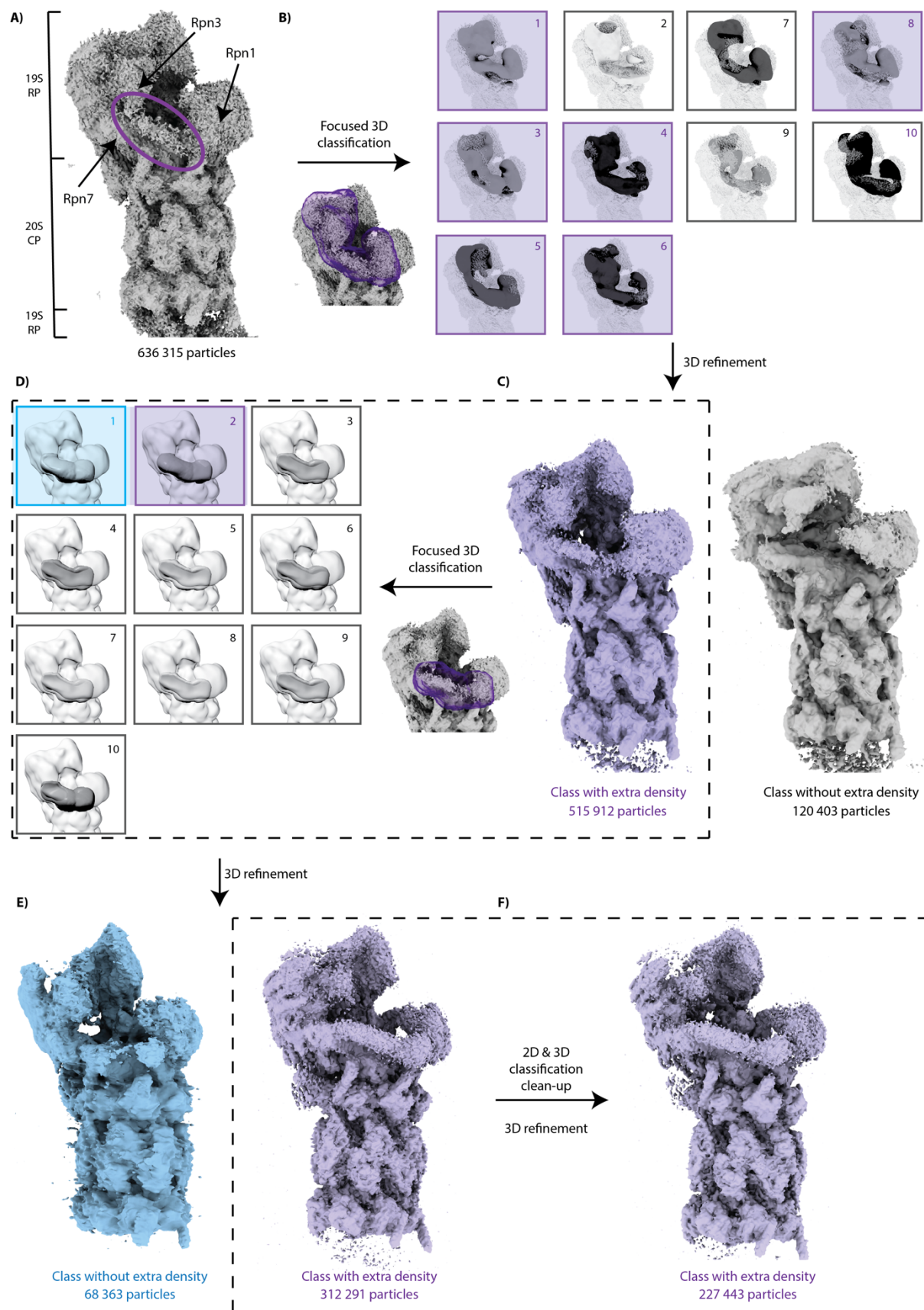


Figure 4.16. 3D processing in Relion.

- A)** Calculated cryo-EM map of the 26S proteasome complex after 3D refinement of particles localized, extracted, and exported from CryoSPARC. The additional density representing bound ZFAND2a is encircled with a purple ellipse. The black arrows indicate the proteasomal subunits Rpn1, Rpn3, and Rpn7 that are in the contact with ZFAND2a density. The brackets on the left side indicate the map regions occupied by 19S RP and 20S CP density.
- B)** Resulting 3D classes after the first round of focused 3D classification. The classes that contain ZFAND2a density are shaded in purple and classes without ZFAND2a density are enclosed in a black square.
- C)** Calculated cryo-EM maps of the 26S proteasome complexes after 3D refinement representing separated 26S proteasome class with ZFAND2a density and 26S proteasome class without ZFAND2a density.
- D)** Resulting 3D classes after the second round of focused 3D classification. Two classes with identified extra densities are enclosed in shaded blue and purple squares.
- E)** Calculated cryo-EM maps of 26S proteasome complexes after 3D refinement of blue and purple shaded classes in panel D).
- F)** Final calculated cryo-EM map of 26S proteasome with ZFAND2a density after an additional particle stack clean-up.

With the aim to achieve a better resolution, additional rounds of 2D and 3D classification were performed on a selected particle stack to remove any remaining contaminants and sort for heterogeneity that might have contributed to the poor resolution. Further cleaned and sorted particle stack was once more subjected to 3D refinement. The resulting cryo-EM map (**Figure 4.16 F**) still had the same quality as the previous one. This result indicated that the resolution limit might be due to the overall data quality and not due to conformational heterogeneity present in the sample or contamination particles.

In another attempt to improve the map quality, the particles belonging to the second class from **Figure 4.16 D** were analyzed with CryoDRGN (Zhong et al., 2021) (**Figure 4.17 A**). CryoDRGN is a very powerful neural-network-based tool used for sorting compositional and conformational heterogeneity as well as for the effective separation of bad or broken particles from intact particles. For this purpose, two rounds of CryoDRGN heterogeneous 3D reconstructions and selection of good 3D class averages (**Figure S3**) resulted in a stack of 94,738 particles that were then re-imported back to Relion and subjected to 3D refinement (**Figure 4.17 B**). The resulting cryo-EM map showed minimal visual improvement in overall quality. Nevertheless, ZFAND2a density was much less noisy and distributed around. Hence,

an additional round of focused 3D classification was repeated using a mask surrounding the further improved ZFAND2a density and the resulting 3D classes were inspected (**Figure 4.17 C**). Only one class containing most of the input particles, was selected and the particles belonging to the respective class were subjected to 3D refinement (**Figure 4.17 D**). The final obtained cryo-EM map resulted in similar quality as the one before the final focused 3D classification procedure. This once more confirmed my hypothesis that the data quality, and not the conformational heterogeneity, is most likely the cause of resolution limit in this data set.

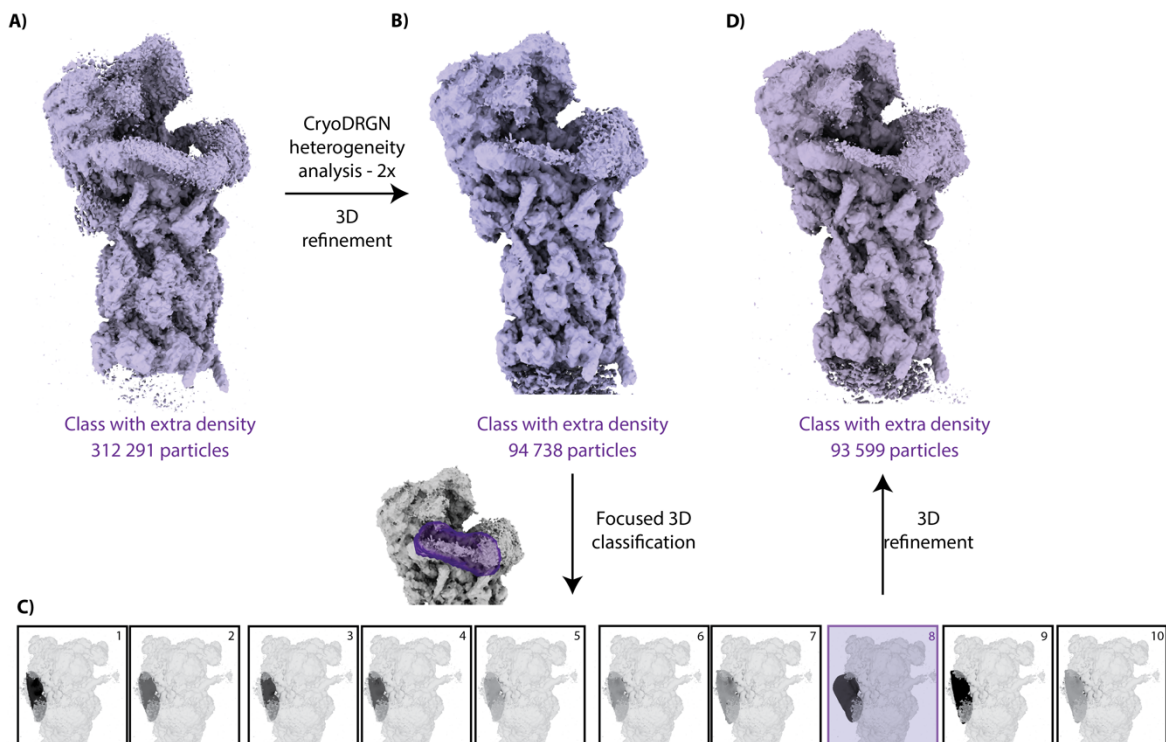


Figure 4.17. 3D refinement in Relion after heterogeneity sorting procedure in CryoDRGN.

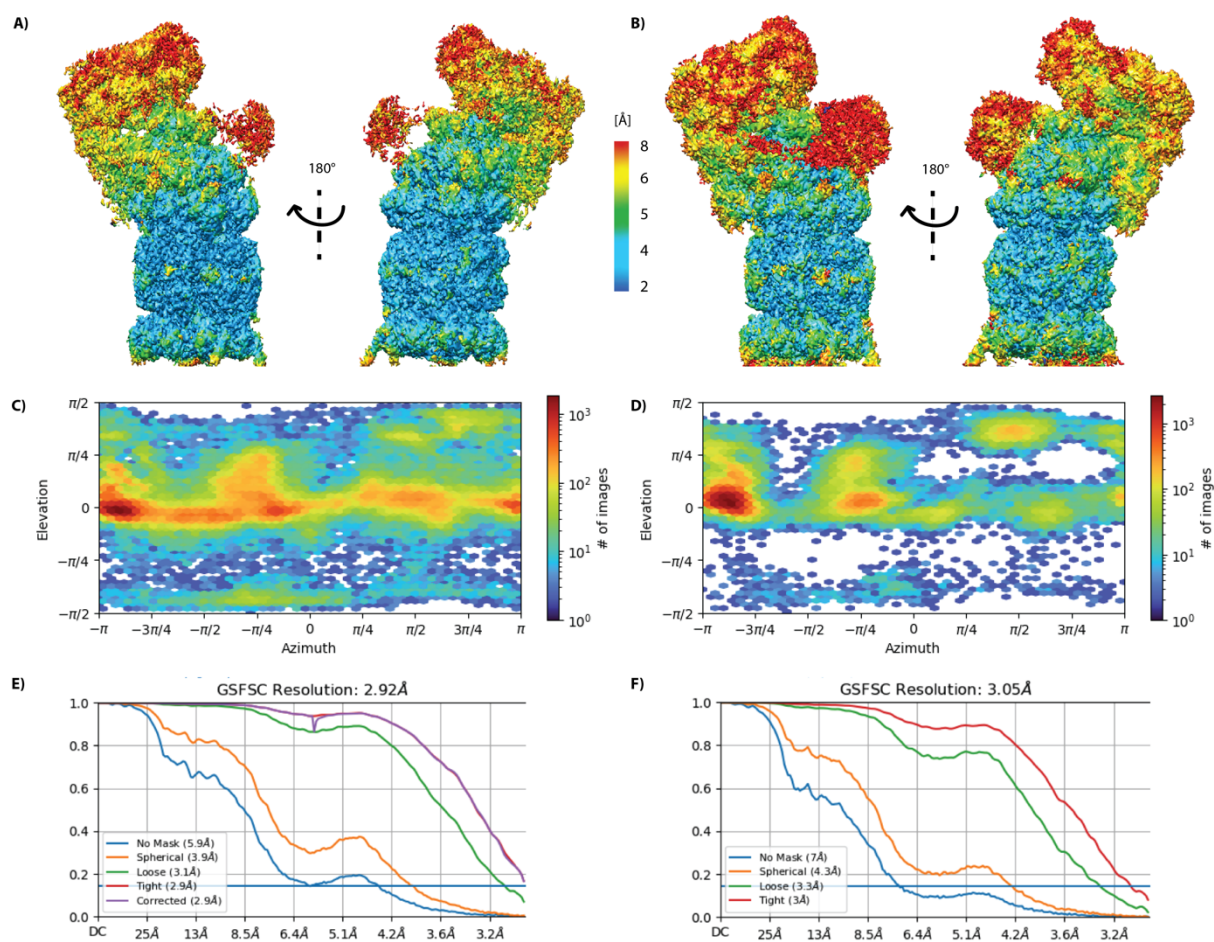
A) Starting cryo-EM map whose particles were imported into CryoDRGN heterogeneity analysis.
B) Resulting cryo-EM map after 3D refinement of particles curated through CryoDRGN procedure.

C) Resulting 3D classes after final round of focused 3D classification. The class shaded in purple contained most of the particles and ZFAND2a density.

D) Final cryo-EM map of the ZFAND2a-bound 26S proteasome complex obtained by 3D refinement of particles belonging to the class shaded in purple from panel C).

4.4.3. Comparison of ZFAND2a-bound and ZFAND2a-free 26S proteasome complexes

After obtaining the final cryo-EM maps of ZFAND2a-bound and ZFAND2a-free 26S proteasome, local resolution and corresponding angular distribution plots and Fourier Shell Correlation curves were calculated in CryoSPARC software (**Figure 4.18**). Local resolution estimation shows that the 20S CP in both cryo-EM maps is resolved to a much higher resolution ($<5\text{\AA}$) than the 19S RP ($>6\text{\AA}$). Only the ATPase domains of the Rpt hexameric ring had a resolution that was of a quality close to the 20S CP (**Figure 4.18 A and B**). Such distribution of local resolution is commonly observed for the 26S proteasome complex. This is the case because the 19S RP is a very flexible subcomplex, whereas the 20S CP undergoes rather short-range conformational movements. ZFAND2a density was in the worst resolution range ($>8\text{\AA}$) (**Figure 4.18 B**). This was partially expected because it is a disordered and most likely a flexible protein. Moreover, ZFAND2a binds the 19S RP through Rpn1 subunit located in one of the most flexible regions of the whole complex, thus contributing to the poor resolution. The angular distribution plots of both cryo-EM maps, though not filled, do have a feature tendency of a tomographic series (**Figure 4.18 C and D**). This means that there are 360° views of the specimen assigned. This distribution is most obvious in the angular distribution plot of ZFAND2a-free 26S proteasome cryo-EM map where a line with red-orange color code can be followed almost throughout the whole plot (**Figure 4.18 C**). Contrary, in the ZFAND2a-bound 26S proteasome cryo-EM map plot the series is much weaker and the two preferred orientations represented by red regions are easily detected (**Figure 4.18 D**). Lastly, the final resolution of both cryo-EM maps was determined using Fourier Shell Correlation (FSC). According to the gold-standard FSC criterion of 0.143 the determined overall resolution of ZFAND2a-free 26S proteasome complex was 2.9\AA , and that of ZFAND2a-bound 26S proteasome complex 3.1\AA (**Figure 4.18 E and F**).



4.18. Analysis of final 26S proteasome cryo-EM maps in CryoSPARC.

A) and B) Local resolution map of ZFAND2a-free (A) and ZFAND2a-bound (B) 26S proteasome. The density color corresponds to the local resolution value as indicated in the color bar. The resolution range is from 2Å (blue) to 8Å (red).

C) and D) Angular distribution plot of ZFAND2-free (C) and ZFAND2a-bound (D) 26S proteasome.

E) and F) Fourier shell correlation (FSC) curve of ZFAND2-free (E) and ZFAND2a-bound (F) 26S proteasome. Gold-standard FSC criterion of 0.143 was used to estimate the final resolution.

Next, I closely compared low-resolution cryo-EM maps of ZFAND2a-bound (**Figure 4.19 A**) and ZFAND2a-free 26S proteasome complex (**Figure 4.19 B**). The most striking difference between the two cryo-EM maps can be observed in the conformational states of the two complexes. The ZFAND2a-bound 26S proteasome is found in ground or substrate accepting state. This state can be recognized by the absence of the contact between the Rpt4/5 coiled coil with the Rpn10 ubiquitin receptor (**Figure 4.19 A**). In contrast, the ZFAND2a-free 26S proteasome complex is found in an activated state in which Rpt4/5 coiled coil is in contact

with the Rpn10 ubiquitin receptor (**Figure 4.19 A**). However, I did not observe any additional density in the cryo-EM map of ZFAND2a-free 26S proteasome complex that could be assigned to the bound substrate. This could be due to the high substrate flexibility on the 19S RP in the initial stages of substrate recruitment and engagement.

Finding ZFAND2a bound only to 26S proteasome particles that are not engaged with a substrate indicates that ZFAND2a regulatory role is most likely exerted prior to substrate recruitment. This further suggests that ZFAND2a binding potentially has no direct regulatory influence on the 26S proteasome while the degradation is taking place. Such conclusion agrees with the previous observations I made in this study that the degradation profile of model proteasome substrate remained unchanged in the presence of ZFAND2a.

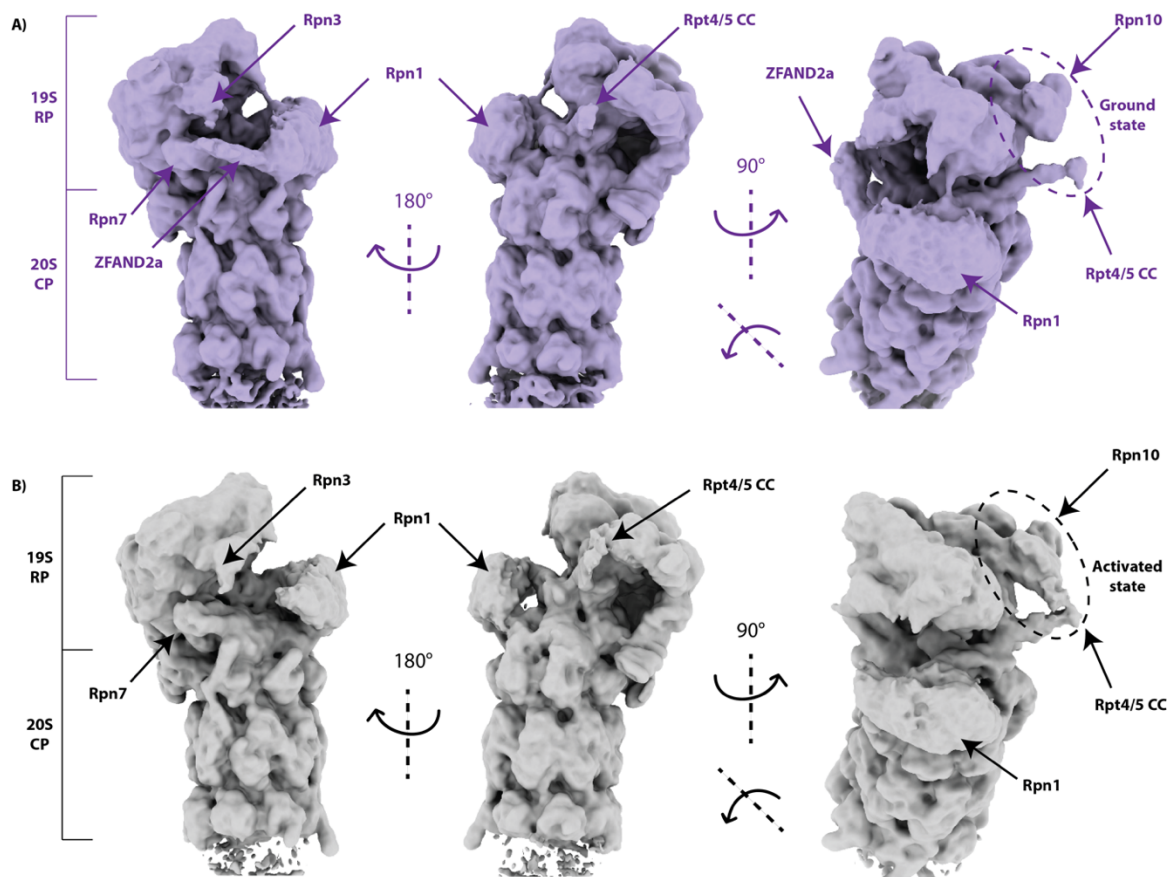


Figure 4.19. Comparison between ZFAND2a-bound and ZFAND2a-free 26S proteasome.

A) ZFAND2a-bound 26S proteasome with indicated ZFAND2a density.

B) ZFAND2a-free 26S proteasome.

Proteasome subunits surrounding ZFAND2a (Rpn1, Rpn3 and Rpn7) are indicated with an arrow in both complexes. The major structural feature of conformational state (ground vs. activated state) of both complexes is indicated with dashed ellipse and the relevant proteasome subunits, Rpn10 and Rpt4/5 coiled coil (CC), are indicated with an arrow.

4.4.4. Rigid body fitting of ZFAND2a predicted structure into ZFAND2a density

Since there is no structure available for ZFAND2a, I used AlphaFold (Jumper et al., 2021) to predict the ZFAND2a structure (**Figure 4.20 A**, **Supplementary Figure S5**). ZFAND2a contains two zinc-finger AN1 domains positioned at the N- and C-terminus of the protein connected with a linker. Previous pulldown experiments showed that both AN1 domains are required and necessary for 26S proteasome binding (**Figure 4.20 B**) (Stanhill et al., 2006). ZFAND2a is predicted to be intrinsically disordered protein with only a small stretch forming short α -helix in the linker region. The predicted ZFAND2a structure was overall successfully docked inside the ZFAND2a density together with structures of surrounding proteasome subunits Rpn1, Rpn3, and Rpn7 (**Figure 4.20 C**).

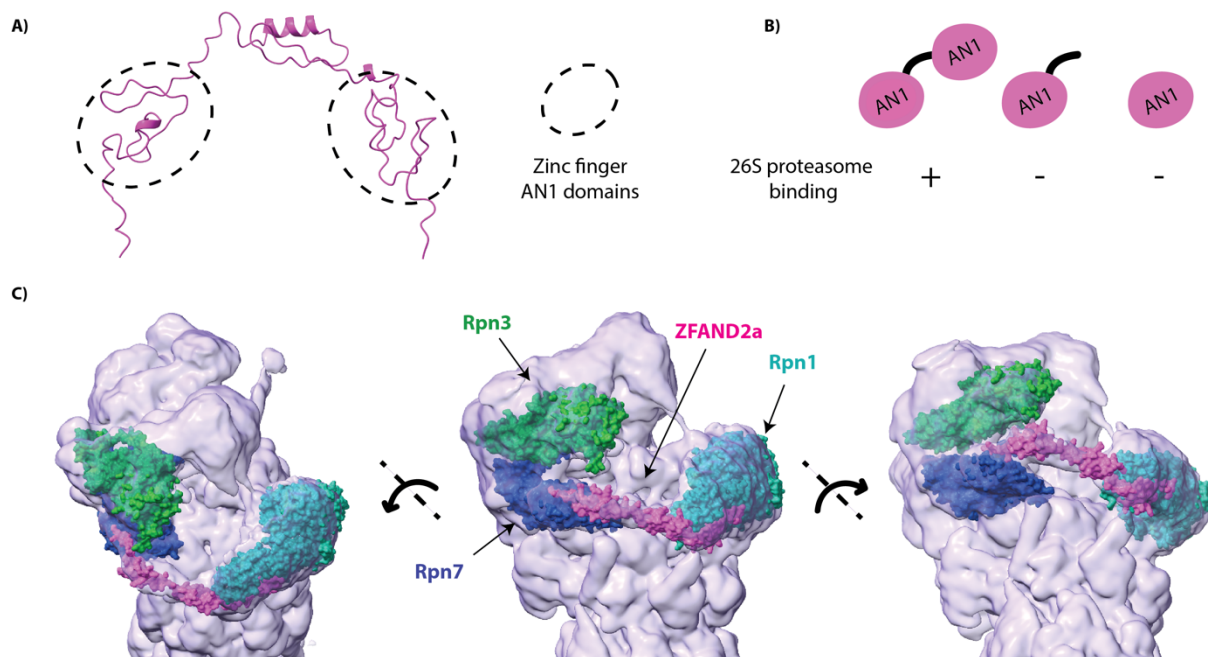


Figure 4.20. Rigid body fitting of ZFAND2a AlphaFold predicted structure and Rpn1, Rpn3, and Rpn7 structures into the cryo-EM map of ZFAND2a-bound 26S proteasome complex.

A) Exemplary AlphaFold prediction of ZFAND2a structure. Zinc finger AN1 domains are encircled with dashed ellipses.

B) Schematic of ZFAND2a structural elements and requirements for 26S proteasome binding.

C) Close-up of the 19S RP cryo-EM map region of ZFAND2a-bound 26S proteasome with docked ZFAND2a predicted structure, Rpn1, Rpn3, and Rpn7 proteasome subunits represented in space-filling preset (PDB ID: 6FVT).

From the five different conformations of the predicted ZFAND2a structures, the structure that is most elongated, fitted better in terms of size and length into the density. ZFAND2a density bridges the N-terminal region of the Rpn1 ubiquitin receptor and the N-terminal region of the Rpn7 subunit of the 19S RP lid. In this configuration of the 19 RP, the Rpn1 subunit that is otherwise rather free to rotate and change its position in relation to the ATPase ring, is now linked by ZFAND2a to a more static region of the 19S RP. I hypothesize that such a link restricts Rpn1 movements and potentially couples them with the movements of the 19S RP lid. Such arrangement could have direct impact on the 19S RP's functionality in terms of polyubiquitinated substrates recruitment or the occupancy of different PIPs. The nature behind this impact should ultimately benefit the 26S proteasome function under proteotoxic conditions to allow more efficient substrate degradation.

5. Summary and Conclusions

The impairment of the Ubiquitin-Proteasome System (UPS) is one of the central research questions in neurodegenerative pathologies. The shared hallmark of many neurodegenerative conditions is inefficient removal of disease-associated toxic proteins despite them being targeted for degradation by the UPS (Ciechanover and Kwon, 2015). Consequently, these proteins accumulate over time and form cytotoxic aggregates that ultimately disrupt normal cellular functioning and lead to neuronal death (Soto and Pritzkow, 2018). As the main proteolytic engine of the UPS, the 26S proteasome is considered to play a major role in the development and progression of neurodegenerative diseases (Myeku and Duff, 2018). Therefore, the 26S proteasome functional insufficiency and/or malfunction have been suggested as the underlying causes of inefficient removal of toxic proteins.

One extensively studied example of 26S proteasome malfunction is caused by stalling of substrates that contain stretches of glutamines (polyQ stretches) longer than 35 residues (Holmberg et al., 2004). In the case of other substrate-stalled protein complexes, such as ribosomes or DNA-polymerase, rescue mechanisms are known to resolve the malfunction through binding to the stalled protein complex (Bengtson and Joazeiro, 2010; Edenberg et al., 2014). However, thus far no such rescue mechanisms have been understood for the stalled 26S proteasome, although candidate mechanisms can be found throughout the literature (Kopp et al., 2001; Tsvetkov et al., 2015; Wang et al., 2017b; Welk et al., 2016). One candidate proteasome rescue mechanism might involve zinc-finger protein ZFAND2a. The ZFAND2a protein expression is induced under proteotoxic conditions where almost all ZFAND2a in cells associates with the 26S proteasomes, indicating that ZFAND2a's functional role is connected with the 26S proteasome function (Rossi et al., 2014). On a cellular level, in the presence of ZFAND2a, the cells accumulate fewer misfolded proteins when treated with arsenite indicating a role of ZFAND2a in regulating 26S proteasome turnover of misfolded proteins (Stanhill et al., 2006). Moreover, ZFAND2a homolog in *C.elegans*, AIP-1 was shown to increase general protein turnover and reduce the toxicity caused by A β -peptide and polyQ fusion proteins present in Alzheimer's and Huntington's disease, respectively (Hassan et al., 2009; Yun et al., 2008). Guided by these observations, I questioned if human ZFAND2a might show similar functional properties in rescuing 26S proteasome stalled by substrate containing long polyQ stretch and/or enhance the 26S proteasome's degradation capacity in general.

5.1. *In vitro* system preparation for investigation of ZFAND2a potential role in rescuing stalled 26S proteasome complex

Inside cells, the 26S proteasome binds many different regulatory factors simultaneously (Verma et al., 2000). This makes it hard to discern the exact regulatory role of an individual factor when performing *in vivo* functional analyses. For this reason, many studies, including the one I conducted in this work, take advantage of an *in vitro* approach with individual components. One of the biggest caveats of an *in vitro* approach is the possibility that some regulatory mechanisms might involve more than one factor. Since during this work I did not have any information indicating this could be the case with ZFAND2a, I reasoned that approaching the question with a minimal *in vitro* setup could serve as a starting point for driving any further hypotheses and experiments.

Having a structural investigation in mind, I favored the *in vitro* approach in terms of preparation of the required sample for the structural analysis. Aiming for the structural investigation of the complex directly in the cellular environment would be much more challenging as current state-of-the-art *in situ* structural biology is still largely mastered in only a few labs in the whole world. Moreover, even if the expertise would not be a limiting factor, the *in situ* structural approach highly depends on the molecular size of the complex of interest as this determines the likelihood of finding the complex inside a crowded cellular milieu.

As part of the preparatory phase for the *in vitro* experimental approach, I purified 26S proteasome complexes from cell extracts using two different methods and produced recombinant ZFAND2a protein. Furthermore, I constructed seven different substrates whose backbone consisted of the following components fused from N- to C-terminus in a single construct: first 95 amino acids from Cyclin B (N95CycB), dihydrofolate reductase (DHFR), enhanced green fluorescent protein (EGFP), and ubiquitin (Ub). Individual substrates differed in position, number, and lengths of polyQ stretches. I positioned either a polyQ stretch of non-pathological length (polyQ19) and/or pathological length (polyQ89) in front of and/or after DHFR in all possible combinations. Finally, all purified substrate proteins were marked for 26S proteasome degradation by attaching either a single linear K48 polyubiquitin chain or two branched K11/K63 polyubiquitin chains.

5.2. 26S proteasome degradation of model substrates in the presence or absence of ZFAND2a

Despite many research efforts, it is still not entirely clear what is the exact mechanism by which long polyQ stretch causes stalling of the 26S proteasome and terminates degradation of substrate protein. The available literature reports are full of contradictory findings on almost every suggested mechanism (Holmberg et al., 2004; Juenemann et al., 2013; Michalik and Van Broeckhoven, 2004; Pratt and Rechsteiner, 2008; Venkatraman et al., 2004). However, some consistency can be found throughout numerous reports, namely that the presence of long polyQ stretch doesn't necessarily lead to 26S proteasome stalling, but it depends on the protein context around the polyQ stretch (Schipper-Krom et al., 2012). For example, positioning of long polyQ stretch upstream from a stable protein domain that represents unfolding challenge for proteasome's ATPase motor results in 26S proteasome stalling (Holmberg et al., 2004). However, when a long polyQ stretch is positioned downstream from a stable protein domain, the stalling does not occur and protein degradation proceeds to completion, including the degradation of polyQ stretch (Michalik and Van Broeckhoven, 2004). I observed similar polyQ stalling pattern in the results of *in vitro* degradation assays performed in this study. Upon 26S proteasome degradation of designed proteasome substrate only polyQ89 stretch preceding the EGFP caused stalling of the 26S proteasome and resulted in partial substrate processing that retained the polyQ89 stretch and everything downstream from the stretch. Intriguingly, when polyQ89 stretch was positioned in front of a folded domain of DHFR, I did not observe 26S proteasome stalling and both polyQ89 stretch and DHFR were successfully processed. Thus, it appears that the domain downstream of long polyQ stretch needs to have a certain degree of structural stability to result in 26S proteasome stalling mediated by long polyQ stretch.

Another poorly investigated biological question is what happens once the 26S proteasome degradation is stalled by the long polyQ stretch. One possible scenario could be that the 26S proteasome is permanently impaired, as suggested previously (Holmberg et al., 2004), upon which a potential rescue factor that recognizes stalled 26S proteasomes is recruited. The rescue factor could act to promote either efficient substrate processing or disengaging of the stuck substrate to relieve impairment. Another possible scenario could be that the impairment caused by the long polyQ stretch is not permanent, and the stalled substrate can disengage on its own at some point. In this case, a rescue mechanism might act to ensure that disengaging does not happen while at the same time it promotes efficient processing. The results I obtained in this work partially support the latter scenario as I observed that the stalled

polyQ substrate is at some point being released from the 26S proteasome. These results open up the possibility that the 26S proteasome is not necessarily permanently impaired upon degradation stalling by the polyQ stretch of pathological length as previous literature suggests (Holmberg et al., 2004). The release of the partially processed substrate upon polyQ-mediated stalling would also exclude the need for a rescue mechanism that would need to actively disengage the stalled substrate from the translocation channel of the 26S proteasomes, the mechanism previously suggested for potential VCP-mediated rescue (Isakov and Stanhill, 2011). Whether the substrate stalled by long polyQ stretch is being released on its own in cells needs to be tested. It could also be that in cells the 26S proteasome bound E3 ligases counteract this *in vitro* observed release of stalled substrate to ensure more time for the substrate to get degraded.

Regardless of if the release is indeed taking place in cells, even the temporary nature of stalling is more than sufficient to cause alterations in 26S proteasome processing capacity. This is supported by the observed downregulation of caspase-like and chymotrypsin activities of the 20S CP together with the increased half-life of polyubiquitinated reporter substrate in cells expressing model substrates containing long polyQ stretch (Hunter et al., 2007). In either case, polyQ-mediated stalling renders the 26S proteasome incapable to meet degradation demands while ever-increasing amount of aggregation-prone protein is being shuttled for degradation. Furthermore, another issue related to the spontaneous release of partially processed polyQ-containing substrates is the fact that the released protein fragments still contain aggregation-prone long polyQ stretches. Meanwhile, only the complete removal of disease-related aggregation-prone proteins from the cell's interior proved to be the most efficient approach to rescuing cells from neurodegeneration phenotype (Ortega and Lucas, 2014). Thus, achieving the complete removal of toxic proteins through modulation of 26S proteasome function could be an extremely promising therapeutic approach in treating neurodegenerative diseases.

In this work I investigated the potential rescue role of ZFAND2a protein in promoting efficient degradation of substrates whose degradation is stalled by long polyQ stretch using an *in vitro* degradation system. The results I obtained indicate that ZFAND2a binding alone to the 26S proteasome does not lead to complete degradation of model proteasome substrate whose degradation is stalled by long polyQ stretch. Additionally, I also did not observe any difference in the processing rate of non-stalling model proteasome substrate by ZFAND2a-bound 26S proteasomes in comparison to ZFAND2a-free 26S proteasomes, suggesting that ZFAND2a binding does not influence the overall degradation by the 26S proteasome, as reported for AIP-1 (Hassan et al., 2009). However, the conclusions drawn from the *in vitro* degradation assays

should always be taken with caution since the choice of individual substrate elements and their combinations have an impact on the 26S degradation properties and have the potential to influence the outcome that does not necessarily reflect the situation with native substrates (Inobe et al., 2011; Martinez-Fonts and Matouschek, 2016). Hence, I cannot exclude that by designing proteasome substrates that are not native by their composition, the obtained results could have different outcome when investigating ZFAND2a regulatory role. Taking this into consideration, it would be worthwhile to perform *in vitro* degradation assay with ZFAND2a that I established in this study with native substrates, both that are completely degradable and stalling substrates containing long polyQ stretch such as mutant huntingtin.

5.3. Structural characteristics of ZFAND2a-bound 26S proteasome complex

At the time I started this study little was known about ZFAND2a interaction sites on the 26S proteasome; moreover, the structure of ZFAND2a was not available. Earlier studies have speculated that ZFAND2a might bind close to the DUB subunit Rpn11 or indicated that the binding site is on the ubiquitin receptor subunit Rpn1 (Stanhill et al., 2006; Sukenik et al., 2021). To fill in this important information gap, I determined the first low-resolution cryo-EM map of the ZFAND2a-bound 26S proteasome in the presence of stalling proteasome substrate.

Although the overall map quality in the ZFAND2a binding region was insufficient for atomic model building, it did allow me to perform rigid body fitting of available atomic models of individual proteasomal subunits. Since for ZFAND2a there was no atomic model available, I used AlphaFold (Jumper et al., 2021) to obtain the predicted structure, which I then fitted into the cryo-EM density. In the obtained cryo-EM map of ZFAND2a-bound 26S proteasome, I identified N-terminal regions of subunits Rpn1 and Rpn7 of the 19S RP as ZFAND2a binding sites. Additionally, some intermediate cryo-EM maps throughout the processing procedure indicated another possible ZFAND2a interaction site in the N-terminal region of subunit Rpn3. In the future, binding assays with individual subunits and/or cross-linking mass spectrometry approach could be undertaken to further verify and confirm these interactions.

The identified binding position of ZFAND2a on the 26S proteasome has two potential functional implications. Firstly, ZFAND2a is positioned far away from the translocation channel and Rpn11 subunit where the steps of active substrate processing physically take place. This would refute previously suggested role of ZFAND2a in rescuing catalytic activity of

arsenite-bound Rpn11 by zinc-arsenite exchange that assumes ZFAND2a binding close to Rpn11 (Sukenik et al., 2021). Secondly, the elongated shape and positioning of ZFAND2a acts as a molecular bridge between the Rpn1 ubiquitin receptor and the rest of the 19S RP lid. Rpn1 ubiquitin receptor subunit is known to have large mobility and to change its relative location on the ATPase ring, a characteristic most likely required to accommodate substrate initiation. I would expect that with ZFAND2a bound, the Rpn1 mobility might be restricted, or it might be differently coordinated with the movements of the 19S RP lid compared to when this molecular connection through ZFAND2a is not present. It is possible that ZFAND2a exerts its regulatory role by introducing a change in the conformational freedom of the 19SRP. Describing the nature of this change could further reveal functional implications behind ZFAND2a binding.

Today, with the advancements in computational algorithms, single-particle cryo-EM is being routinely employed for not only determining the static structures of proteins and protein complexes but it is also used for analyzing their dynamical properties (Zhong et al., 2021). This is possible because upon sample vitrification, an equilibrium of different conformational and/or occupancy states of protein of interest exist and are represented in the data set. In the case of cryo-EM sample I prepared in this work, the sample contained an equilibrium of ZFAND2a-bound and ZFAND2a-free 26S proteasomes, of which both species assumed certain and different conformational states. Upon comparison of low-resolution cryo-EM maps of ZFAND2a-bound and ZFAND2a-free 26S proteasome, I identified that ZFAND2a-bound 26S proteasome is mainly found in ground or substrate accepting state whereas ZFAND2a-free 26S proteasome was mainly in activated or substrate processing state. This observation suggests that the change in conformational landscape introduced by ZFAND2a binding is most likely not involved, either directly or indirectly, in regulation of active substrate processing, thus explaining the reported lack of functional effect observed. Obtaining a better resolved cryo-EM dataset of ZFAND2a-bound 26S proteasome could allow a more in-depth investigation of any subtle conformational differences between ground states of ZFAND2a-free and ZFAND2a-bound 26S proteasomes and whether ZFAND2a-bound 26S proteasome is even able to engage substrates.

Taken all together, these results suggest that ZFAND2a protein might have more of a structural than a functional role upon binding the 26S proteasome under proteotoxic conditions. One possibility could be that ZFAND2a binding ensures structural integrity of the 19S RP under harsh conditions, thus acting as a chaperone in between two active substrate processing cycles. Another possibility could be that ZFAND2a binding stabilizes ground-like state that

hinders substrate engagement until certain additional factors bind that are required for a more complex regulation of the 26S proteasome under proteotoxic conditions, such as UBE3C or another, yet unidentified regulator.

Hence, future studies on ZFAND2a role in regulation of malfunctioning 26S proteasomes should preferably include the factor of cellular environment and potential additional interactors. For this purpose, it might be useful for future structural and conformational analysis of ZFAND2a-bound 26S proteasomes to obtain the complex directly from cells. This would also allow a more in-depth investigation of the novel dynamic and compositional properties introduced by ZFAND2a binding and their implications in overall functioning of the 26S proteasome. Ultimately, it would be interesting to investigate potential effects of ZFAND2a expression in cellular models of different neurodegenerative diseases such as Huntington's to explore the potential of ZFAND2a-mediated regulatory pathway in combating more efficient removal of disease-related proteins that cause proteasome malfunction.

6. Appendix

Table S1. Protein identification by mass spectrometry of affinity purification of 26S proteasomes from HEK293GP cells

Gene	Description	NaCl Wash Norm.Area	Elution Norm.Area
PSMA1	Proteasome subunit alpha type-1	5.58E+05	5.03E+07
PSMA7	Proteasome subunit alpha type-7	2.29E+04	4.14E+07
PSMC2	26S proteasome regulatory subunit 7	2.29E+04	3.76E+07
PSMD3	26S proteasome non-ATPase regulatory subunit 3	2.29E+04	3.74E+07
PSMD6	26S proteasome non-ATPase regulatory subunit 6	2.29E+04	3.64E+07
PSMD7	26S proteasome non-ATPase regulatory subunit 7	2.29E+04	2.94E+07
PSMD4	26S proteasome non-ATPase regulatory subunit 4	2.29E+04	2.41E+07
PSMD11	26S proteasome non-ATPase regulatory subunit 11	2.29E+04	2.36E+07
PSMD14	26S proteasome non-ATPase regulatory subunit 14	2.29E+04	2.32E+07
PSMA5	Proteasome subunit alpha type-5	2.29E+04	2.28E+07
PSMB7	Proteasome subunit beta type-7	4.72E+05	2.27E+07
PSMA2	Proteasome subunit alpha type-2	2.29E+04	2.07E+07
PSMC1	26S proteasome regulatory subunit 4	2.29E+04	2.03E+07
PSMC6	26S proteasome regulatory subunit 10B	2.29E+04	1.98E+07
PSMB2	Proteasome subunit beta type-2	2.29E+04	1.92E+07
PSMD2	26S proteasome non-ATPase regulatory subunit 2	2.29E+04	1.81E+07
PSMD1	26S proteasome non-ATPase regulatory subunit 1	2.29E+04	1.76E+07
PSMD13	26S proteasome non-ATPase regulatory subunit 13	2.29E+04	1.58E+07
PSMC5	26S proteasome regulatory subunit 8	2.29E+04	1.48E+07
PSMB6	Proteasome subunit beta type-6	1.74E+05	1.48E+07
PSMA6	Proteasome subunit alpha type-6	2.29E+04	1.22E+07
PSMB5	Proteasome subunit beta type-5	2.29E+04	1.01E+07
PSMB4	Proteasome subunit beta type-4	2.29E+04	9.89E+06
PSMD8	26S proteasome non-ATPase regulatory subunit 8	2.29E+04	8.50E+06
PSMC4	26S proteasome regulatory subunit 6B	2.29E+04	8.28E+06
PSMA4	Proteasome subunit alpha type-4	2.29E+04	7.81E+06
PSMB1	Proteasome subunit beta type-1	2.29E+04	7.80E+06
ADRM1	Proteasomal ubiquitin receptor ADRM1	2.29E+04	7.50E+06
PSMC3	26S proteasome regulatory subunit 6A	2.29E+04	6.86E+06
RAD23B	UV excision repair protein RAD23 homolog B	1.16E+06	4.48E+06

PSMD12	26S proteasome non-ATPase regulatory subunit 12	2.29E+04	3.56E+06
PSMA3	Proteasome subunit alpha type-3	2.29E+04	3.46E+06
PSMB3	Proteasome subunit beta type-3	2.29E+04	2.53E+06
PSMD10	26S proteasome non-ATPase regulatory subunit 10	2.29E+04	1.47E+06
UCHL5	Ubiquitin carboxyl-terminal hydrolase isozyme L5	2.29E+04	1.32E+06
TXNL1	Thioredoxin-like protein 1	5.01E+05	9.58E+05
VCP	Transitional endoplasmic reticulum ATPase	2.29E+04	4.73E+05
PAAF1	Proteasomal ATPase-associated factor 1	2.29E+04	3.78E+05
USP14	Ubiquitin carboxyl-terminal hydrolase 14	2.97E+05	3.11E+05
KIAA0368	Proteasome adapter and scaffold protein ECM29	2.74E+05	1.21E+05
UBE3A	Ubiquitin-protein ligase E3A	2.29E+04	1.03E+05
RAD23A	UV excision repair protein RAD23 homolog A	2.29E+04	2.74E+04

NOTE: Proteasome interacting proteins are marked in red.

Table S2. Protein identification by mass spectrometry of affinity purification of 26S proteasomes from HeLa cells

Gene	Description	Elution Norm.Area
RAD23B	UV excision repair protein RAD23 homolog B	2.26E+10
PSMD11	26S proteasome non-ATPase regulatory subunit 11	4.80E+08
PSMC2	26S proteasome regulatory subunit 7	4.45E+08
PSMC4	26S proteasome regulatory subunit 6B	4.57E+08
PSMC5	26S proteasome regulatory subunit 8	3.92E+08
PSMD3	26S proteasome non-ATPase regulatory subunit 3	3.61E+08
PSMD13	26S proteasome non-ATPase regulatory subunit 13	3.48E+08
PSMD7	26S proteasome non-ATPase regulatory subunit 7	3.21E+08
PSMD2	26S proteasome non-ATPase regulatory subunit 2	3.29E+08
PSMD6	26S proteasome non-ATPase regulatory subunit 6	3.14E+08
PSMD4	26S proteasome non-ATPase regulatory subunit 4	3.06E+08
PSMD5	26S proteasome non-ATPase regulatory subunit 5	2.55E+08
VCP	Transitional endoplasmic reticulum ATPase	2.40E+08
PSMD8	26S proteasome non-ATPase regulatory subunit 8	2.38E+08
PSMC1	26S proteasome regulatory subunit 4	2.64E+08
TXNL1	Thioredoxin-like protein 1	2.33E+08
USP14	Ubiquitin carboxyl-terminal hydrolase 14	2.31E+08
PSMD12	26S proteasome non-ATPase regulatory subunit 12	1.99E+08
PSMD14	26S proteasome non-ATPase regulatory subunit 14	2.00E+08
PSMD1	26S proteasome non-ATPase regulatory subunit 1	2.34E+08
PSMC3	26S proteasome regulatory subunit 6A	1.87E+08
UCHL5	Ubiquitin carboxyl-terminal hydrolase isozyme L5	1.69E+08
PSMC6	26S proteasome regulatory subunit 10B	1.84E+08
PSMD10	26S proteasome non-ATPase regulatory subunit 10	1.26E+08
PSMA7	Proteasome subunit alpha type-7	1.12E+08
PSMA1	Proteasome subunit alpha type-1	9.22E+07

PSMA5	Proteasome subunit alpha type-5	9.19E+07
ADRM1	Proteasomal ubiquitin receptor ADRM1	6.72E+07
PSMB2	Proteasome subunit beta type-2	7.66E+07
PSMB5	Proteasome subunit beta type-5	6.57E+07
PSMB1	Proteasome subunit beta type-1	6.25E+07
PSMA6	Proteasome subunit alpha type-6	6.58E+07
PSMB3	Proteasome subunit beta type-3	5.54E+07
PSMA3	Proteasome subunit alpha type-3	5.38E+07
PSMA4	Proteasome subunit alpha type-4	5.55E+07
PSMB6	Proteasome subunit beta type-6	4.94E+07
HSPB1	Heat shock protein beta-1	4.05E+07
PSMB7	Proteasome subunit beta type-7	3.60E+07
PSMA2	Proteasome subunit alpha type-2	4.58E+07
PSMB4	Proteasome subunit beta type-4	3.65E+07
UBE3A	Ubiquitin-protein ligase E3A	2.51E+07
UBE3C	Ubiquitin-protein ligase E3C	2.93E+06
PAAF1	Proteasomal ATPase-associated factor 1	1.34E+06
KIAA0368	Proteasome adapter and scaffold protein ECM29	7.24E+05

NOTE: Proteasome interacting proteins are marked in red.

Table S3. Peptide coverage of proteasome substrate proteins (NoQ, Q19-DHFR, Q89-DHFR, DHFR-Q19, DHFR-Q89 and Q89-DHFR-Q19) determined by mass spectrometry.

Substrate (Coverage percentage)	Coverage details
NoQ (63.23%)	<p>MKHHHHHHNTSSNSMSPILGYWKIKGLVQPTRLLLEYLEEKYEEHLYERDE GDKWRNKKFELGLEFPNLPYYIDGDVKLTQSMAIRYIADKHNMLGGCPKE RAEISMLEGAVLDIRYGVSR IAYSKDFETLKVDFLSKLP EMLKMFEDRLCHK TYLNGDHVTHPDFM L YDALDVVLYMDPMCLDAFPKLVCFKKRIEAIPOIDK YLKSSKYIAWPLQGWQATFGGGDHPPKSDLEVL FQGPMALRVTRNSKINA ENKAKINMAGAKRVPTAPAATSKPGLRPRTALGDIGNKVSEQLQAKMP MKKEAKPSATGKVIDKKLPKPLEKVPMLVPVPVSGSMVRPLNCIVAVS QNMGIGKNGDLPWPPLRNEFKYFQRM TTTSSVEGKQNLVIMGRKTWFSI PEKNRPLKDRINIVLSRELKEPPRG AHFLAKsLddALRLIEQPELASKVDM VWIVGGSSVYQ EAMNQPGHLRL FVTRIMQEFESDTFFPEIDL GKYKLLPE YPGVLSEVQEEKGIKYKFEVYEKKDGSMVSKGEELFTGVVPILVELDGD VNGHKFSVSGEGEGDATY GKLTLKFICTTGKLPVPWP TLVTTLT YGVQC FSRYPDHMKQHDFFKSAMPEGYVQERTIFFK DdGNyKTRA EVKFE GDT LVNRIELKGIDFKEDGNILGHKLEYNYNSHNVYIMADKQKNGIKVNFKI HHNIEDG SVQLADHYQONTPIGDGPVLLPDNHYLstQSALS KDPNEKRDH MVLLEFVTAAGITLGMDELYKGSMQIFVKTLTGKTITLeVePSDTIENVK AKIQDKEGIPPDQORLIFAGKQLEDGRTLSDYNIQKESTLHLVLR LSA WSHPQFEKGGGSGGSGGSAWSHPQFEK</p>
Q19-DHFR (61.74%)	<p>MKHHHHHHNTSSNSMSPILGYWKIKGLVQPTRLLLEYLEEKYEEHLYERDE GDKWRNKKFELGLEFPNLPYYIDGDVKLTQSMAIRYIADKHNMLGGCPKE RAEISMLEGAVLDIRYGVSR IAYSKDFETLKVDFLSKLP EMLKMFEDRLCHK TYLNGDHVTHPDFM L YDALDVVLYMDPMCLDAFPKLVCFKKRIEAIPOIDK YLKSSKYIAWPLQGWQATFGGGDHPPKSDLEVL FQGPMALRVTRNSKINA ENKAKINMAGAKRVPTAPAATSKPGLRPRTALGDIGNKVSEQLQAKMP MKKEAKPSATGKVIDKKLPKPLEKVPMLVPVPVSGSQQQQQQQQQQQQQ QQQQQQQGSMVRPLNCIVAVSQNMGIGKNGDLPWPPLRNEFKYFQRM T TSSVEGKQNLVIMGRKTWFSIPEKNRPLKDRINIVLSRELKEPPRG AHFL</p>

	<p><u>AKsLddALRLIEOPELASKVDMVWVGGSSVYQEAMNQPGLRLFLVTRI</u> <u>MQEFESDTFFPEIDLGKYKLLPEYPGVLSEVQEEKGIKYKFEVYEKKDGS</u> <u>MVSKGEELFTGVVPILVELDGDVNGHKFSVSGEGEDATYGKLTCLKFIC</u> <u>TTGKLPVPWPTLVTTLTYGVCFSRYPDHMKQHDFFKSAMPEGYVQER</u> <u>TIFFKDdGNyKTRAEVKFEGDTLVNRIELKGIDFKEDGNILGHKLEYNIN</u> <u>SHNVYIMADKQKNGIKVNFKIHNIENIEDGSVQLADHYQONTPIGDGPVLL</u> <u>PDNHYLstQSALSKDPNEKRDHMLVLEFVTAAGITLGMDELYKGSMOIFV</u> <u>KTLTGKTITLEVePSDTIENVKAKIQDKEGIPPDQORLIFAGKQLEDGRTL</u> <u>SDYNIQKESTLHLVLRRLRSAWSHPQFEKGGGSGGGSGGSAWSHPQFEK</u></p>
Q89-DHFR (57.26%)	<p>MKHHHHHHNTSSNSMSPILGYWKIKGLVQPTRLLLEYLEEKYEEHLYERDE GDKWRNKKFELGLEFPNLPYYIDGDVCLTQSMARIYIADKHNMLGGCPKE RAEISMLEGAVLDIRYGVSRIAYSKDFETLKVDFLSKLPMLKMFEDRLCHK TYLNGDHVTHPDFMLYDALDVVLYMDPMCLDAFPKLVCFKKRIEAIQIDK YLKSSKYIAWPLQGWQATFGGGDHPPKSDLEVLFGQPMALRVTRNSKINA ENKAKINMAGAKRVPTAPAATSKPGLRPRTALGDIGNKVSEQLQAKMP MKKEAKPSATGKVIDKKLPKPLEKVPMLVPVPVSGSQQQQQQQQQQQQQ QQ QQ QQ GSMVRPLNCIVAVSQNM GIGKNGDLPWPPLRNEFKYFQRMTTTSSVEGKQNLVIMGRKTWFSIPEKN RPLKDRINIVLSRELKEPPRGAFHFLAKsLddALRLIEOPELASKVDMVWV GGSSVYQEAMNQPGLRLFLVTRIMQEFESDTFFPEIDLGKYKLLPEYPGV LSEVQEEKGIKYKFEVYEKKDGSMVSKGEELFTGVVPILVELDGDVNGH KFSVSGEGEDATYGKLTCLKFICTTGKLPVPWPTLVTTLTYGVCFSRYP DHMKQHDFFKSAMPEGYVQERTIFFKDdGNyKTRAEVKFEGDTLVNRI ELKGIDFKEDGNILGHKLEYNINSHNVYIMADKQKNGIKVNFKIHNIENIE DGSVQLADHYQONTPIGDGPVLLPDNHYLstQSALSKDPNEKRDHMLVLL EFVTAAGITLGMDELYKGSMOIFVKTLTGKTITLEVePSDTIENVKAKIQD KEGIPPDQORLIFAGKQLEDGRTLSDYNIQKESTLHLVLRRLRSAWSHPQF EKGGGSGGGSGGSAWSHPQFEK</p>
DHFR-Q19 (61.86%)	<p>MKHHHHHHNTSSNSMSPILGYWKIKGLVQPTRLLLEYLEEKYEEHLYERDE GDKWRNKKFELGLEFPNLPYYIDGDVCLTQSMARIYIADKHNMLGGCPKE RAEISMLEGAVLDIRYGVSRIAYSKDFETLKVDFLSKLPMLKMFEDRLCHK TYLNGDHVTHPDFMLYDALDVVLYMDPMCLDAFPKLVCFKKRIEAIQIDK YLKSSKYIAWPLQGWQATFGGGDHPPKSDLEVLFGQPMALRVTRNSKINA ENKAKINMAGAKRVPTAPAATSKPGLRPRTALGDIGNKVSEQLQAKMP MKKEAKPSATGKVIDKKLPKPLEKVPMLVPVPVSGSMVRPLNCIVAVS QNMGIGKNGDLPWPPLRNEFKYFQRMTTTSSVEGKQNLVIMGRKTWFSI PEKNRPLKDRINIVLSRELKEPPRGAFHFLAKsLddALRLIEOPELASKVDM VWVGGSSVYQEAMNQPGLRLFLVTRIMQEFESDTFFPEIDLGKYKLLPE YPGVLSEVQEEKGIKYKFEVYEKKDGSQQQQQQQQQQQQQQQQQQQQGS MVSKGEELFTGVVPILVELDGDVNGHKFSVSGEGEDATYGKLTCLKFIC TTGKLPVPWPTLVTTLTYGVCFSRYPDHMKQHDFFKSAMPEGYVQER TIFFKDdGNyKTRAEVKFEGDTLVNRIELKGIDFKEDGNILGHKLEYNIN SHNVYIMADKQKNGIKVNFKIHNIENIEDGSVQLADHYQONTPIGDGPVLL PDNHYLstQSALSKDPNEKRDHMLVLEFVTAAGITLGMDELYKGSMOIFV KTLTGKTITLEVePSDTIENVKAKIQDKEGIPPDQORLIFAGKQLEDGRTL SDYNIQKESTLHLVLRRLRSAWSHPQFEKGGGSGGGSGGSAWSHPQFEK</p>
DHFR-Q89 (57.37%)	<p>MKHHHHHHNTSSNSMSPILGYWKIKGLVQPTRLLLEYLEEKYEEHLYERDE GDKWRNKKFELGLEFPNLPYYIDGDVCLTQSMARIYIADKHNMLGGCPKE RAEISMLEGAVLDIRYGVSRIAYSKDFETLKVDFLSKLPMLKMFEDRLCHK TYLNGDHVTHPDFMLYDALDVVLYMDPMCLDAFPKLVCFKKRIEAIQIDK YLKSSKYIAWPLQGWQATFGGGDHPPKSDLEVLFGQPMALRVTRNSKINA ENKAKINMAGAKRVPTAPAATSKPGLRPRTALGDIGNKVSEQLQAKMP MKKEAKPSATGKVIDKKLPKPLEKVPMLVPVPVSGSMVRPLNCIVAVS QNMGIGKNGDLPWPPLRNEFKYFQRMTTTSSVEGKQNLVIMGRKTWFSI PEKNRPLKDRINIVLSRELKEPPRGAFHFLAKsLddALRLIEOPELASKVDM VWVGGSSVYQEAMNQPGLRLFLVTRIMQEFESDTFFPEIDLGKYKLLPE YPGVLSEVQEEKGIKYKFEVYEKKDGSQQQQQQQQQQQQQQQQQQQQQQ QQ</p>

Q89-DHFR-Q19 (56.14%)	<p> <u>QQQQQQQQQQQQQQQQQQQQQQ</u><u>GS</u><u>MVSKGEELFTG</u><u>VVPILVELDGDVNG</u> <u>HKFSVSGEGEGDATYGKLT</u><u>TLKFICTTGKLPVPWPTLVTTLT</u><u>YGVQCFSR</u> <u>YPDHMKQHDFFKSAMPEGYVQERTIFFK</u><u>DdGNyKTRAEVKFEGDTLVN</u> <u>RIELKGIDFKEDGNILGHKLEYNYN</u><u>SHNVYIMADKQKNGIKVNF</u><u>KIHHN</u> <u>IEDGSVQLADHYQONTPIGDGPVLLPDNH</u><u>YLstQSALSKDPNEKRDH</u><u>MVL</u> <u>LEFVTAAGITLGMDELYK</u><u>GS</u><u>MQIFVKTLTGKTITLE</u><u>VePSDTIENVKAKIQ</u> <u>DKEGIPPDQORLIFAGKQLEDGRTLSDYNIQKESTLHLVLR</u><u>LSA</u><u>WSHP</u> <u>QFEKGGGSGGGSGGSAWSHPQFEK</u> </p>
	<p> MKHHHHHHNTSSNSMSPILGYWKIKGLVQPTRLLLEYLEEKYEEHLYERDE GDKWRNKKFELGLEFPNLPYYIDGDVKLTQSMAIIRYIADKHNLGGCPKE RAEISMLEGAVLDIRYGVSRIAYSKDFETLKVDFLSKLPEMLKMFEDRLCHK TYLNGDHVTHPDFMLYDALDVVLYMDPMCLDAFPKLVCFKKRIEAIQIDK YLKSSKYIAWPLQGWQATFGGGDHPPKSDLEVLFG<u>GP</u><u>MALRVTRNSKINA</u> <u>ENKAKINMAGAKRVPTAPAATSKPGLRPRTALGDIGNKVSEQLQAKMP</u> <u>MKKEAKPSATGKVIDKKLPKPLEKVPMLVPVPVS</u><u>GS</u><u>QQQQQQQQQQQQQQ</u> <u>QQ</u> <u>QQ</u> <u>QQ</u><u>GS</u><u>MVRPLNCIVAVSQNM</u> <u>GIGKNGDLPWPPLRNEFKYFQRM</u><u>TTTSSVEGKQNLVIMGRKTWFSIPEKN</u> <u>RPLKDRINIVLSRELKEPPRGAFHAKsLddALRLIEQPELASKVDMVWIV</u> <u>GGSSVYQEAMNQPGHLRLFVTRIMQEFESDTFFPEIDL</u><u>GKYKLLPEYPGV</u> <u>LSEVQEEKGIKYKFEVYEKKD</u><u>GS</u><u>QQQQQQQQQQQQQQQQQQQQQQ</u><u>GS</u><u>MVSK</u> <u>GEELFTG</u><u>VVPILVELDGDVNGHKFSVSGEGEGDATYGKLT</u><u>TLKFICTTGK</u> <u>LPVPWPTLVTTLT</u><u>YGVQCFSRYPDHMKQHDFFKSAMPEGYVQERTIFFK</u> <u>DdGNyKTRAEVKFEGDTLVNRIELKGIDFKEDGNILGHKLEYNYN</u><u>SHNV</u> <u>YIMADKQKNGIKVNF</u><u>KIHHNIEDGSVQLADHYQONTPIGDGPVLLPDNH</u> <u>YLstQSALSKDPNEKRDH</u><u>MVLLEFVTAAGITLGMDELYK</u><u>GS</u><u>MQIFVKTLT</u> <u>GKTITLE</u><u>VePSDTIENVKAKIQDKEGIPPDQORLIFAGKQLEDGRTLSDYN</u> <u>IQKESTLHLVLR</u><u>LSA</u><u>WSHPQFEKGGGSGGGSGGSAWSHPQFEK</u> </p>

NOTE: Each substrate component is represented by different color: 6xHis tag – green, GST tag – brown, N(95)CyclinB – red, polyQ – pink, DHFR – blue/green, GFP – yellow, ubiquitin – purple, TwinStrep tag – orchid. Only bold and underlined parts of the protein sequence contribute to coverage percentage.

Table S4. Software and computational tools.

Software	Version	Reference
CryoSPARC	3.3.1	Punjani et al., 2017
Relion	4.0	Kimanius et al., 2021
CryoDRGN	0.3.3/4	Zhong et al., 2021
UCSF Chimera	1.14	Pettersen et al., 2004
UCSF ChimeraX	1.3	Pettersen et al., 2021

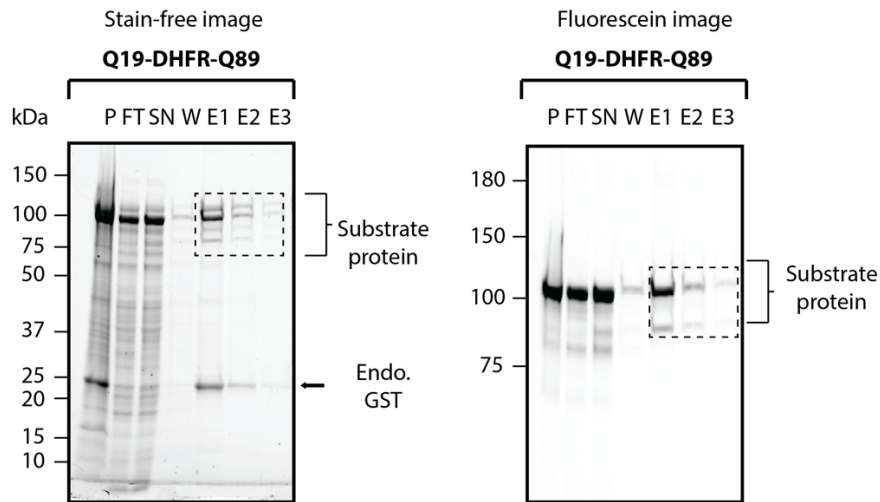


Figure S1. SDS-PAGE analysis of affinity purification of Q19-DHFR-Q89.

On the right the enclosing brackets and dashed squares on the gel image mark the positions of individual bands corresponding to substrate proteins and the arrow indicates the position of endogenous *E.coli* GST (Endo. GST) co-pulled with tagged protein. P – pellet, FT – flowthrough, SN – supernatant, W – wash, E – elution.

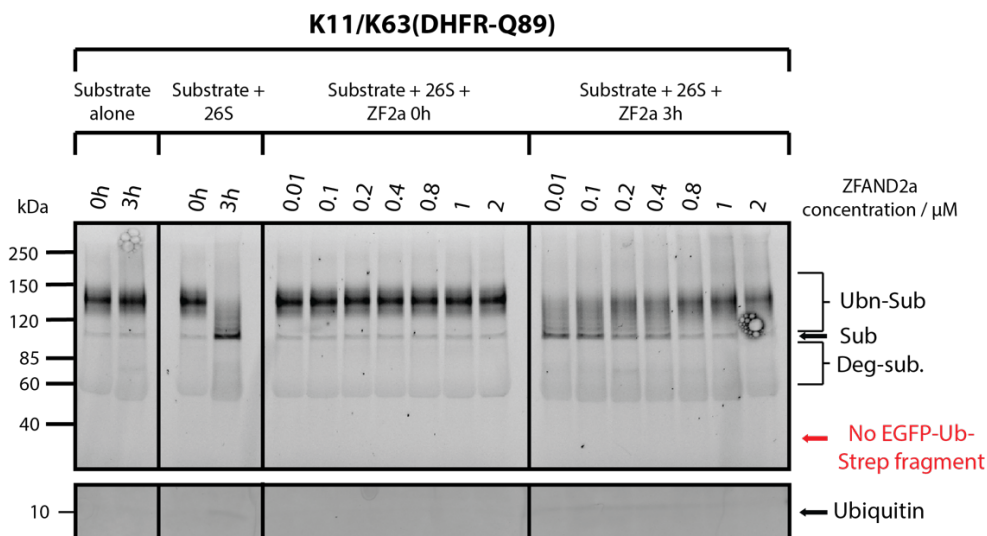


Figure S2. SDS-PAGE analysis of *in vitro* degradation assay with HEK293GP 26S proteasomes and K11/K63(DHFR-Q89) substrate with increasing concentration of ZFAND2a.

On the right side of the gel the band position of non-ubiquitinated substrate (Sub) is indicated with an arrow, the band range representing polyubiquitinated substrate (Ubn-Sub) and degradation products (Deg-sub) is indicated with enclosing brackets and ubiquitin band is indicated with an arrow in lower panel. The upper image was taken using Fluorescein channel. Bottom image was taken after overnight staining of the gel with SafeBlue and imaging with Coomassie channel.

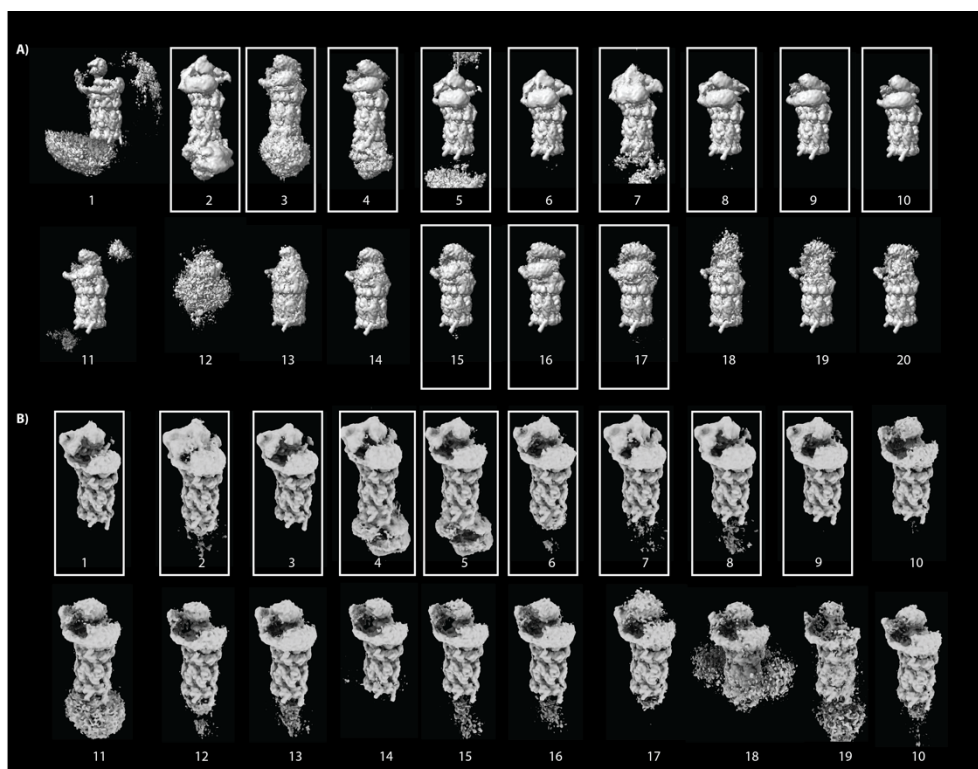


Figure S3. 3D classification in CryoDRGN.

A) First round of 3D classification and resulting 3D class averages. Particles belonging to models in white squares were selected for B) Second round of 3D classification and resulting 3D class averages. Particles belonging to models in white squares were selected for further processing.

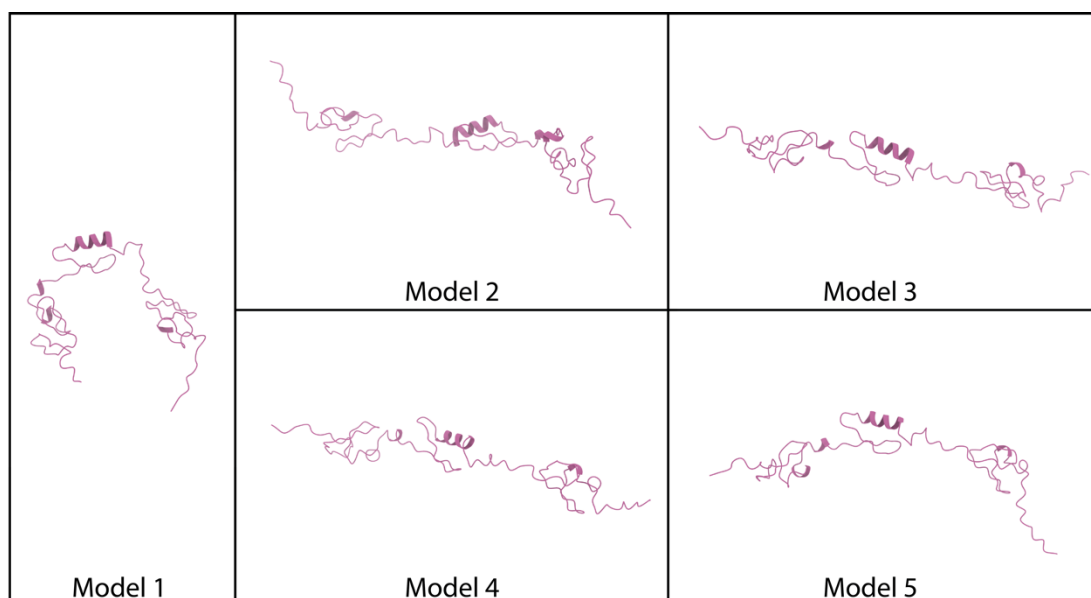


Figure S4. ZFAND2a structure prediction with AlphaFold. Model 5 was used for rigid body fitting into ZFAND2a cryo-EM density.

7. References

- Agard, D., Cheng, Y., Glaeser, R.M., Subramaniam, S., 2014. Chapter Two - Single-Particle Cryo-Electron Microscopy (Cryo-EM): Progress, Challenges, and Perspectives for Further Improvement, in: Hawkes, P.W. (Ed.), *Advances in Imaging and Electron Physics*. Elsevier, pp. 113–137. <https://doi.org/10.1016/B978-0-12-800144-8.00002-1>
- Akutsu, M., Dikic, I., Bremm, A., 2016. Ubiquitin chain diversity at a glance. *J Cell Sci* 129, 875–880. <https://doi.org/10.1242/jcs.183954>
- Ambagala, A.P.N., Solheim, J.C., Srikumaran, S., 2005. Viral interference with MHC class I antigen presentation pathway: The battle continues. *Veterinary Immunology and Immunopathology* 107, 1–15. <https://doi.org/10.1016/j.vetimm.2005.04.006>
- Amici, M., Sagratini, D., Pettinari, A., Pucciarelli, S., Angeletti, M., Eleuteri, A.M., 2004. 20S proteasome mediated degradation of DHFR: implications in neurodegenerative disorders. *Archives of Biochemistry and Biophysics* 422, 168–174. <https://doi.org/10.1016/j.abb.2003.12.014>
- Arrasate, M., Finkbeiner, S., 2012. Protein aggregates in Huntington's disease. *Exp Neurol* 238, 1–11. <https://doi.org/10.1016/j.expneurol.2011.12.013>
- Aviram, S., Kornitzer, D., 2010. The Ubiquitin Ligase Hsl5 Promotes Proteasomal Processivity. *Molecular and Cellular Biology*. <https://doi.org/10.1128/MCB.00909-09>
- Bai, X., McMullan, G., Scheres, S.H.W., 2015. How cryo-EM is revolutionizing structural biology. *Trends in Biochemical Sciences* 40, 49–57. <https://doi.org/10.1016/j.tibs.2014.10.005>
- Bajorek, M., Glickman, M.H., 2004. Ubiquitin-proteasome system. *CMLS, Cell. Mol. Life Sci.* 61, 1579–1588. <https://doi.org/10.1007/s00018-004-4131-y>
- Bard, J.A.M., Bashore, C., Dong, K.C., Martin, A., 2019. The 26S Proteasome Utilizes a Kinetic Gateway to Prioritize Substrate Degradation. *Cell* 177, 286-298.e15. <https://doi.org/10.1016/j.cell.2019.02.031>
- Bard, J.A.M., Goodall, E.A., Greene, E.R., Jonsson, E., Dong, K.C., Martin, A., 2018. Structure and Function of the 26S Proteasome. *Annu. Rev. Biochem.* 87, 697–724. <https://doi.org/10.1146/annurev-biochem-062917-011931>
- Baumeister, W., Walz, J., Zühl, F., Seemüller, E., 1998. The Proteasome: Paradigm of a Self-Compartmentalizing Protease. *Cell* 92, 367–380. [https://doi.org/10.1016/S0092-8674\(00\)80929-0](https://doi.org/10.1016/S0092-8674(00)80929-0)
- Bedford, L., Hay, D., Paine, S., Rezvani, N., Mee, M., Lowe, J., Mayer, R.J., 2008. Is malfunction of the ubiquitin proteasome system the primary cause of α -synucleinopathies and other chronic human neurodegenerative disease? *Biochimica et Biophysica Acta (BBA) - Molecular Basis of Disease, Ubiquitin, Proteasomes, and Disease* 1782, 683–690. <https://doi.org/10.1016/j.bbadis.2008.10.009>
- Bence, N.F., 2001. Impairment of the Ubiquitin-Proteasome System by Protein Aggregation. *Science* 292, 1552–1555. <https://doi.org/10.1126/science.292.5521.1552>
- Bengtson, M.H., Joazeiro, C.A.P., 2010. Role of a ribosome-associated E3 ubiquitin ligase in protein quality control. *Nature* 467, 470–473. <https://doi.org/10.1038/nature09371>
- Besche, H.C., Goldberg, A.L., 2012. Affinity Purification of Mammalian 26S Proteasomes Using an Ubiquitin-Like Domain, in: Dohmen, R.J., Scheffner, M. (Eds.), *Ubiquitin Family Modifiers and the Proteasome: Reviews and Protocols, Methods in Molecular*

- Biology. Humana Press, Totowa, NJ, pp. 423–432. https://doi.org/10.1007/978-1-61779-474-2_29
- Besche, H.C., Haas, W., Gygi, S.P., Goldberg, A.L., 2009. Isolation of Mammalian 26S Proteasomes and p97/VCP Complexes Using the Ubiquitin-like Domain from HHR23B Reveals Novel Proteasome-Associated Proteins. *Biochemistry* 48, 10.1021/bi802198q. <https://doi.org/10.1021/bi802198q>
- Besche, H.C., Sha, Z., Kukushkin, N.V., Peth, A., Hock, E.-M., Kim, W., Gygi, S., Gutierrez, J.A., Liao, H., Dick, L., Goldberg, A.L., 2014. Autoubiquitination of the 26S Proteasome on Rpn13 Regulates Breakdown of Ubiquitin Conjugates. *EMBO J* 33, 1159–1176. <https://doi.org/10.1002/embj.201386906>
- Bett, J.S., Cook, C., Petrucelli, L., Bates, G.P., 2009. The Ubiquitin-Proteasome Reporter GFPu Does Not Accumulate in Neurons of the R6/2 Transgenic Mouse Model of Huntington's Disease. *PLoS One* 4, e5128. <https://doi.org/10.1371/journal.pone.0005128>
- Bodnar, N.O., Rapoport, T.A., 2017. Molecular Mechanism of Substrate Processing by the Cdc48 ATPase Complex. *Cell* 169, 722–735.e9. <https://doi.org/10.1016/j.cell.2017.04.020>
- Boughton, A.J., Liu, L., Lavy, T., Kleifeld, O., Fushman, D., 2021. A novel recognition site for polyubiquitin and ubiquitin-like signals in an unexpected region of proteasomal subunit Rpn1. *Journal of Biological Chemistry* 297, 101052. <https://doi.org/10.1016/j.jbc.2021.101052>
- Bragança, C.E., Kraut, D.A., 2020. Mode of targeting to the proteasome determines GFP fate. *J Biol Chem* 295, 15892–15901. <https://doi.org/10.1074/jbc.RA120.015235>
- Braunstein, I., Zach, L., Allan, S., Kalies, K.-U., Stanhill, A., 2015. Proteasomal degradation of preemptive quality control (pQC) substrates is mediated by an AIRAPL-p97 complex. *Mol Biol Cell* 26, 3719–3727. <https://doi.org/10.1091/mbc.E15-02-0085>
- Brüning, A., Jücker, J., 2015. Misfolded Proteins: From Little Villains to Little Helpers in the Fight Against Cancer. *Frontiers in Oncology* 5.
- Carroll, E.C., Latorraca, N.R., Lindner, J.M., Maguire, B.C., Pelton, J.G., Marqusee, S., 2021. Mechanistic basis for ubiquitin modulation of a protein energy landscape. *PNAS* 118. <https://doi.org/10.1073/pnas.2025126118>
- Cascio, P., 2014. PA28 $\alpha\beta$: The Enigmatic Magic Ring of the Proteasome? *Biomolecules* 4, 566–584. <https://doi.org/10.3390/biom4020566>
- Chai, Y., Koppenhafer, S.L., Shoesmith, S.J., Perez, M.K., Paulson, H.L., 1999. Evidence for Proteasome Involvement in Polyglutamine Disease: Localization to Nuclear Inclusions in SCA3/MJD and Suppression of Polyglutamine Aggregation in vitro. *Human Molecular Genetics* 8, 673–682. <https://doi.org/10.1093/hmg/8.4.673>
- Chen, S., Wu, J., Lu, Y., Ma, Y.-B., Lee, B.-H., Yu, Z., Ouyang, Q., Finley, D.J., Kirschner, M.W., Mao, Y., 2016. Structural basis for dynamic regulation of the human 26S proteasome. *Proc Natl Acad Sci U S A* 113, 12991–12996. <https://doi.org/10.1073/pnas.1614614113>
- Chondrogianni, N., Georgila, K., Kourtis, N., Tavernarakis, N., Gonos, E.S., 2015. 20S proteasome activation promotes life span extension and resistance to proteotoxicity in *Caenorhabditis elegans*. *FASEB j.* 29, 611–622. <https://doi.org/10.1096/fj.14-252189>
- Chu, B.W., Kovary, K.M., Guillaume, J., Chen, L., Teruel, M.N., Wandless, T.J., 2013. The E3 Ubiquitin Ligase UBE3C Enhances Proteasome Processivity by Ubiquitinating Partially

- Proteolyzed Substrates *. *Journal of Biological Chemistry* 288, 34575–34587.
<https://doi.org/10.1074/jbc.M113.499350>
- Ciechanover, A., Brundin, P., 2003. The Ubiquitin Proteasome System in Neurodegenerative Diseases: Sometimes the Chicken, Sometimes the Egg. *Neuron* 40, 427–446.
[https://doi.org/10.1016/S0896-6273\(03\)00606-8](https://doi.org/10.1016/S0896-6273(03)00606-8)
- Ciechanover, A., Kwon, Y.T., 2015. Degradation of misfolded proteins in neurodegenerative diseases: therapeutic targets and strategies. *Exp Mol Med* 47, e147–e147.
<https://doi.org/10.1038/emm.2014.117>
- Collins, G.A., Goldberg, A.L., 2017. The Logic of the 26S Proteasome. *Cell* 169, 792–806.
<https://doi.org/10.1016/j.cell.2017.04.023>
- Coll-Martínez, B., Crosas, B., 2019. How the 26S Proteasome Degrades Ubiquitinated Proteins in the Cell. *Biomolecules* 9, 395. <https://doi.org/10.3390/biom9090395>
- Coux, O., Tanaka, K., Goldberg, A.L., 1996. Structure and Functions of the 20s and 26s Proteasomes. *Annual Review of Biochemistry* 65, 801–847.
<https://doi.org/10.1146/annurev.bi.65.070196.004101>
- Cummings, C.J., Mancini, M.A., Antalffy, B., DeFranco, D.B., Orr, H.T., Zoghbi, H.Y., 1998. Chaperone suppression of aggregation and altered subcellular proteasome localization imply protein misfolding in SCA1. *Nat Genet* 19, 148–154.
<https://doi.org/10.1038/502>
- Dahlmann, B., 2016. Mammalian proteasome subtypes: Their diversity in structure and function. *Archives of Biochemistry and Biophysics* 591, 132–140.
<https://doi.org/10.1016/j.abb.2015.12.012>
- Dantuma, N.P., Heessen, S., Lindsten, K., Jellne, M., Masucci, M.G., 2000. Inhibition of proteasomal degradation by the Gly-Ala repeat of Epstein–Barr virus is influenced by the length of the repeat and the strength of the degradation signal. *Proc Natl Acad Sci U S A* 97, 8381–8385.
- Dasgupta, S., Fishman, M.A., Mahallati, H., Castro, L.M., Tashima, A.K., Ferro, E.S., Fricker, L.D., 2015. Reduced Levels of Proteasome Products in a Mouse Striatal Cell Model of Huntington’s Disease. *PLOS ONE* 10, e0145333.
<https://doi.org/10.1371/journal.pone.0145333>
- Daskalogianni, C., Apcher, S., Candeias, M.M., Naski, N., Calvo, F., Fåhræus, R., 2008. Gly-Ala Repeats Induce Position- and Substrate-specific Regulation of 26 S Proteasome-dependent Partial Processing. *J Biol Chem* 283, 30090–30100.
<https://doi.org/10.1074/jbc.M803290200>
- David, Y., Ternette, N., Edelmann, M.J., Ziv, T., Gayer, B., Sertchook, R., Dadon, Y., Kessler, B.M., Navon, A., 2011. E3 Ligases Determine Ubiquitination Site and Conjugate Type by Enforcing Specificity on E2 Enzymes *. *Journal of Biological Chemistry* 286, 44104–44115. <https://doi.org/10.1074/jbc.M111.234559>
- de Pril, R., 2004. Accumulation of aberrant ubiquitin induces aggregate formation and cell death in polyglutamine diseases. *Human Molecular Genetics* 13, 1803–1813.
<https://doi.org/10.1093/hmg/ddh188>
- Deol, K.K., Crowe, S.O., Du, J., Bisbee, H.A., Guenette, R.G., Strieter, E.R., 2020. Proteasome-Bound UCH37/UCL5 Debranches Ubiquitin Chains to Promote Degradation. *Molecular Cell* 80, 796–809.e9. <https://doi.org/10.1016/j.molcel.2020.10.017>
- Deriziotis, P., Tabrizi, S.J., 2008. Prions and the proteasome. *Biochimica et Biophysica Acta (BBA) - Molecular Basis of Disease, Ubiquitin, Proteasomes, and Disease* 1782, 713–722. <https://doi.org/10.1016/j.bbadis.2008.06.011>

- Díaz-Hernández, M., Valera, A.G., Morán, M.A., Gómez-Ramos, P., Alvarez-Castelao, B., Castaño, J.G., Hernández, F., Lucas, J.J., 2006. Inhibition of 26S proteasome activity by huntingtin filaments but not inclusion bodies isolated from mouse and human brain. *J Neurochem* 98, 1585–1596. <https://doi.org/10.1111/j.1471-4159.2006.03968.x>
- Ding, F., Xiao, H., Wang, M., Xie, X., Hu, F., 2014. The role of the ubiquitin-proteasome pathway in cancer development and treatment. *Front Biosci (Landmark Ed)* 19, 886–895. <https://doi.org/10.2741/4254>
- Ding, Q., Lewis, J.J., Strum, K.M., Dimayuga, E., Bruce-Keller, A.J., Dunn, J.C., Keller, J.N., 2002. Polyglutamine Expansion, Protein Aggregation, Proteasome Activity, and Neural Survival*. *Journal of Biological Chemistry* 277, 13935–13942. <https://doi.org/10.1074/jbc.M107706200>
- Ding, Z., Fu, Z., Xu, C., Wang, Yifan, Wang, Yanxing, Li, J., Kong, L., Chen, J., Li, N., Zhang, R., Cong, Y., 2017. High-resolution cryo-EM structure of the proteasome in complex with ADP-AlFx. *Cell Res* 27, 373–385. <https://doi.org/10.1038/cr.2017.12>
- Edenberg, E.R., Downey, M., Toczyski, D., 2014. Polymerase Stalling during Replication, Transcription and Translation. *Current Biology* 24, R445–R452. <https://doi.org/10.1016/j.cub.2014.03.060>
- Eisele, M.R., Reed, R.G., Rudack, T., Schweitzer, A., Beck, F., Nagy, I., Pfeifer, G., Plitzko, J.M., Baumeister, W., Tomko, R.J., Sakata, E., 2018. Expanded Coverage of the 26S Proteasome Conformational Landscape Reveals Mechanisms of Peptidase Gating. *Cell Reports* 24, 1301-1315.e5. <https://doi.org/10.1016/j.celrep.2018.07.004>
- Ferrell, K., Wilkinson, C.R.M., Dubiel, W., Gordon, C., 2000. Regulatory subunit interactions of the 26S proteasome, a complex problem. *Trends in Biochemical Sciences* 25, 83–88. [https://doi.org/10.1016/S0968-0004\(99\)01529-7](https://doi.org/10.1016/S0968-0004(99)01529-7)
- Förster, F., Unverdorben, P., Ślędz, P., Baumeister, W., 2013. Unveiling the Long-Held Secrets of the 26S Proteasome. *Structure* 21, 1551–1562. <https://doi.org/10.1016/j.str.2013.08.010>
- Frank, J., 2002. Single-particle imaging of macromolecules by cryo-electron microscopy. *Annu Rev Biophys Biomol Struct* 31, 303–319. <https://doi.org/10.1146/annurev.biophys.31.082901.134202>
- Frankland-Searby, S., Bhaumik, S.R., 2012. The 26S proteasome complex: an attractive target for cancer therapy. *Biochim Biophys Acta* 1825, 64–76. <https://doi.org/10.1016/j.bbcan.2011.10.003>
- Fw, S., 2005. Protein production by auto-induction in high density shaking cultures. *Protein expression and purification* 41. <https://doi.org/10.1016/j.pep.2005.01.016>
- Gasteiger, E., Hoogland, C., Gattiker, A., Duvaud, S., Wilkins, M.R., Appel, R.D., Bairoch, A., 2005. Protein Identification and Analysis Tools on the ExPASy Server, in: Walker, J.M. (Ed.), *The Proteomics Protocols Handbook*, Springer Protocols Handbooks. Humana Press, Totowa, NJ, pp. 571–607. <https://doi.org/10.1385/1-59259-890-0:571>
- Glickman, M.H., Rubin, D.M., Fried, V.A., Finley, D., 1998. The Regulatory Particle of the *Saccharomyces cerevisiae* Proteasome. *Mol Cell Biol* 18, 3149–3162.
- Glinka, T., Alter, J., Braunstein, I., Tzach, L., Wei Sheng, C., Geifman, S., Edelmann, M.J., Kessler, B.M., Stanhill, A., 2013. Signal-peptide-mediated translocation is regulated by a p97–AIRAPL complex. *Biochemical Journal* 457, 253–261. <https://doi.org/10.1042/BJ20130710>

- Gottlieb, C.D., Thompson, A.C.S., Ordureau, A., Harper, J.W., Kopito, R.R., 2019. Acute unfolding of a single protein immediately stimulates recruitment of ubiquitin protein ligase E3C (UBE3C) to 26S proteasomes. *J Biol Chem* 294, 16511–16524. <https://doi.org/10.1074/jbc.RA119.009654>
- Groll, M., Ditzel, L., Löwe, J., Stock, D., Bochtler, M., Bartunik, H.D., Huber, R., 1997. Structure of 20S proteasome from yeast at 2.4Å resolution. *Nature* 386, 463–471. <https://doi.org/10.1038/386463a0>
- Groll, M., Huber, R., 2003. Substrate access and processing by the 20S proteasome core particle. *The International Journal of Biochemistry & Cell Biology, The proteasome in the regulation of cell function* 35, 606–616. [https://doi.org/10.1016/S1357-2725\(02\)00390-4](https://doi.org/10.1016/S1357-2725(02)00390-4)
- Grune, T., Merker, K., Sandig, G., Davies, K.J.A., 2003. Selective degradation of oxidatively modified protein substrates by the proteasome. *Biochem Biophys Res Commun* 305, 709–718. [https://doi.org/10.1016/S0006-291X\(03\)00809-X](https://doi.org/10.1016/S0006-291X(03)00809-X)
- Guo, Q., Lehmer, C., Martínez-Sánchez, A., Rudack, T., Beck, F., Hartmann, H., Pérez-Berlanga, M., Frotin, F., Hipp, M.S., Hartl, F.U., Edbauer, D., Baumeister, W., Fernández-Busnadiego, R., 2018. In Situ Structure of Neuronal C9ORF72 Poly-GA Aggregates Reveals Proteasome Recruitment. *Cell* 172, 696–705.e12. <https://doi.org/10.1016/j.cell.2017.12.030>
- Gusella, J.F., MacDonald, M.E., Ambrose, C.M., Duyao, M.P., 1993. Molecular Genetics of Huntington's Disease. *Archives of Neurology* 50, 1157–1163. <https://doi.org/10.1001/archneur.1993.00540110037003>
- Haas, A.L., Warms, J.V., Hershko, A., Rose, I.A., 1982. Ubiquitin-activating enzyme. Mechanism and role in protein-ubiquitin conjugation. *Journal of Biological Chemistry* 257, 2543–2548. [https://doi.org/10.1016/S0021-9258\(18\)34958-5](https://doi.org/10.1016/S0021-9258(18)34958-5)
- Hamazaki, J., Iemura, S., Natsume, T., Yashiroda, H., Tanaka, K., Murata, S., 2006. A novel proteasome interacting protein recruits the deubiquitinating enzyme UCH37 to 26S proteasomes. *EMBO J* 25, 4524–4536. <https://doi.org/10.1038/sj.emboj.7601338>
- Hanna, J., Waterman, D., Isasa, M., Elsasser, S., Shi, Y., Gygi, S., Finley, D., 2014. Cuz1/Ynl155w, a Zinc-dependent Ubiquitin-binding Protein, Protects Cells from Metalloid-induced Proteotoxicity* *This work was supported by National Institutes of Health Grant GM043601 (to D. F.). *Journal of Biological Chemistry* 289, 1876–1885. <https://doi.org/10.1074/jbc.M113.534032>
- Harding, R.J., Tong, Y., 2018. Proteostasis in Huntington's disease: disease mechanisms and therapeutic opportunities. *Acta Pharmacol Sin* 39, 754–769. <https://doi.org/10.1038/aps.2018.11>
- Hartmann-Petersen, R., Seeger, M., Gordon, C., 2003. Transferring substrates to the 26S proteasome. *Trends in Biochemical Sciences* 28, 26–31. [https://doi.org/10.1016/S0968-0004\(02\)00002-6](https://doi.org/10.1016/S0968-0004(02)00002-6)
- Hassan, W.M., Merin, D.A., Fonte, V., Link, C.D., 2009. AIP-1 ameliorates β -amyloid peptide toxicity in a *Caenorhabditis elegans* Alzheimer's disease model. *Hum Mol Genet* 18, 2739–2747. <https://doi.org/10.1093/hmg/ddp209>
- He, J., Kulkarni, K., da Fonseca, P.C.A., Krutauz, D., Glickman, M.H., Barford, D., Morris, E.P., 2012. The Structure of the 26S Proteasome Subunit Rpn2 Reveals Its PC Repeat Domain as a Closed Toroid of Two Concentric α -Helical Rings. *Structure* 20, 513–521. <https://doi.org/10.1016/j.str.2011.12.015>

- Hershko, A., Ciechanover, A., 1998. The Ubiquitin System. *Annual Review of Biochemistry* 67, 425–479. <https://doi.org/10.1146/annurev.biochem.67.1.425>
- Hershko, A., Ciechanover, A., Heller, H., Haas, A.L., Rose, I.A., 1980. Proposed role of ATP in protein breakdown: conjugation of protein with multiple chains of the polypeptide of ATP-dependent proteolysis. *Proc Natl Acad Sci U S A* 77, 1783–1786. <https://doi.org/10.1073/pnas.77.4.1783>
- Hershko, A., Heller, H., Elias, S., Ciechanover, A., 1983. Components of ubiquitin-protein ligase system. Resolution, affinity purification, and role in protein breakdown. *J Biol Chem* 258, 8206–8214.
- Hershko, A., Leshinsky, E., Ganoth, D., Heller, H., 1984. ATP-dependent degradation of ubiquitin-protein conjugates. *Proc Natl Acad Sci U S A* 81, 1619–1623. <https://doi.org/10.1073/pnas.81.6.1619>
- Hishiya, A., Iemura, S., Natsume, T., Takayama, S., Ikeda, K., Watanabe, K., 2006. A novel ubiquitin-binding protein ZNF216 functioning in muscle atrophy. *EMBO J* 25, 554–564. <https://doi.org/10.1038/sj.emboj.7600945>
- Hochstrasser, M., 2016. Gyre and gimble in the proteasome. *PNAS* 113, 12896–12898. <https://doi.org/10.1073/pnas.1616055113>
- Holmberg, C.I., Staniszewski, K.E., Mensah, K.N., Matouschek, A., Morimoto, R.I., 2004. Inefficient degradation of truncated polyglutamine proteins by the proteasome. *EMBO J* 23, 4307–4318. <https://doi.org/10.1038/sj.emboj.7600426>
- Hoyt, M.A., Zich, J., Takeuchi, J., Zhang, M., Govaerts, C., Coffino, P., 2006. Glycine–alanine repeats impair proper substrate unfolding by the proteasome. *EMBO J* 25, 1720–1729. <https://doi.org/10.1038/sj.emboj.7601058>
- Huber, E.M., Basler, M., Schwab, R., Heinemeyer, W., Kirk, C.J., Groettrup, M., Groll, M., 2012. Immuno- and constitutive proteasome crystal structures reveal differences in substrate and inhibitor specificity. *Cell* 148, 727–738. <https://doi.org/10.1016/j.cell.2011.12.030>
- Hunter, J.M., Lesort, M., Johnson, G.V.W., 2007. Ubiquitin-proteasome system alterations in a striatal cell model of huntington’s disease. *Journal of Neuroscience Research* 85, 1774–1788. <https://doi.org/10.1002/jnr.21287>
- Husnjak, K., Dikic, I., 2012. Ubiquitin-Binding Proteins: Decoders of Ubiquitin-Mediated Cellular Functions. *Annual Review of Biochemistry* 81, 291–322. <https://doi.org/10.1146/annurev-biochem-051810-094654>
- Inobe, T., Fishbain, S., Prakash, S., Matouschek, A., 2011. Defining the geometry of the two-component proteasome degron. *Nat Chem Biol* 7, 161–167. <https://doi.org/10.1038/nchembio.521>
- Isakov, E., Stanhill, A., 2011. Stalled Proteasomes Are Directly Relieved by P97 Recruitment. *J Biol Chem* 286, 30274–30283. <https://doi.org/10.1074/jbc.M111.240309>
- Jana, N.R., Zemskov, E.A., Wang, G., Nukina, N., 2001. Altered proteasomal function due to the expression of polyglutamine-expanded truncated N-terminal huntingtin induces apoptosis by caspase activation through mitochondrial cytochrome c release. *Human Molecular Genetics* 10, 1049–1059. <https://doi.org/10.1093/hmg/10.10.1049>
- Jiang, T.-X., Zhao, M., Qiu, X.-B., 2018. Substrate receptors of proteasomes. *Biological Reviews* 93, 1765–1777. <https://doi.org/10.1111/brv.12419>
- Johnston, J.A., Johnson, E.S., Waller, P.R.H., Varshavsky, A., 1995. Methotrexate Inhibits Proteolysis of Dihydrofolate Reductase by the N-end Rule Pathway (*). *Journal of Biological Chemistry* 270, 8172–8178. <https://doi.org/10.1074/jbc.270.14.8172>

- Jonsson, E., Htet, Z.M., Bard, J.A.M., Dong, K.C., Martin, A., 2021. Ubiquitin modulates 26S proteasome conformational dynamics and promotes substrate degradation (preprint). *Biochemistry*. <https://doi.org/10.1101/2021.08.18.456915>
- Juenemann, K., Schipper-Krom, S., Wiemhoefer, A., Kloss, A., Sanz, A.S., Reits, E.A.J., 2013. Expanded Polyglutamine-containing N-terminal Huntingtin Fragments Are Entirely Degraded by Mammalian Proteasomes. *The Journal of Biological Chemistry* 288, 27068. <https://doi.org/10.1074/jbc.M113.486076>
- Jumper, J., Evans, R., Pritzel, A., Green, T., Figurnov, M., Ronneberger, O., Tunyasuvunakool, K., Bates, R., Židek, A., Potapenko, A., Bridgland, A., Meyer, C., Kohli, S.A.A., Ballard, A.J., Cowie, A., Romera-Paredes, B., Nikolov, S., Jain, R., Adler, J., Back, T., Petersen, S., Reiman, D., Clancy, E., Zielinski, M., Steinegger, M., Pacholska, M., Berghammer, T., Bodenstein, S., Silver, D., Vinyals, O., Senior, A.W., Kavukcuoglu, K., Kohli, P., Hassabis, D., 2021. Highly accurate protein structure prediction with AlphaFold. *Nature* 596, 583–589. <https://doi.org/10.1038/s41586-021-03819-2>
- Kahana, C., Asher, G., Shaul, Y., 2005. Mechanisms of Protein Degradation: An Odyssey with ODC. *Cell Cycle* 4, 1461–1464. <https://doi.org/10.4161/cc.4.11.2115>
- Kim, K.B., 2021. Proteasomal adaptations to FDA-approved proteasome inhibitors: a potential mechanism for drug resistance? *Cancer Drug Resistance* 4, 634–645. <https://doi.org/10.20517/cdr.2021.27>
- Kimanius, D., Dong, L., Sharov, G., Nakane, T., Scheres, S.H.W., 2021. New tools for automated cryo-EM single-particle analysis in RELION-4.0. *Biochemical Journal* 478, 4169–4185. <https://doi.org/10.1042/BCJ20210708>
- King, R.W., Peters, J.-M., Tugendreich, S., Rolfe, M., Hieter, P., Kirschner, M.W., 1995. A 20S complex containing CDC27 and CDC16 catalyzes the mitosis-specific conjugation of ubiquitin to cyclin B. *Cell* 81, 279–288. [https://doi.org/10.1016/0092-8674\(95\)90338-0](https://doi.org/10.1016/0092-8674(95)90338-0)
- Kish-Trier, E., Hill, C.P., 2013. Structural Biology of the Proteasome. *Annual Review of Biophysics* 42, 29–49. <https://doi.org/10.1146/annurev-biophys-083012-130417>
- Kisselev, A.F., Akopian, T.N., Woo, K.M., Goldberg, A.L., 1999. The Sizes of Peptides Generated from Protein by Mammalian 26 and 20 S Proteasomes: IMPLICATIONS FOR UNDERSTANDING THE DEGRADATIVE MECHANISM AND ANTIGEN PRESENTATION*. *Journal of Biological Chemistry* 274, 3363–3371. <https://doi.org/10.1074/jbc.274.6.3363>
- Kitajima, Y., Yoshioka, K., Suzuki, N., 2020. The ubiquitin–proteasome system in regulation of the skeletal muscle homeostasis and atrophy: from basic science to disorders. *The Journal of Physiological Sciences* 70, 40. <https://doi.org/10.1186/s12576-020-00768-9>
- Kopp, F., Dahlmann, B., Kuehn, L., 2001. Reconstitution of hybrid proteasomes from purified PA700-20 S complexes and PA28alpha/beta activator: ultrastructure and peptidase activities. *J Mol Biol* 313, 465–471. <https://doi.org/10.1006/jmbi.2001.5063>
- Kunjappu, M.J., Hochstrasser, M., 2014. Assembly of the 20S Proteasome. *Biochim Biophys Acta* 1843, 10.1016/j.bbamcr.2013.03.008. <https://doi.org/10.1016/j.bbamcr.2013.03.008>
- Lavalée, M., Curdy, N., Laurent, C., Fournié, J.-J., Franchini, D.-M., 2021. Cancer cell adaptability: turning ribonucleoprotein granules into targets. *Trends in Cancer* 7, 902–915. <https://doi.org/10.1016/j.trecan.2021.05.006>

- Lecker, S.H., Goldberg, A.L., Mitch, W.E., 2006. Protein Degradation by the Ubiquitin–Proteasome Pathway in Normal and Disease States. *JASN* 17, 1807–1819. <https://doi.org/10.1681/ASN.2006010083>
- Lee, D., Takayama, S., Goldberg, A.L., 2018. ZFAND5/ZNF216 is an activator of the 26S proteasome that stimulates overall protein degradation. *PNAS* 115, E9550–E9559. <https://doi.org/10.1073/pnas.1809934115>
- Leggett, D.S., Hanna, J., Borodovsky, A., Crosas, B., Schmidt, M., Baker, R.T., Walz, T., Ploegh, H., Finley, D., 2002. Multiple Associated Proteins Regulate Proteasome Structure and Function. *Molecular Cell* 10, 495–507. [https://doi.org/10.1016/S1097-2765\(02\)00638-X](https://doi.org/10.1016/S1097-2765(02)00638-X)
- Levitskaya, J., Sharipo, A., Leonchiks, A., Ciechanover, A., Masucci, M.G., 1997. Inhibition of ubiquitin/proteasome-dependent protein degradation by the Gly-Ala repeat domain of the Epstein–Barr virus nuclear antigen 1. *Proc Natl Acad Sci U S A* 94, 12616–12621.
- Li, S.-H., Li, X.-J., 1998. Aggregation of N-Terminal Huntingtin is Dependent on the Length of Its Glutamine Repeats. *Human Molecular Genetics* 7, 777–782. <https://doi.org/10.1093/hmg/7.5.777>
- Li, X., Mooney, P., Zheng, S., Booth, C.R., Braunfeld, M.B., Gubbens, S., Agard, D.A., Cheng, Y., 2013. Electron counting and beam-induced motion correction enable near-atomic-resolution single-particle cryo-EM. *Nat Methods* 10, 584–590. <https://doi.org/10.1038/nmeth.2472>
- Lindersson, E., Beedholm, R., Højrup, P., Moos, T., Gai, W., Hendil, K.B., Jensen, P.H., 2004. Proteasomal Inhibition by α -Synuclein Filaments and Oligomers *. *Journal of Biological Chemistry* 279, 12924–12934. <https://doi.org/10.1074/jbc.M306390200>
- Linnen, J.M., Bailey, C.P., Weeks, D.L., 1993. Two related localized mRNAs from *Xenopus laevis* encode ubiquitin-like fusion proteins. *Gene* 128, 181–188. [https://doi.org/10.1016/0378-1119\(93\)90561-G](https://doi.org/10.1016/0378-1119(93)90561-G)
- Livneh, I., Cohen-Kaplan, V., Cohen-Rosenzweig, C., Avni, N., Ciechanover, A., 2016. The life cycle of the 26S proteasome: from birth, through regulation and function, and onto its death. *Cell Res* 26, 869–885. <https://doi.org/10.1038/cr.2016.86>
- Löwe, J., Stock, D., Jap, B., Zwickl, P., Baumeister, W., Huber, R., 1995. Crystal Structure of the 20S Proteasome from the Archaeon *T. acidophilum* at 3.4 Å Resolution. *Science*. <https://doi.org/10.1126/science.7725097>
- Mao, I., Liu, J., Li, X., Luo, H., 2008. REGy, a proteasome activator and beyond? *Cell. Mol. Life Sci.* 65, 3971. <https://doi.org/10.1007/s00018-008-8291-z>
- Marques, A.J., Palanimurugan, R., Matias, A.C., Ramos, P.C., Dohmen, R.J., 2009. Catalytic Mechanism and Assembly of the Proteasome. *Chem. Rev.* 109, 1509–1536. <https://doi.org/10.1021/cr8004857>
- Marquez-Lona, E.M., Torres-Machorro, A.L., Gonzales, F.R., Pillus, L., Patrick, G.N., 2017. Phosphorylation of the 19S regulatory particle ATPase subunit, Rpt6, modifies susceptibility to proteotoxic stress and protein aggregation. *PLoS ONE* 12, e0179893. <https://doi.org/10.1371/journal.pone.0179893>
- Marshall, R.S., Vierstra, R.D., 2019. Dynamic Regulation of the 26S Proteasome: From Synthesis to Degradation. *Frontiers in Molecular Biosciences* 6.
- Martinez-Fonts, K., Davis, C., Tomita, T., Elsasser, S., Nager, A.R., Shi, Y., Finley, D., Matouschek, A., 2020. The proteasome 19S cap and its ubiquitin receptors provide a

- versatile recognition platform for substrates. *Nat Commun* 11, 477.
<https://doi.org/10.1038/s41467-019-13906-8>
- Martinez-Fonts, K., Matouschek, A., 2016. A Rapid and Versatile Method for Generating Proteins with Defined Ubiquitin Chains. *Biochemistry* 55, 1898–1908.
<https://doi.org/10.1021/acs.biochem.5b01310>
- Matyskiela, M.E., Lander, G.C., Martin, A., 2013. Conformational switching of the 26S proteasome enables substrate degradation. *Nat Struct Mol Biol* 20, 781–788.
<https://doi.org/10.1038/nsmb.2616>
- Maynard, C.J., Böttcher, C., Ortega, Z., Smith, R., Florea, B.I., Díaz-Hernández, M., Brundin, P., Overkleeft, H.S., Li, J.-Y., Lucas, J.J., Dantuma, N.P., 2009. Accumulation of ubiquitin conjugates in a polyglutamine disease model occurs without global ubiquitin/proteasome system impairment. *Proc Natl Acad Sci U S A* 106, 13986–13991. <https://doi.org/10.1073/pnas.0906463106>
- McKinnon, C., Tabrizi, S.J., 2014. The Ubiquitin-Proteasome System in Neurodegeneration. *Antioxidants & Redox Signaling* 21, 2302–2321.
<https://doi.org/10.1089/ars.2013.5802>
- Meyer, H.-J., Rape, M., 2014. Enhanced Protein Degradation by Branched Ubiquitin Chains. *Cell* 157, 910–921. <https://doi.org/10.1016/j.cell.2014.03.037>
- Michalik, A., Van Broeckhoven, C., 2004. Proteasome degrades soluble expanded polyglutamine completely and efficiently. *Neurobiology of Disease* 16, 202–211.
<https://doi.org/10.1016/j.nbd.2003.12.020>
- Mishra, A., Dikshit, P., Purkayastha, S., Sharma, J., Nukina, N., Jana, N.R., 2008. E6-AP Promotes Misfolded Polyglutamine Proteins for Proteasomal Degradation and Suppresses Polyglutamine Protein Aggregation and Toxicity*. *Journal of Biological Chemistry* 283, 7648–7656. <https://doi.org/10.1074/jbc.M706620200>
- Morimoto, D., Walinda, E., Fukada, H., Sou, Y.-S., Kageyama, S., Hoshino, M., Fujii, T., Tsuchiya, H., Saeki, Y., Arita, K., Ariyoshi, M., Tochio, H., Iwai, K., Namba, K., Komatsu, M., Tanaka, K., Shirakawa, M., 2015. The unexpected role of polyubiquitin chains in the formation of fibrillar aggregates. *Nat Commun* 6, 6116.
<https://doi.org/10.1038/ncomms7116>
- Myeku, N., Duff, K.E., 2018. Targeting the 26S Proteasome To Protect Against Proteotoxic Diseases. *Trends in Molecular Medicine* 24, 18–29.
<https://doi.org/10.1016/j.molmed.2017.11.006>
- Nandi, D., Tahiliani, P., Kumar, A., Chandu, D., 2006. The ubiquitin-proteasome system. *J. Biosci.* 19.
- Nath, S.R., Lieberman, A.P., 2017. The Ubiquitination, Disaggregation and Proteasomal Degradation Machineries in Polyglutamine Disease. *Front Mol Neurosci* 10.
<https://doi.org/10.3389/fnmol.2017.00078>
- Nedelsky, N.B., Todd, P.K., Taylor, J.P., 2008. Autophagy and the ubiquitin-proteasome system: Collaborators in neuroprotection. *Biochimica et Biophysica Acta (BBA) - Molecular Basis of Disease, Ubiquitin, Proteasomes, and Disease* 1782, 691–699.
<https://doi.org/10.1016/j.bbadis.2008.10.002>
- Njomen, E., Tepe, J.J., 2019. Proteasome Activation as a New Therapeutic Approach To Target Proteotoxic Disorders. *J Med Chem* 62, 6469–6481.
<https://doi.org/10.1021/acs.jmedchem.9b00101>
- Oddo, S., 2008. The ubiquitin-proteasome system in Alzheimer's disease. *J Cell Mol Med* 12, 363–373. <https://doi.org/10.1111/j.1582-4934.2008.00276.x>

- Ohi, M., Li, Y., Cheng, Y., Walz, T., 2004. Negative Staining and Image Classification – Powerful Tools in Modern Electron Microscopy. *Biol Proced Online* 6, 23–34. <https://doi.org/10.1251/bpo70>
- Olszewski, M.M., Williams, C., Dong, K.C., Martin, A., 2019. The Cdc48 unfoldase prepares well-folded protein substrates for degradation by the 26S proteasome. *Commun Biol* 2, 1–8. <https://doi.org/10.1038/s42003-019-0283-z>
- Ortega, Z., Díaz-Hernández, M., Maynard, C.J., Hernández, F., Dantuma, N.P., Lucas, J.J., 2010. Acute Polyglutamine Expression in Inducible Mouse Model Unravels Ubiquitin/Proteasome System Impairment and Permanent Recovery Attributable to Aggregate Formation. *J Neurosci* 30, 3675–3688. <https://doi.org/10.1523/JNEUROSCI.5673-09.2010>
- Ortega, Z., Lucas, J.J., 2014. Ubiquitin–proteasome system involvement in Huntington’s disease. *Front Mol Neurosci* 7, 77. <https://doi.org/10.3389/fnmol.2014.00077>
- Paul, S., 2008. Dysfunction of the ubiquitin–proteasome system in multiple disease conditions: therapeutic approaches. *BioEssays* 30, 1172–1184. <https://doi.org/10.1002/bies.20852>
- Peña, A.H. de la, Goodall, E.A., Gates, S.N., Lander, G.C., Martin, A., 2018. Substrate-engaged 26S proteasome structures reveal mechanisms for ATP-hydrolysis–driven translocation. *Science*.
- Penney Jr, J.B., Vonsattel, J.-P., Macdonald, M.E., Gusella, J.F., Myers, R.H., 1997. CAG repeat number governs the development rate of pathology in Huntington’s disease. *Annals of Neurology* 41, 689–692. <https://doi.org/10.1002/ana.410410521>
- Petroski, M.D., Deshaies, R.J., 2003. Context of Multiubiquitin Chain Attachment Influences the Rate of Sic1 Degradation. *Molecular Cell* 11, 1435–1444. [https://doi.org/10.1016/S1097-2765\(03\)00221-1](https://doi.org/10.1016/S1097-2765(03)00221-1)
- Pettersen, E.F., Goddard, T.D., Huang, C.C., Couch, G.S., Greenblatt, D.M., Meng, E.C., Ferrin, T.E., 2004. UCSF Chimera--a visualization system for exploratory research and analysis. *J Comput Chem* 25, 1605–1612. <https://doi.org/10.1002/jcc.20084>
- Pettersen, E.F., Goddard, T.D., Huang, C.C., Meng, E.C., Couch, G.S., Croll, T.I., Morris, J.H., Ferrin, T.E., 2021. UCSF ChimeraX: Structure visualization for researchers, educators, and developers. *Protein Sci* 30, 70–82. <https://doi.org/10.1002/pro.3943>
- Pickering, Andrew.M., Davies, Kelvin.J.A., 2012. Differential Roles of Proteasome and Immunoproteasome Regulators Pa28 $\alpha\beta$, Pa28 γ and Pa200 in the Degradation of Oxidized Proteins. *Arch Biochem Biophys* 523, 181–190. <https://doi.org/10.1016/j.abb.2012.04.018>
- Powell, S.R., Herrmann, J., Lerman, A., Patterson, C., Wang, X., 2012. The Ubiquitin–Proteasome System and Cardiovascular Disease. *Prog Mol Biol Transl Sci* 109, 295–346. <https://doi.org/10.1016/B978-0-12-397863-9.00009-2>
- Prakash, S., Tian, L., Ratliff, K.S., Lehotzky, R.E., Matouschek, A., 2004. An unstructured initiation site is required for efficient proteasome-mediated degradation. *Nat Struct Mol Biol* 11, 830–837. <https://doi.org/10.1038/nsmb814>
- Pratt, G., Rechsteiner, M., 2008. Proteasomes Cleave at Multiple Sites within Polyglutamine Tracts: ACTIVATION BY PA28 γ (K188E)* *This work was supported, in whole or in part, by National Institutes of Health Grant NS042892 (to M. R.). The costs of publication of this article were defrayed in part by the payment of page charges. This article must therefore be hereby marked “advertisement” in accordance with 18

- U.S.C. Section 1734 solely to indicate this fact. *Journal of Biological Chemistry* 283, 12919–12925. <https://doi.org/10.1074/jbc.M709347200>
- Punjani, A., Rubinstein, J.L., Fleet, D.J., Brubaker, M.A., 2017. cryoSPARC: algorithms for rapid unsupervised cryo-EM structure determination. *Nat Methods* 14, 290–296. <https://doi.org/10.1038/nmeth.4169>
- Rabl, J., Smith, D.M., Yu, Y., Chang, S.-C., Goldberg, A.L., Cheng, Y., 2008. Mechanism of gate opening in the 20S proteasome by the proteasomal ATPases. *Mol Cell* 30, 360–368. <https://doi.org/10.1016/j.molcel.2008.03.004>
- Rahighi, S., Braunstein, I., Ternette, N., Kessler, B., Kawasaki, M., Kato, R., Matsui, T., Weiss, T.M., Stanhill, A., Wakatsuki, S., 2016. Selective binding of AIRAPL tandem UIMs to Lys48-linked tri-ubiquitin chains. *Structure* 24, 412–422. <https://doi.org/10.1016/j.str.2015.12.017>
- Rao, G., Croft, B., Teng, C., Awasthi, V., 2015. Ubiquitin-Proteasome System in Neurodegenerative Disorders. *J Drug Metab Toxicol* 6, 187. <https://doi.org/10.4172/2157-7609.1000187>
- Raspe, M., Gillis, J., Krol, H., Krom, S., Bosch, K., van Veen, H., Reits, E., 2009. Mimicking proteasomal release of polyglutamine peptides initiates aggregation and toxicity. *Journal of Cell Science* 122, 3262–3271. <https://doi.org/10.1242/jcs.045567>
- Ravid, T., Hochstrasser, M., 2008. Diversity of degradation signals in the ubiquitin–proteasome system. *Nat Rev Mol Cell Biol* 9, 679–689. <https://doi.org/10.1038/nrm2468>
- Rechsteiner, M., Hill, C.P., 2005. Mobilizing the proteolytic machine: cell biological roles of proteasome activators and inhibitors. *Trends Cell Biol* 15, 27–33. <https://doi.org/10.1016/j.tcb.2004.11.003>
- Reeg, S., Castro, J.P., Hugo, M., Grune, T., 2020. Accumulation of polyubiquitinated proteins: A consequence of early inactivation of the 26S proteasome. *Free Radical Biology and Medicine* 160, 293–302. <https://doi.org/10.1016/j.freeradbiomed.2020.08.008>
- Rosano, G.L., Ceccarelli, E.A., 2014. Recombinant protein expression in *Escherichia coli*: advances and challenges. *Frontiers in Microbiology* 5.
- Rosenthal, P.B., Henderson, R., 2003. Optimal Determination of Particle Orientation, Absolute Hand, and Contrast Loss in Single-particle Electron Cryomicroscopy. *Journal of Molecular Biology* 333, 721–745. <https://doi.org/10.1016/j.jmb.2003.07.013>
- Rosenzweig, R., Glickman, M.H., 2008. Chaperone-driven proteasome assembly. *Biochemical Society Transactions* 36, 807–812. <https://doi.org/10.1042/BST0360807>
- Rossi, A., Riccio, A., Coccia, M., Trotta, E., La Frazia, S., Santoro, M.G., 2014. The Proteasome Inhibitor Bortezomib Is a Potent Inducer of Zinc Finger AN1-type Domain 2a Gene Expression. *J Biol Chem* 289, 12705–12715. <https://doi.org/10.1074/jbc.M113.513242>
- Rossi, A., Trotta, E., Brandi, R., Arisi, I., Coccia, M., Santoro, M.G., 2010. AIRAP, a New Human Heat Shock Gene Regulated by Heat Shock Factor 1. *J Biol Chem* 285, 13607–13615. <https://doi.org/10.1074/jbc.M109.082693>
- Sahu, I., Glickman, M.H., 2021a. Proteasome in action: substrate degradation by the 26S proteasome. *Biochemical Society Transactions* 49, 629–644. <https://doi.org/10.1042/BST20200382>
- Sahu, I., Glickman, M.H., 2021b. Structural Insights into Substrate Recognition and Processing by the 20S Proteasome. *Biomolecules* 11, 148. <https://doi.org/10.3390/biom11020148>

- Sá-Moura, B., Funakoshi, M., Tomko, R.J., Dohmen, R.J., Wu, Z., Peng, J., Hochstrasser, M., 2013. A Conserved Protein with AN1 Zinc Finger and Ubiquitin-like Domains Modulates Cdc48 (p97) Function in the Ubiquitin-Proteasome Pathway. *J Biol Chem* 288, 33682–33696. <https://doi.org/10.1074/jbc.M113.521088>
- Saric, T., Graef, C.I., Goldberg, A.L., 2004. Pathway for Degradation of Peptides Generated by Proteasomes: A KEY ROLE FOR THIMET OLIGOPEPTIDASE AND OTHER METALLOPEPTIDASES *. *Journal of Biological Chemistry* 279, 46723–46732. <https://doi.org/10.1074/jbc.M406537200>
- Scanlon, T.C., Gottlieb, B., Durcan, T.M., Fon, E.A., Beitel, L.K., Trifiro, M.A., 2009. Isolation of human proteasomes and putative proteasome-interacting proteins using a novel affinity chromatography method. *Experimental Cell Research* 315, 176–189. <https://doi.org/10.1016/j.yexcr.2008.10.027>
- Schipper-Krom, S., Juenemann, K., Jansen, A.H., Wiemhoefer, A., van den Nieuwendijk, R., Smith, D.L., Hink, M.A., Bates, G.P., Overkleeft, H., Ovaa, H., Reits, E., 2014. Dynamic recruitment of active proteasomes into polyglutamine initiated inclusion bodies. *FEBS Letters* 588, 151–159. <https://doi.org/10.1016/j.febslet.2013.11.023>
- Schipper-Krom, S., Juenemann, K., Reits, E.A.J., 2012. The Ubiquitin-Proteasome System in Huntington's Disease: Are Proteasomes Impaired, Initiators of Disease, or Coming to the Rescue? *Biochemistry Research International* 2012, e837015. <https://doi.org/10.1155/2012/837015>
- Schmidt, M., Finley, D., 2014. Regulation of proteasome activity in health and disease. *Biochim Biophys Acta* 1843, 13–25. <https://doi.org/10.1016/j.bbamcr.2013.08.012>
- Schwartz, A.L., PhD, MD, Ciechanover, A., MD, PhD, 1999. The Ubiquitin-Proteasome Pathway and Pathogenesis of Human Diseases. *Annual Review of Medicine* 50, 57–74. <https://doi.org/10.1146/annurev.med.50.1.57>
- Schweitzer, A., Aufderheide, A., Rudack, T., Beck, F., Pfeifer, G., Plitzko, J.M., Sakata, E., Schulten, K., Förster, F., Baumeister, W., 2016. Structure of the human 26S proteasome at a resolution of 3.9 Å. *PNAS* 113, 7816–7821. <https://doi.org/10.1073/pnas.1608050113>
- Scomazzon, S.P., Riccio, A., Santopolo, S., Lanzilli, G., Coccia, M., Rossi, A., Santoro, M.G., 2019. The Zinc-Finger AN1-Type Domain 2a Gene Acts as a Regulator of Cell Survival in Human Melanoma: Role of E3-Ligase cIAP2. *Mol Cancer Res* 17, 2444–2456. <https://doi.org/10.1158/1541-7786.MCR-19-0243>
- Seo, H., Sonntag, K.-C., Kim, W., Cattaneo, E., Isacson, O., 2007. Proteasome Activator Enhances Survival of Huntington's Disease Neuronal Model Cells. *PLOS ONE* 2, e238. <https://doi.org/10.1371/journal.pone.0000238>
- Shabek, N., Herman-Bachinsky, Y., Buchsbaum, S., Lewinson, O., Haj-Yahya, M., Hejjaoui, M., Lashuel, H.A., Sommer, T., Brik, A., Ciechanover, A., 2012. The Size of the Proteasomal Substrate Determines Whether Its Degradation Will Be Mediated by Mono- or Polyubiquitylation. *Molecular Cell* 48, 87–97. <https://doi.org/10.1016/j.molcel.2012.07.011>
- Shibatani, T., Carlson, E.J., Larabee, F., McCormack, A.L., Früh, K., Skach, W.R., 2006. Global Organization and Function of Mammalian Cytosolic Proteasome Pools: Implications for PA28 and 19S Regulatory Complexes. *Mol Biol Cell* 17, 4962–4971. <https://doi.org/10.1091/mbc.E06-04-0311>

- Smith, D.M., 2018. Could a Common Mechanism of Protein Degradation Impairment Underlie Many Neurodegenerative Diseases? *J Exp Neurosci* 12, 1179069518794675. <https://doi.org/10.1177/1179069518794675>
- Sok, J., Calfon, M., Lu, J., Lichtlen, P., Clark, S.G., Ron, D., 2001. Arsenite-inducible RNA-associated protein (AIRAP) protects cells from arsenite toxicity. *Cell Stress Chaperones* 6, 6–15.
- Sonn-Segev, A., Belacic, K., Bodrug, T., Young, G., VanderLinden, R.T., Schulman, B.A., Schimpf, J., Friedrich, T., Dip, P.V., Schwartz, T.U., Bauer, B., Peters, J.-M., Struwe, W.B., Benesch, J.L.P., Brown, N.G., Haselbach, D., Kukura, P., 2020. Quantifying the heterogeneity of macromolecular machines by mass photometry. *Nature Communications* 11, 1772. <https://doi.org/10.1038/s41467-020-15642-w>
- Soto, C., Pritzkow, S., 2018. Protein misfolding, aggregation, and conformational strains in neurodegenerative diseases. *Nat Neurosci* 21, 1332–1340. <https://doi.org/10.1038/s41593-018-0235-9>
- Stadtmueller, B.M., Hill, C.P., 2011. Proteasome Activators. *Molecular Cell* 41, 8–19. <https://doi.org/10.1016/j.molcel.2010.12.020>
- Stanhill, A., Haynes, C.M., Zhang, Y., Min, G., Steele, M.C., Kalinina, J., Martinez, E., Pickart, C.M., Kong, X.-P., Ron, D., 2006. An Arsenite-Inducible 19S Regulatory Particle-Associated Protein Adapts Proteasomes to Proteotoxicity. *Molecular Cell* 23, 875–885. <https://doi.org/10.1016/j.molcel.2006.07.023>
- Stenoien, D.L., Cummings, C.J., Adams, H.P., Mancini, M.G., Patel, K., DeMartino, G.N., Marcelli, M., Weigel, N.L., Mancini, M.A., 1999. Polyglutamine-Expanded Androgen Receptors Form Aggregates That Sequester Heat Shock Proteins, Proteasome Components and SRC-1, and Are Suppressed by the HDJ-2 Chaperone. *Human Molecular Genetics* 8, 731–741. <https://doi.org/10.1093/hmg/8.5.731>
- Sukenik, S., Braunstein, I., Stanhill, A., 2021. An Arsenite Relay between PSMD14 and AIRAP Enables Revival of Proteasomal DUB Activity. *Biomolecules* 11, 1317. <https://doi.org/10.3390/biom11091317>
- Tai, H.-C., Besche, H., Goldberg, A., Schuman, E., 2010. Characterization of the brain 26S proteasome and its interacting proteins. *Frontiers in Molecular Neuroscience* 3.
- Tanaka, K., 2009. The proteasome: Overview of structure and functions. *Proc Jpn Acad Ser B Phys Biol Sci* 85, 12–36. <https://doi.org/10.2183/pjab.85.12>
- Thrower, J.S., Hoffman, L., Rechsteiner, M., Pickart, C.M., 2000. Recognition of the polyubiquitin proteolytic signal. *EMBO J* 19, 94–102. <https://doi.org/10.1093/emboj/19.1.94>
- Tillotson, J., Zerio, C.J., Harder, B., Ambrose, A.J., Jung, K.S., Kang, M., Zhang, D.D., Chapman, E., 2017. Arsenic Compromises Both p97 and Proteasome Functions. *Chem Res Toxicol* 30, 1508–1514. <https://doi.org/10.1021/acs.chemrestox.7b00158>
- Tomko, R.J., Hochstrasser, M., 2013. Molecular Architecture and Assembly of the Eukaryotic Proteasome. *Annu Rev Biochem* 82, 10.1146/annurev-biochem-060410–150257. <https://doi.org/10.1146/annurev-biochem-060410-150257>
- Traub, L.M., Lukacs, G.L., 2007. Decoding ubiquitin sorting signals for clathrin-dependent endocytosis by CLASPs. *Journal of Cell Science* 120, 543–553. <https://doi.org/10.1242/jcs.03385>
- Tsvetkov, P., Mendillo, M.L., Zhao, J., Carette, J.E., Merrill, P.H., Cikes, D., Varadarajan, M., van Diemen, F.R., Penninger, J.M., Goldberg, A.L., Brummelkamp, T.R., Santagata, S., Lindquist, S., 2015. Compromising the 19S proteasome complex protects cells from

- reduced flux through the proteasome. *eLife* 4, e08467.
<https://doi.org/10.7554/eLife.08467>
- Turakhiya, A., Meyer, S.R., Marincola, G., Böhm, S., Vanselow, J.T., Schlosser, A., Hofmann, K., Buchberger, A., 2018. ZFAND1 Recruits p97 and the 26S Proteasome to Promote the Clearance of Arsenite-Induced Stress Granules. *Molecular Cell* 70, 906-919.e7.
<https://doi.org/10.1016/j.molcel.2018.04.021>
- Unno, M., Mizushima, T., Morimoto, Y., Tomisugi, Y., Tanaka, K., Yasuoka, N., Tsukihara, T., 2002. The Structure of the Mammalian 20S Proteasome at 2.75 Å Resolution. *Structure* 10, 609–618. [https://doi.org/10.1016/S0969-2126\(02\)00748-7](https://doi.org/10.1016/S0969-2126(02)00748-7)
- Unverdorben, P., Beck, F., Śledź, P., Schweitzer, A., Pfeifer, G., Plitzko, J.M., Baumeister, W., Förster, F., 2014. Deep classification of a large cryo-EM dataset defines the conformational landscape of the 26S proteasome. *Proc Natl Acad Sci U S A* 111, 5544–5549. <https://doi.org/10.1073/pnas.1403409111>
- Venkatraman, P., Wetzel, R., Tanaka, M., Nukina, N., Goldberg, A.L., 2004. Eukaryotic Proteasomes Cannot Digest Polyglutamine Sequences and Release Them during Degradation of Polyglutamine-Containing Proteins. *Molecular Cell* 14, 95–104.
[https://doi.org/10.1016/S1097-2765\(04\)00151-0](https://doi.org/10.1016/S1097-2765(04)00151-0)
- Verbrugge, S.E., Scheper, R.J., Lems, W.F., de Gruijl, T.D., Jansen, G., 2015. Proteasome inhibitors as experimental therapeutics of autoimmune diseases. *Arthritis Research & Therapy* 17, 17. <https://doi.org/10.1186/s13075-015-0529-1>
- Verhoef, L.G.G.C., Lindsten, K., Masucci, M.G., Dantuma, N.P., 2002. Aggregate formation inhibits proteasomal degradation of polyglutamine proteins. *Human Molecular Genetics* 11, 2689–2700. <https://doi.org/10.1093/hmg/11.22.2689>
- Verma, R., Chen, S., Feldman, R., Schieltz, D., Yates, J., Dohmen, J., Deshaies, R.J., 2000. Proteasomal Proteomics: Identification of Nucleotide-sensitive Proteasome-interacting Proteins by Mass Spectrometric Analysis of Affinity-purified Proteasomes. *MBoC* 11, 3425–3439. <https://doi.org/10.1091/mbc.11.10.3425>
- VerPlank, J.J.S., Tyrkalska, S.D., Fleming, A., Rubinsztein, D.C., Goldberg, A.L., 2020. cGMP via PKG activates 26S proteasomes and enhances degradation of proteins, including ones that cause neurodegenerative diseases. *PNAS* 117, 14220–14230.
<https://doi.org/10.1073/pnas.2003277117>
- Wade, R.H., 1992. A brief look at imaging and contrast transfer. *Ultramicroscopy* 46, 145–156. [https://doi.org/10.1016/0304-3991\(92\)90011-8](https://doi.org/10.1016/0304-3991(92)90011-8)
- Waelter, S., Boeddrich, A., Lurz, R., Scherzinger, E., Lueder, G., Lehrach, H., Wanker, E.E., 2001. Accumulation of Mutant Huntingtin Fragments in Aggresome-like Inclusion Bodies as a Result of Insufficient Protein Degradation. *Mol Biol Cell* 12, 1393–1407.
- Wang, J., Maldonado, M.A., 2006. The ubiquitin-proteasome system and its role in inflammatory and autoimmune diseases. *Cell Mol Immunol* 3, 255–261.
- Wang, X., Chemmama, I.E., Yu, C., Huszagh, A., Xu, Y., Viner, R., Block, S.A., Cimermancic, P., Rychnovsky, S.D., Ye, Y., Sali, A., Huang, L., 2017a. The proteasome-interacting Ecm29 protein disassembles the 26S proteasome in response to oxidative stress. *J Biol Chem* 292, 16310–16320. <https://doi.org/10.1074/jbc.M117.803619>
- Wang, X., Cimermancic, P., Yu, C., Schweitzer, A., Chopra, N., Engel, J.L., Greenberg, C., Huszagh, A.S., Beck, F., Sakata, E., Yang, Y., Novitsky, E.J., Leitner, A., Nanni, P., Kahraman, A., Guo, X., Dixon, J.E., Rychnovsky, S.D., Aebersold, R., Baumeister, W., Sali, A., Huang, L., 2017b. Molecular Details Underlying Dynamic Structures and

- Regulation of the Human 26S Proteasome. *Mol Cell Proteomics* 16, 840–854.
<https://doi.org/10.1074/mcp.M116.065326>
- Wehmer, M., Rudack, T., Beck, F., Aufderheide, A., Pfeifer, G., Plitzko, J.M., Förster, F., Schulten, K., Baumeister, W., Sakata, E., 2017. Structural insights into the functional cycle of the ATPase module of the 26S proteasome. *Proc Natl Acad Sci U S A* 114, 1305–1310. <https://doi.org/10.1073/pnas.1621129114>
- Welk, V., Coux, O., Kleene, V., Abeza, C., Trümbach, D., Eickelberg, O., Meiners, S., 2016. Inhibition of Proteasome Activity Induces Formation of Alternative Proteasome Complexes *. *Journal of Biological Chemistry* 291, 13147–13159.
<https://doi.org/10.1074/jbc.M116.717652>
- Wolf, D.H., Hilt, W., 2004. The proteasome: a proteolytic nanomachine of cell regulation and waste disposal. *Biochimica et Biophysica Acta (BBA) - Molecular Cell Research, The Ubiquitin-Proteasome System* 1695, 19–31.
<https://doi.org/10.1016/j.bbamcr.2004.10.007>
- Worden, E.J., Dong, K.C., Martin, A., 2017. An AAA Motor-Driven Mechanical Switch in Rpn11 Controls Deubiquitination at the 26S Proteasome. *Molecular Cell* 67, 799–811.e8. <https://doi.org/10.1016/j.molcel.2017.07.023>
- Worden, E.J., Padovani, C., Martin, A., 2014. Structure of the Rpn11–Rpn8 dimer reveals mechanisms of substrate deubiquitination during proteasomal degradation. *Nat Struct Mol Biol* 21, 220–227. <https://doi.org/10.1038/nsmb.2771>
- Xie, Y., 2010. Structure, Assembly and Homeostatic Regulation of the 26S Proteasome. *Journal of Molecular Cell Biology* 2, 308–317. <https://doi.org/10.1093/jmcb/mjq030>
- Xie, Y., Varshavsky, A., 2002. UFD4 lacking the proteasome-binding region catalyses ubiquitination but is impaired in proteolysis. *Nat Cell Biol* 4, 1003–1007.
<https://doi.org/10.1038/ncb889>
- Yun, C., Stanhill, A., Yang, Y., Zhang, Y., Haynes, C.M., Xu, C.-F., Neubert, T.A., Mor, A., Philips, M.R., Ron, D., 2008. Proteasomal adaptation to environmental stress links resistance to proteotoxicity with longevity in *Caenorhabditis elegans*. *PNAS* 105, 7094–7099. <https://doi.org/10.1073/pnas.0707025105>
- Zaldumbide, A., Ossevoort, M., Wiertz, E.J.H.J., Hoeben, R.C., 2007. In cis inhibition of antigen processing by the latency-associated nuclear antigen I of Kaposi sarcoma herpes virus. *Mol Immunol* 44, 1352–1360.
<https://doi.org/10.1016/j.molimm.2006.05.012>
- Zhang, M., Coffino, P., 2004. Repeat Sequence of Epstein-Barr Virus-encoded Nuclear Antigen 1 Protein Interrupts Proteasome Substrate Processing *. *Journal of Biological Chemistry* 279, 8635–8641. <https://doi.org/10.1074/jbc.M310449200>
- Zhong, E.D., Bepler, T., Berger, B., Davis, J.H., 2021. CryoDRGN: reconstruction of heterogeneous cryo-EM structures using neural networks. *Nat Methods* 18, 176–185. <https://doi.org/10.1038/s41592-020-01049-4>
- Zhu, Y., Wang, W.L., Yu, D., Ouyang, Q., Lu, Y., Mao, Y., 2018. Structural mechanism for nucleotide-driven remodeling of the AAA-ATPase unfoldase in the activated human 26S proteasome. *Nat Commun* 9, 1360. <https://doi.org/10.1038/s41467-018-03785-w>